DROPLET EVAPORATION OF ALCOHOL-BIODIESEL BLENDS

ALEXIS TANNER

Thesis Submitted to the University of Ottawa
in Partial Fulfillment of the Requirements for the
Master of Applied Science Degree in Mechanical Engineering

Ottawa-Carleton Institute for Mechanical and Aerospace Engineering
Department of Mechanical Engineering
Faculty of Engineering
University of Ottawa

Abstract

Biodiesel has been proposed as a substitute for diesel given that biodiesel has lower net average greenhouse gas emissions than diesel. Additionally, alcohol may be added to biodiesel to improve biodiesel's performance in a diesel engine as well to reduce engine emissions. This work will study the droplet evaporation process of alcohol-biodiesel blends.

Due to alcohol's polar nature and the fatty acid methyl esters's (FAME) slightly polar nature, an appropriate method must be chosen to represent the evaporation process of a non-ideal mixture. The vapour-liquid equilibria was modelled in two ways: the first method uses only Raoult's Law, while the second method uses Raoult's law modified with activity coefficients calculated using the UNIFAC method. The comparison of the modelled results with experimental vapour-liquid equilibria data has shown that activity coefficients calculated using the UNIFAC method are able to accurately represent alcohol-biodiesel systems.

Droplet evaporation experiments have been performed for biodiesel-propanol and biodiesel-pentanol blends at temperatures of 450°C and 700°C with the alcohol concentrations of 5%, 10%, 15%, and 20%. Additionally, the droplet evaporation was numerically modelled using two different models to represent the liquid state: a model with a well-mixed liquid phase and a model which includes component diffusion in the liquid phase. Comparing the experimental droplet temperatures to the numerical models has shown that the diffusion-limited model best represents the droplet evaporation process, suggesting that some of the alcohol components remain in the center of the droplet even when the droplet temperature is greater than the boiling temperature of the alcohol. This was further confirmed by observations of bubbling within the droplet during evaporation of the biodiesel-alcohol blends, in which there were both small bubbles and large bubbles forming. The formation of large bubbles has shown to correspond with the difference between experimental droplet diameter and the diffusion-limited model's droplet diameter.

Acknowledgements

First and foremost, the author acknowledges the financial support provided by NSERC for providing funding for this research project.

Secondly, the author would like to thank Simon Doray and Innoltek for providing the biodiesel sample that was needed for this work.

Most importantly, I would like to give special thanks to my thesis supervisor, Dr. William Hallett, for giving me the opportunity to work under your supervision on alcohol-biodiesel droplet evaporation. You always provide great insight and help with my work with your expertise and knowledge. I appreciate how you have been able to adjust my studies and research during the lockdowns and COVID restrictions such that I was able to still make progress on my degree. You have definitely inspired me to pursue an academic/research career in combustion.

Lastly, I would like to thank my family, Mom, Dad, Joshua, and Jacob, who have become my quarantine (stuck at home) coworkers and have kept me somewhat sane during the pandemic and my thesis writing. You always showed interest in my work and made sure I was making progress, even when you may not fully understand my work. A special thanks should be given to Joshua, who always suggested, nearly everyday, that I should include his favourite subject, machine learning, in my thesis.

Table of Contents

Abstract ii
Acknowledgements iii
List of Figures vi
List of Tables xii
Nomenclature xiii
1 Introduction 1
2 Literature Review 2
2.1 Alcohol-Biodiesel Blends 2
2.2 Droplet Evaporation Model 4
2.2.1 Continuous Thermodynamics Model 4
2.2.2 Liquid Transport Processes 5
2.3 Vapour-Liquid Equilibria 6
2.3.1 Raoult's Law 6
2.3.2 UNIFAC Method 6
2.4 Summary of Literature Review 7
3 Model Development 8
3.1 Well-Mixed Continuous Thermodynamics Model 9
3.2 Diffusion-Limited Continuous Thermodynamics Model 11
3.3 Physical Property Correlations 14
3.4 UNIFAC Method 16
4 Distillation Test of Biodiesel and Fitting of Model Biodiesel Composition 20
5 Vapour-Liquid Equilibria of Alcohol-Biodiesel Blends 24
5.1 Determining the Representative Molecule for the UNIFAC Model of a Continuous Mixture 24
5.1.1 Continuous Alcohol Mixture with a Single FAME 24
5.1.2 Single Alcohol with a Continuous FAME Mixture 28
5.2 Comparing VLE Models with Experimental Data 30
5.3 Vapour-Liquid Equilibria of FAME-MGC-Alcohols 35
6 Droplet Evaporation Experiment Methodology 38
6.1 Experimental Setup 38
6.2 Droplet Diameter Measurements 39
6.3 Droplet Temperature Measurements 40

7 Droplet Evaporation Results....41
7.1 Biodiesel Droplets....41
7.2 Propanol-Biodiesel Droplets....47
7.2.1 Droplet Temperatures....48
7.2.2 Droplet Diameters....54
7.2.3 Droplet Boiling Temperatures....65
7.2.4 Summary of Results for Propanol-Biodiesel....70
7.3 Pentanol-Biodiesel Mixtures....71
7.3.1 Droplet Temperatures....71
7.3.2 Droplet Diameters....78
7.3.3 Droplet Boiling Temperatures....87
7.3.4 Summary of Results for Pentanol-Biodiesel....91
7.4 Summary of Droplet Evaporation Results....92
8 Conclusion....93
References....95
Appendix A: Property Correlations Parameters Values....100
Appendix B: Experimental Droplet Diameter Data from Droplet Evaporation Experiments....101
Appendix C: Experimental Droplet Temperature Data from Droplet Evaporation Experiments....110
Appendix D: Additional Results for Biodiesel Propanol Mixtures....119
Appendix E: Additional Results for Biodiesel Pentanol Mixtures....123

List of Figures

Figure 4-1: Apparatus for distillation test 20
Figure 4-2: Distillation curve for biodiesel and distillation model using two continuous mixtures 22
Figure 4-3: Distillation curve for biodiesel and distillation model using individual components 23
Figure 5-1: Numerical model of the distillation of an alcohol mixture with a composition of individual components or as a continuous mixture.....25
Figure 5-2: Vapour liquid equilibria of alcohol mixture with methyl oleate where the alcohol mixture is represented as individual components or as a continuous mixture with the functional groups represented by the molecule with the lowest molecular weight, highest molecular weight, mol average or mass average.....27
Figure 5-3: Vapour liquid equilibria of FAME mixture with propanol where the FAME mixture is represented as individual components or as a continuous mixture with the functional groups represented by the molecule with the lowest molecular weight, highest molecular weight, mol average or mass average.....29
Figure 5-4: Vapour liquid equilibria of FAME mixture with propanol where the FAME mixture is represented as individual components or as a continuous mixture with the functional groups represented by a FAME molecule that has 0, 1, 2, or 3, double bonds.....30
Figure 5-5: Chemical structures of a) methyl laurate, b) methyl myristate, and c) methyl oleate 31
Figure 5-6: Comparison of vapour liquid equilibria modelling using the UNIFAC method and Raoult's Law with experimental data for methyl laurate-ethanol 31
Figure 5-7: Comparison of vapour liquid equilibria modelling using the UNIFAC method and Raoult's Law with experimental data for methyl myristate-ethanol 32
Figure 5-8: Comparison of vapour liquid equilibria modelling using the UNIFAC method and Raoult's Law with experimental data for methyl oleate-ethanol.....33
Figure 5-9: Comparison of vapour liquid equilibria modelling using the UNIFAC method and Raoult's Law with experimental data for biodiesel-ethanol.....34
Figure 5-10: Vapour liquid equilibrium modelling using UNIFAC for FAME-MGC-propanol at 1 atm.....36
Figure 5-11: Vapour liquid equilibrium modelling using UNIFAC for FAME-MGC-pentanol at 1 atm.....37
Figure 6-1: Cross-section and longitudinal section views of furnace and droplet setup 39
Figure 7-1: Droplet diameter of biodiesel during droplet evaporation at 450°C.....42
Figure 7-2: Droplet temperature of biodiesel during droplet evaporation at 450°C.....43
Figure 7-3: Droplet photos of biodiesel during droplet evaporation at 450°C.....44
Figure 7-4: Droplet diameter of biodiesel during droplet evaporation at 700°C.....45
Figure 7-5: Droplet photos of biodiesel during droplet evaporation at 700°C.....46
Figure 7-6: Droplet temperature of biodiesel during droplet evaporation at 700°C.....47
Figure 7-7: Droplet temperature of biodiesel with 5% propanol during droplet evaporation at 450°C.....48

Figure 7-8: Droplet temperature of biodiesel with 20% propanol during droplet evaporation at 450°C.....49
Figure 7-9: Calculated vapour molar flux and vapour mol fractions of well-mixed droplet of biodiesel with 20% during droplet evaporation at 450°C 50
Figure 7-10: Calculated vapour molar flux and vapour mol fractions of diffusion-limited droplet of biodiesel with 20% during droplet evaporation at 450°C 51
Figure 7-11: Droplet temperature of biodiesel with 20% propanol during droplet evaporation at 450°C with varying mixing factor, χ.....52
Figure 7-12: Droplet temperature of biodiesel with 20% propanol during droplet evaporation at 450°C with Varying Mixing Factor, χ, between 0 and 6 seconds 52
Figure 7-13: Droplet temperature of biodiesel with 5% propanol during droplet evaporation at 700°C.....53
Figure 7-14: Droplet temperature of biodiesel with 20% propanol during droplet evaporation at 700°C.....54
Figure 7-15: Droplet diameter of biodiesel with 5% propanol during droplet evaporation at 450°C.....55
Figure 7-16: Droplet photos of biodiesel with 5% propanol during droplet evaporation at 450°C 56
Figure 7-17: Droplet diameter of biodiesel with 20% propanol during droplet evaporation at 450°C.....57
Figure 7-18: Droplet photos of biodiesel with 20% propanol during droplet evaporation at 450°C 58
Figure 7-19: Droplet diameter of biodiesel with 5% propanol during droplet evaporation at 700°C.....59
Figure 7-20: Droplet photos of biodiesel with 5% propanol during droplet evaporation at 700°C 60
Figure 7-21: Stages of bubbling during droplet evaporation.....61
Figure 7-22: Droplet diameter of biodiesel with 20% propanol during droplet evaporation at 700°C.....62
Figure 7-23: Droplet photos of biodiesel with 20% propanol during droplet evaporation at 700°C 63
Figure 7-24: Droplet diameter, with adjusted experimental droplet diameter, of biodiesel with 5% propanol during droplet evaporation at 450°C 64
Figure 7-25: Droplet diameter, with adjusted experimental droplet diameter, of biodiesel with 20% propanol during droplet evaporation at 450°C 65
Figure 7-26: Propanol mol fractions at different radial positions for biodiesel with 5% propanol during droplet evaporation at 450°C, where Z=r/R 66
Figure 7-27: Droplet temperature and boiling temperature at different radial positions for biodiesel with 5% propanol during droplet evaporation at 450°C, where Z=r/R.....67

Figure 7-28: Droplet temperature and boiling temperature at different radial positions for biodiesel with 20% propanol during droplet evaporation at 450°C, where Z=r/R 68
Figure 7-29: Droplet temperature and boiling temperature at different radial positions for biodiesel with 5% propanol during droplet evaporation at 700°C, where Z=r/R 69
Figure 7-30: Droplet temperature and boiling temperature at different radial positions for biodiesel with 20% propanol during droplet evaporation at 700°C, where Z=r/R 70
Figure 7-31: Droplet temperature of biodiesel with 5% pentanol during droplet evaporation at 450°C 72
Figure 7-32: Droplet temperature of biodiesel with 20% pentanol during droplet evaporation at 450°C 73
Figure 7-33: Droplet temperature of biodiesel with 20% pentanol during droplet evaporation at 450°C with varying mixing factor, χ 74
Figure 7-34: Droplet temperature of biodiesel with 20% pentanol during droplet evaporation at 450°C with Varying Mixing Factor, χ, between 0 and 6 seconds 74
Figure 7-35: Droplet temperature of biodiesel with 5% pentanol during droplet evaporation at 700°C 75
Figure 7-36: Droplet temperature of biodiesel with 20% pentanol during droplet evaporation at 700°C 76
Figure 7-37: Droplet temperature of biodiesel with 20% pentanol during droplet evaporation at 700°C with diffusion-limited model using χ=10 77
Figure 7-38: Droplet diameter of biodiesel with 5% pentanol during droplet evaporation at 450°C 78
Figure 7-39: Droplet photos of biodiesel with 5% pentanol during droplet evaporation at 450°C 79
Figure 7-40: Droplet diameter of biodiesel with 20% pentanol during droplet evaporation at 450°C 80
Figure 7-41: Droplet photos of biodiesel with 20% pentanol during droplet evaporation at 450°C 81
Figure 7-42: Droplet diameter of biodiesel with 5% pentanol during droplet evaporation at 700°C 82
Figure 7-43: Droplet photos of biodiesel with 5% pentanol during droplet evaporation at 700°C 83
Figure 7-44: Droplet diameter of biodiesel with 20% pentanol during droplet evaporation at 700°C 84
Figure 7-45: Droplet photos of biodiesel with 20% pentanol during droplet evaporation at 700°C 85
Figure 7-46: Droplet diameter, with adjusted experimental droplet diameter, of biodiesel with 5% pentanol during droplet evaporation at 450°C 86
Figure 7-47: Droplet diameter, with adjusted experimental droplet diameter, of biodiesel with 20% pentanol during droplet evaporation at 450°C 87

Figure 7-48: Droplet temperature and boiling temperature at different radial positions for biodiesel with 5% pentanol during droplet evaporation at 450°C, where Z=r/R 88
Figure 7-49: Droplet temperature and boiling temperature at different radial positions for biodiesel with 20% pentanol during droplet evaporation at 450°C, where Z=r/R 89
Figure 7-50: Droplet temperature and boiling temperature at different radial positions for biodiesel with 5% pentanol during droplet evaporation at 700°C, where Z=r/R 90
Figure 7-51: Droplet temperature and boiling temperature at different radial positions for biodiesel with 20% pentanol during droplet evaporation at 700°C, where Z=r/R 91
Figure B-1: Trial results of droplet diameter of biodiesel during droplet evaporation at 450°C 101
Figure B-2: Trial results of droplet diameter of biodiesel during droplet evaporation at 700°C 101
Figure B-3: Trial results droplet diameter of biodiesel with 5% propanol during droplet evaporation at 450°C.....102
Figure B-4: Trial results droplet diameter of biodiesel with 5% propanol during droplet evaporation at 700°C.....102
Figure B-5: Trial results droplet diameter of biodiesel with 10% propanol during droplet evaporation at 450°C.....103
Figure B-6: Trial results droplet diameter of biodiesel with 10% propanol during droplet evaporation at 700°C.....103
Figure B-7: Trial results droplet diameter of biodiesel with 15% propanol during droplet evaporation at 450°C.....104
Figure B-8: Trial results droplet diameter of biodiesel with 15% propanol during droplet evaporation at 700°C.....104
Figure B-9: Trial results droplet diameter of biodiesel with 20% propanol during droplet evaporation at 450°C.....105
Figure B-10: Trial results droplet diameter of biodiesel with 20% propanol during droplet evaporation at 700°C.....105
Figure B-11: Trial results droplet diameter of biodiesel with 5% pentanol during droplet evaporation at 450°C.....106
Figure B-12: Trial results droplet diameter of biodiesel with 5% pentanol during droplet evaporation at 700°C.....106
Figure B-13: Trial results droplet diameter of biodiesel with 10% pentanol during droplet evaporation at 450°C.....107
Figure B-14: Trial results droplet diameter of biodiesel with 10% pentanol during droplet evaporation at 700°C.....107
Figure B-15: Trial results droplet diameter of biodiesel with 15% pentanol during droplet evaporation at 450°C.....108
Figure B-16: Trial results droplet diameter of biodiesel with 15% pentanol during droplet evaporation at 700°C.....108
Figure B-17: Trial results droplet diameter of biodiesel with 20% pentanol during droplet evaporation at 450°C.....109

Figure B-18: Trial results droplet diameter of biodiesel with 20% pentanol during droplet evaporation at 700°C.....109
Figure C-1: Trial results of droplet temperature of biodiesel during droplet evaporation at 450°C 110
Figure C-2: Trial results of droplet temperature of biodiesel during droplet evaporation at 700°C 110
Figure C-3: Trial results droplet temperature of biodiesel with 5% propanol during droplet evaporation at 450°C.....111
Figure C-4: Trial results droplet temperature of biodiesel with 5% propanol during droplet evaporation at 700°C.....111
Figure C-5: Trial results droplet temperature of biodiesel with 10% propanol during droplet evaporation at 450°C.....112
Figure C-6: Trial results droplet temperature of biodiesel with 10% propanol during droplet evaporation at 700°C.....112
Figure C-7: Trial results droplet temperature of biodiesel with 15% propanol during droplet evaporation at 450°C.....113
Figure C-8: Trial results droplet temperature of biodiesel with 15% propanol during droplet evaporation at 700°C.....113
Figure C-9: Trial results droplet temperature of biodiesel with 20% propanol during droplet evaporation at 450°C.....114
Figure C-10: Trial results droplet temperature of biodiesel with 20% propanol during droplet evaporation at 700°C.....114
Figure C-11: Trial results droplet temperature of biodiesel with 5% pentanol during droplet evaporation at 450°C.....115
Figure C-12: Trial results droplet temperature of biodiesel with 5% pentanol during droplet evaporation at 700°C.....115
Figure C-13: Trial results droplet temperature of biodiesel with 10% pentanol during droplet evaporation at 450°C.....116
Figure C-14: Trial results droplet temperature of biodiesel with 10% pentanol during droplet evaporation at 700°C.....116
Figure C-15: Trial results droplet temperature of biodiesel with 15% pentanol during droplet evaporation at 450°C.....117
Figure C-16: Trial results droplet temperature of biodiesel with 15% pentanol during droplet evaporation at 700°C.....117
Figure C-17: Trial results droplet temperature of biodiesel with 20% pentanol during droplet evaporation at 450°C.....118
Figure C-18: Trial results droplet temperature of biodiesel with 20% pentanol during droplet evaporation at 700°C.....118
Figure D-1: Droplet diameter of biodiesel with 10% propanol during droplet evaporation at 450°C.....119

Figure D-2: Droplet temperature of biodiesel with 10% propanol during droplet evaporation at 450°C.....119
Figure D-3: Droplet diameter of biodiesel with 10% propanol during droplet evaporation at 700°C.....120
Figure D-4: Droplet temperature of biodiesel with 10% propanol during droplet evaporation at 700°C.....120
Figure D-5: Droplet diameter of biodiesel with 15% propanol during droplet evaporation at 450°C.....121
Figure D-6: Droplet temperature of biodiesel with 15% propanol during droplet evaporation at 450°C.....121
Figure D-7: Droplet diameter of biodiesel with 15% propanol during droplet evaporation at 700°C.....122
Figure D-8: Droplet temperature of biodiesel with 15% propanol during droplet evaporation at 700°C.....122
Figure E-1: Droplet diameter of biodiesel with 10% pentanol during droplet evaporation at 450°C.....123
Figure E-2: Droplet temperature of biodiesel with 10% pentanol during droplet evaporation at 450°C.....123
Figure E-3: Droplet diameter of biodiesel with 10% pentanol during droplet evaporation at 700°C.....124
Figure E-4: Droplet temperature of biodiesel with 10% pentanol during droplet evaporation at 700°C.....124
Figure E-5: Droplet diameter of biodiesel with 15% pentanol during droplet evaporation at 450°C.....125
Figure E-6: Droplet temperature of biodiesel with 15% pentanol during droplet evaporation at 450°C.....125
Figure E-7: Droplet diameter of biodiesel with 15% pentanol during droplet evaporation at 700°C.....126
Figure E-8: Droplet temperature of biodiesel with 15% pentanol during droplet evaporation at 450°C.....126

List of Tables

Table 3-1: Film thickness δ for diffusion-limited model at different ambient temperatures T_∞ ...14
Table 3-2: UNIFAC functional group volume and area parameters [46], [47] ...18
Table 3-3: UNIFAC functional group interaction parameters, a_{mn}, in Kelvins [46], [47] ...19
Table 4-1: Composition of biodiesel as two continuous mixtures ...22
Table 4-2: Composition of biodiesel as individual components ...23
Table 5-1: Composition of alcohol mixture as a continuous mixture ...25
Table 5-2: Composition of alcohol mixture as individual components ...25
Table 5-3: Number of each functional group k in each alcohol component i, $N_k^{(i)}$ ...26
Table 5-4: Different methods to approximate the number of each functional group k in alcohol mixture i, $N_k^{(i)}$ ...26
Table 5-5: Number of each functional group k in each fame component i, $N_k^{(i)}$ ...28
Table 5-6: Different methods to approximate the number of each functional group k in FAME mixture i, $N_k^{(i)}$ ...28
Table 5-7: Number of functional groups present in FAME with a carbon chain length of 17 carbons with varying number of double bonds ...29
Table A-1: Parameter values used in property correlations ...100

Nomenclature

a: functional group interaction parameter (K)

a_b, b_b: boiling temperature parameters

a_C, a_0, a_1, a_2, a_3, b_C, b_0, b_1, b_2, b_3: vapour specific heat parameters

a_D, b_D, ϕ_H, b_Φ: diffusivity parameters

a_H, b_H, ϕ_H: constants in h_{fg} configuration

a_K, b_K, a_{KC}, a_{KT}, b_{KC}, b_{KT}: thermal conductivity parameters

a_L, b_L, c_L: liquid specific heat parameters

a_p, b_p: critical pressure parameters

a_T, b_T: critical temperature parameters

a_v, b_v, α_P: specific volume parameters

A_w: functional group van der Waals surface area

B: mass transfer number

B_T: thermal transfer number

c: molar density (kmol/m^3)

Cp: specific heat (kJ/kmol·K)

d: droplet diameter (m)

$\overline{D}, \widetilde{D}, \widehat{D}$: average diffusivity ($m^2$/s)

e: interaction energy between molecules (K)

E: interaction energy between functional groups (K)

f(I): gamma distribution function

G: molar flux (kmol/m^2s)

Gr: Grashof number based on droplet diameter

h_{fg}: enthalpy of vaporization (kJ/kmol·K)

h_0: heat transfer coefficient (W/m^2s)

I: distribution variable (= species molecular weight (g/mol))

l: molecular van der Waals parameter

Nu_0: Nusselt number at 0 mass transfer rate

P: vapour pressure of component in a mixture (kPa)

P_{vp}: vapour pressure of individual component (kPa)

Pr: Prandtl number

q: heat flux (W/m^2)

r: radial component (m)

R: droplet radius (m)

$\bar{R}$: universal gas constant (8.314 kJ/kmol·K)

Sh_0: Sherwood number at 0 mass transfer rate

T: temperature (K)

u: molecular van der Waals surface area

U: functional group surface area parameter

v*: molar average velocity (m/s)

V: volume of droplet

V_w: functional group van der Waals volume

w: molecular van der Waals volume

W: functional group volume parameter

x: liquid mol fraction

X: functional group mol fraction

y: vapour mol fraction

z: coordination number

Z: ratio of radial position over droplet radius (=r/R)

α, β, γ: distribution parameters

Γ(x): gamma function

δ: film thickness (m)

Z_N: ratio between film thickness and droplet radius

θ: mean of distribution (= mean molecular weight (g/mol))

Θ: surface area fraction

λ: thermal conductivity (W/m·K)

ν: specific volume

N: number of functional groups

Π: functional group residual activity coefficient

σ: standard deviation of distribution (=standard deviation molecular weight (g/mol))

τ: temperature dependent molecular interaction parameter

φ: segment fraction

Φ: $=y_F\theta$ or $y_F\Psi$ in Equation (*17*

χ: mixing factor (= D_{Leff}/D_L)

Ψ: distribution second central moment ($=\theta^2+ \sigma^2$)

ω: activity coefficient

Ω: temperature dependent functional group interaction parameter

Subscripts:

B: boiling

cr: critical

eff: effective, including effects of internal flow

EQ: equivalent (diameter)

F: fuel

i, l: individual species index

j: distribution function index

k, m, n: functional group index

L: liquid

MAJ: major diameter of prolate spheroid

MIN: minor diameter of prolate spheroid

net: heat flux to droplet from vapour phase

R: at droplet surface

RAD: radiation

∞: ambient conditions

Subscripts:

C: combinational term

R: residual term

Abbreviations:

FAME: Fatty Acid Methyl Esters

MGC: Monoglycerides

PENT5: Biodiesel with 5% (v/v) pentanol

PENT20: Biodiesel with 20% (v/v) pentanol

PROP5: Biodiesel with 5% (v/v) propanol

PROP20: Biodiesel with 20% (v/v) propanol

VLE: Vapour Liquid Equilibrium

1 Introduction

Due to the rising CO_2 emissions, interest in bio-based renewable fuels has increased over the years. One of the bio-based fuels that are of interest is biodiesel, a replacement of traditional diesel that can be made of plant oils. Interest in biodiesel has grown given that biodiesel has lower net greenhouse emissions than traditional diesel. The use and production of biodiesel has grown over the years. Additionally, alcohol, which is also a bio-based renewable fuel, is of interest as a fuel additive. Alcohol blended into diesel fuels has been shown to decrease engine emissions of diesel engines with no decrease in diesel engine performance.

Liquid fuel is typically sprayed into combustors or engine cylinders as a spray of droplets, in which individual droplets evaporate into vapour and this vapour then burns at the edge of a droplet cloud. As discussed in the next chapter, droplet evaporation experiments have been performed on alcohol-biodiesel blends, but this evaporation process has yet to be numerically modelled. The droplet evaporation process of other multi-component liquid fuels, such as biodiesel, has been numerically modelled using continuous thermodynamics.

The goal of this work is to perform droplet evaporation experiments on propanol-biodiesel and pentanol-biodiesel blends, and then numerically model this evaporation process. The evaporation process, specifically the vapour-liquid equilibria, of alcohol-biodiesel blends are further studied by comparing vapour-liquid equilibria calculations with experimental data. The numerical models will use two methods to determine the vapour pressure of components in a mixture: the first method is Raoult's Law, and the second method is Raoult's Law modified with activity coefficients calculated by the UNIFAC method. Droplet evaporation experiments were performed in this work at ambient temperatures of 450°C and 700°C with 2μL droplets of propanol-biodiesel blends and pentanol-blends, and the droplet's diameters and temperatures were measured throughout the evaporation process. The droplet evaporation experimental data are then compared to calculated droplet diameters and droplet temperatures produced by a well-mixed continuous thermodynamic droplet model and a diffusion-limited continuous thermodynamics droplet model. The goal of this work is to identify the best model to represent the droplet evaporation of alcohol-biodiesel blends.

2 Literature Review

2.1 Alcohol-Biodiesel Blends

Biodiesel use has become more prevalent given that biodiesel can be used as a potential substitute for traditional diesel in order to reduce greenhouse gas emissions. Biodiesel is an ideal replacement for diesel produced from fossil fuels, given that the carbon fixation during the growing phase of the plants used to produce biodiesel can offset the carbon emissions during biodiesel combustion. Additionally, replacing diesel with biodiesel has shown an average net reduction of 54% in greenhouse gas emissions [1]. Global biodiesel production has increased significantly from 300 thousand barrels per day in 2010 to 716 thousand barrels per day in 2020 [2], and global biodiesel consumption has increased from 294 thousand barrels per day in 2010 to 682 thousand barrels per day in 2020 [2]. The United States' biodiesel production has increased from 204 thousand barrels in 2001 to 43,036 thousand barrels in 2020 [3], and US biodiesel consumption has increased from 244 thousand barrels in 2001 to 44,375 thousand barrels in 2020 [3]. Governments have also given incentives to use alcohol with diesel fuel as a way to reduce greenhouse gas emissions, given that alcohols blended into diesel fuels have shown a reduction of diesel engine emissions with no effect on diesel engine performance [4]. The government of Ontario currently has a regulation that requires 10% of gasoline and 4% of diesel fuel by volume to be bio-based [5].

The process of producing biodiesel is known as transesterification [6], [7]. The transesterification process takes a plant oil (or other oils or fats), which is composed of triacylglycerols, and reacts it with a monohydric alcohol to produce a mono-alkyl ester and a glycerol. The most common oils used as a feedstock for biodiesel production are plant oils such as canola, palm, soybean, and coconut [7]. Most plant oils are composed of five common fatty acids, which are palmitic (hexadecanoic), stearic (octadecanoic), oleic (9(Z)-octadecenoic), linoleic (9(Z),12(Z)-octadecadienoic), and linolenic (9(Z),12(Z),15(Z)-octadecatrienoic) fatty acids [7]. Typically, a less expensive common alcohol, such as methanol, is used in the production of biodiesel [7]. The choice to use methanol during the transesterification process produces fatty acid methyl esters (FAME) [7]. During the production of biodiesel, not all of the triacylglycerols convert to FAME, meaning that there are typically mono-, di-, and tri-glycerides left over in the biodiesel [8]. However, biodiesel composition measurements have shown that monoglycerides

(MGC) represent 0.5% by mass compared to less than 0.1% by mass for di- and tri-glycerides, making the di- and tri-glyceride composition negligible in the analysis of biodiesel [9], [10].

Adding ethanol to biodiesel has been able to improve biodiesel fuel properties at cold temperatures, such as improving the cloud point (CP), pour point (PP), and cold filter plugging point (CFPP) [11]. Experimental work on diesel engines fueled with 80% biodiesel and 20% ethanol has found that this fuel blend was able to produce similar engine power and average brake specific fuel consumption as diesel fuel while seeing a reduction in CO and soot emissions [12]. Biodiesel mixed with butanol has been shown to have lower smoke, hydrocarbon, and CO emissions than diesel [13]. Another experimental study has shown that a diesel engine fueled with biodiesel-butanol blends has given lower exhaust gas temperatures than with diesel fuels [14]. Engines fueled with biodiesel-methanol blends and biodiesel-ethanol blends have been shown to have lower NO emissions than engines fueled with diesel [15], [16].

Combustion experiments on 220-250 μm droplets made of diesel-ethanol and biodiesel-ethanol blends have shown that the droplet burns in three stages, which include a first stage in which the more volatile component burns, a second stage where burning transitions from the more volatile component to the least volatile component, and a third stage of constant burning with co-gasification of remaining components in the droplet [17]. This experimental work has also shown liquid-phase diffusional resistance trapping the ethanol in the center of the droplet causing internal gasification and rupturing of the droplet [17]. Another experimental study with 500 μm droplets made of methanol-biodiesel, ethanol-biodiesel, and propanol-biodiesel blends has shown that microexplosions of the droplet occur due to the low boiling point of the alcohol, making it easy for the superheat of the liquid alcohol to be reached [18]. Experimental results for droplet combustion of butanol-pentanol-biodiesel blends show “puffing” events in which internal boiling occurs while the droplet remains intact and a microexplosion occurs when internal boiling is strong enough within the droplet to rip the droplet apart [19]. The experimental results have shown that puffing and microexplosions occur for all butanol-pentanol blends, but a blend with equi-volumes of biodiesel-pentanol-butanol was able to produce the most significant puffing and microexplosion events [19]. Microexplosions have also occurred for 0.61-1.00 mm biodiesel-butanol droplets in which droplets with initially equi-volume concentrations of butanol and biodiesel have shown the most frequent and most intensive microexplosions [20].

Typically, liquid fuel is sprayed as a cloud of small droplets into an engine cylinder or a combustor, in which the individual droplets will evaporate into a gaseous vapour and the vapour will combust at the edge of the droplet cloud [8], [21]. Therefore, the fundamentals of the evaporation process of single droplets of alcohol-biodiesel blends should be studied. Gasoline-ethanol and rapeseed methyl ester droplet evaporation have been investigated using a numerical model that used Raoult's law to determine the vaporization of individual species and included convection/diffusion of individual species within the droplet [22]. Biodiesel droplet evaporation has been experimentally studied and numerically modelled using continuous thermodynamics and assuming a well-mixed droplet [8]. Unfortunately, modelling of biodiesel-alcohol blends has yet to be accomplished, hence the motivation of this work.

Individual FAME compounds mixed with ethanol, specifically methyl laurate, methyl myristate, and methyl oleate, have had experimental vapour liquid equilibrium results taken at a pressure of 1 atm [23]. Experimental vapour liquid equilibria measurements have also been taken for biodiesel – ethanol systems at pressures of 100 kPa [24], 91.4 kPa [25], and 101.32 kPa [26]. The vapour liquid equilibrium has also successfully been numerically modelled for biodiesel and ethanol system using the UNIFAC method and the NRTL method [26].

2.2 Droplet Evaporation Model

2.2.1 Continuous Thermodynamics Model

The models used in this work are based on the theory of continuous thermodynamics, which treats a mixture of two or more discrete components as a continuous distribution function. Continuous thermodynamics allows multi-component mixtures to be represented by one or more continuous distribution function, such that the number of calculations is reduced during computations [27], [28]. Another advantage of continuous thermodynamics is that the fuel model can be determined from distillation data with general knowledge of the chemistry present in the fuel. This removes the need to know the detailed chemical analysis of the fuel and allows the model to be easily used on different fuels. The model used in this work represents this continuous distribution function as a gamma distribution function shown in Equation 1, where I is a property of the molecules within the distribution, such as molecular weight or boiling point, and $f_{Lj}(I)$ represents the gamma distribution function for a particular continuous fraction j of the mixture [27], [28]. In this work I will represent the molecular weight of a component.

$$f_{Lj}(I) = \frac{\left(I - \gamma_j\right)^{\alpha_{Lj}-1}}{\beta_{Lj}^{\alpha_{Lj}}\Gamma\left(\alpha_{Lj}\right)} exp\left(-\left(I - \gamma_j\right)/\beta_{Lj}\right) \quad (1)$$

The values α_{Lj} and β_{Lj} are related to the mean molecular weight, θ_{Lj}, and the standard deviation molecular weight, σ_{Lj}, of a mixture j, shown in Equations 2 and 3.

$$\theta_{Lj} = \alpha_{Lj}\beta_{Lj} + \gamma_j \quad (2)$$

$$\sigma_{Lj}^2 = \alpha_{Lj}\beta_{Lj}^2 \quad (3)$$

The mean and the standard deviation of a continuous distribution can be determined by fitting a numerical simulation of a distillation test with experimental distillation test results. In this work the distribution origin γ_j is assumed to be zero. A pure component, such as the alcohols used in this study, can be modelled with a very narrow distribution function, using σ = 1 or 2 kg/kmol. Previous work has been able to represent biodiesel as a combination of three continuous mixtures: a light FAME continuous mixture, a FAME continuous mixture, and a MGC continuous mixture [8].

2.2.2 Liquid Transport Processes

There are two types of models that can represent the liquid state of the droplet: a well-mixed model and a diffusion-limited model. The well-mixed model is the simplest model and assumes that the droplet has a constant concentration of components throughout, so that the droplet evaporation process occurs as a batch distillation process [29], [30]. The diffusion-limited model allows for a non-uniform liquid concentration which varies radially throughout the droplet and includes diffusion processes within the liquid droplet, making it a more complex model compared to the well-mixed model [31], [32], [33]. The diffusion-limited model is of interest in this work given that previous droplet evaporation experiments of alcohol-biodiesel droplets have shown that the alcohol component can be concentrated in the center of the droplet longer in the droplet's lifetime, such that internal boiling of the alcohol component occurs [17], [18], [19], [20]. This is because the alcohol components which are initially present at the center of the droplet during the start of the droplet evaporation depend on diffusion processes to reach the surface of the droplet to evaporate. Droplets have shown that some internal mixing still does occur due to an internal flow caused by shear of the liquid surface during atomization of droplets and/or by natural or

forced convection. This internal circulation has most often been represented as a Hill's vortex [34], [35]. This internal circulation can be represented in modelling using an enhanced radial diffusivity coefficient [36], [37]. Both models assume constant temperature throughout the droplet, given that liquid thermal diffusivities are quite large when compared to mass diffusivities, so that any change to the surface temperature is assumed to result in a corresponding change nearly instantaneously in the droplet internal liquid temperature.

2.3 Vapour-Liquid Equilibria

2.3.1 Raoult's Law

Previous work on droplet evaporation assumed ideal mixture behaviour during vapour liquid equilibrium calculations [8], [27], [28], [38]. Previous droplet evaporation models used the Clausius-Clapeyron equation to calculate the vapour pressure of individual components and Raoult's law, shown in Equation 4, to determine the vapour pressure of a component in a mixture:

$$P_i = x_i P_{vpi} \tag{4}$$

2.3.2 UNIFAC Method

Given that alcohols are polar and the FAME components in the biodiesel are slightly polar, Raoult's law alone can not be used to determine the vapour pressure of a component in a mixture. Therefore, Raoult's law must be modified to use activity coefficients to correct for the non-ideal behaviour, as shown in Equation 5.

$$P_i = \omega_i x_i P_{vpi} \tag{5}$$

where ω_i is the activity coefficient of component i in the mixture.

Previous work by Hallett and Beauchamp-Kiss has developed a continuous thermodynamic model using activity coefficients calculated from Wilson's equation for ethanol-fuel oil mixtures [39]. In this work the UNIFAC method will be used instead of Wilson's equation because Wilson's equation requires experimental data for the vapour liquid equilibrium between each individual FAME component in biodiesel and each individual alcohol in order to develop the coefficients, and unfortunately these experimental data are unavailable. The UNIFAC method works for this purpose, given that activity coefficients of a pure component i are calculated using functional

groups found in pure component i and the interactions between functional groups of pure component i with functional groups in other components in the mixture.

The activity coefficients calculated using the UNIFAC method have successfully been used to determine the surface tensions of 78 different biodiesel blends with an average absolute relative deviation of 1.86% [40]. The UNIFAC method has been successfully used to model the vapour liquid equilibrium behaviour of a biodiesel-ethanol system [26]. The UNIFAC method was also able to calculate the liquid-liquid equilibria of biodiesel-glycerol-methanol and biodiesel-glycerol-ethanol systems with a root mean square deviation of 6.2% and 8.8% respectively [41].

2.4 Summary of Literature Review

Review of literature has shown that droplet evaporation experiments have been performed on alcohol-biodiesel blends, but droplet evaporation modelling has yet to be performed. These experiments do report some internal boiling within the droplet during evaporation, in which the cause of internal boiling deserves more attention. Droplet evaporation experiments performed with other fuel mixtures have shown that the liquid state of the droplet depends on mainly liquid diffusion processes with some internal mixing. The vapour-liquid equilibrium of alcohol-biodiesel blends have shown non-ideal behaviour that can't be represented by Raoult's law but can be represented using the UNIFAC method. Therefore, the goal of this work should be to investigate droplet evaporation of alcohol-biodiesel blends by performing droplet evaporation experiments on propanol-biodiesel and pentanol-biodiesel blends and comparing these experimental results to numerical models to determine a suitable model to represent droplet evaporation of alcohol-biodiesel blends. Numerical models should implement a correct method to represent the non-ideal behaviour of alcohol-biodiesel blends by comparing VLE numerical models that use either Raoult's law or modified Raoult's law with activity coefficients calculated using UNIFAC method. Additionally, numerical modelling should compare different methods to model liquid transport processes to determine if liquid diffusion processes is the cause for internal boiling in alcohol-biodiesel droplets.

3 Model Development

This work will look into modelling the droplet evaporation process of alcohol-biodiesel droplets. The two models that will be used in this work will apply continuous thermodynamics while representing the liquid phase of the droplet as either well-mixed or diffusion-limited. All models assume spherical symmetry, so that the problem is one-dimensional in the radial direction.

The fundamental governing equations for the vapour phase during droplet evaporation are shown in the Equations 6 to 8 below [27]. These equations give a full transient description of the vapour phase, where y_{Fj} is the vapour mol fraction of continuous mixture j, c is the molar density, v* is the molar average velocity, θ_j is the mean molecular weight for vapour continuous mixture j, and $\Psi_j = \theta_j^2 + \sigma_j^2$:

$$\frac{\partial}{\partial t}\left(cy_{Fj}\right) + \nabla \cdot \left(cv^* y_{Fj}\right) = \nabla \cdot \left(c\bar{D}_j \nabla y_{Fj}\right) \tag{6}$$

$$\frac{\partial}{\partial t}\left(cy_{Fj}\theta_j\right) + \nabla \cdot \left(cv^* y_{Fj}\theta_j\right) = \nabla \cdot \left(c\widetilde{D}_j \nabla\left(y_{Fj}\theta_j\right)\right) \tag{7}$$

$$\frac{\partial}{\partial t}\left(cy_{Fj}\Psi_j\right) + \nabla \cdot \left(cv^* y_{Fj}\Psi_j\right) = \nabla \cdot \left(c\widehat{D}_j \nabla\left(y_{Fj}\Psi_j\right)\right) \tag{8}$$

These equations describe the transport of the vapour y_{Fj} of the fuel fraction j and of the mean θ_j and standard deviation σ_j of the distribution function j. A full derivation is given by Tamim and Hallett [27].

Equation 9 shows the energy transport equation for the vapour phase; the interdiffusion term is written so as to accommodate multiple distributions [38]. This energy equation includes the thermal conductivity λ, the specific heat of air C_{PA}, and the vapour phase specific heat parameters a_C, and b_C.

$$\bar{C}_P \frac{\partial}{\partial t}(cT) + \bar{C}_P \nabla \cdot (cv^* T) = \nabla \cdot \lambda \nabla T + \sum_{j=1}^{J} \left\{\left[\left(a_{Cj} - C_{PA}\right)c\bar{D}_j + b_{Cj}\theta_j c\widetilde{D}_j\right]\nabla y_{Fj}\right\} \cdot \nabla T \tag{9}$$

The average gas phase diffusivities of continuous mixture j shown in the above equations are calculated using Equations 10 to 12. $D_j(I)$ is the diffusivity of an individual species I in the continuous mixture fraction j as a function of I in the gas phase. Each fuel fraction j has its own gas phase diffusivity.

$$\bar{D}_j = \int_0^\infty D_j(I) f_j(I) dI \tag{10}$$

$$\widetilde{D}_j \theta_j = \int_0^\infty D_j(I) f_j(I) I dI \tag{11}$$

$$\widehat{D}_j \Psi_j = \int_0^\infty D_j(I) f_j(I) I^2 dI \tag{12}$$

3.1 Well-Mixed Continuous Thermodynamics Model

A previously developed well-mixed continuous thermodynamic model will be used in this work [27], [28], and the calculations done within the model will be explained in this section. A well-mixed model assumes that the droplet's mixture concentration and temperature is the same throughout the droplet due to continuous mixing that occurs within the droplet, and that any changes to the surface of the droplet due to evaporation of components will be instantly reflected in the droplet's mixture concentration and temperature. The model also includes the quasi-steady state vapour assumption, in which the vapour field changes instantaneously with changes in droplet temperature and droplet radius, which this is justified by the fact that the liquid phase changes at a slower rate than the vapour phase processes [21], [28].

The vapour phase equations shown in Equations 6 to 9 are solved analytically for the well-mixed model to get expressions for the rate of evaporation that are similar to classical droplet theory, shown in Equation 13. The evaporation rate, or evaporating mol flux G, depends on either the mass transfer number B calculated in Equation 14 or the thermal transfer number B_T calculated in Equation 15. The vapour mol fraction of the evaporated fuel can be calculated at different radially positions using Equation 16.

$$G = \frac{c\bar{D}}{R}\ln(1+B) = \frac{\lambda}{C_{PF}R}\ln(1+B_T) \tag{13}$$

$$B = \frac{y_{FR} - y_{F\infty}}{1 - y_{FR}} \tag{14}$$

$$B_T = \frac{C_{PF}(T_\infty - T_R)}{h_{fg} + q_L/G} \tag{15}$$

$$y_F(r) = 1 - (1 - y_{F\infty})(1 + B)^{-1/Z} \tag{16}$$

where Z=r/R. Additionally, the solution gives the distribution mean θ and the distribution second central moment Ψ as functions of radial position in Equation 17, in which Φ stands for either $y_F\theta$ or $y_F\Psi$ in the equation below.

$$\Phi(r) = \Phi_R - \frac{1}{B}(\Phi_R - \Phi_\infty) \cdot \left[(1 + B)(1 + B)^{-1/Z} - 1\right] \tag{17}$$

The model also incorporates the following equations to represent the changes to the droplet during evaporation which are based on mol balances on individual components and then integrated over the distribution [28]. The total molar flux, G, can be calculated using Equation 18, where the vapour mol fraction is determined using one of the two methods to represent vapour-liquid equilibria in this work. The changes to the liquid phase continuous mixture parameters, θ_{Lj} and Ψ_{Lj}, are determined using Equations 19 and 20 where $\Psi_{Lj} = \theta_{Lj}^2 + \sigma_{Lj}^2$ and c_L is the molar density of the liquid phase.

$$G\left(1 - \sum_{j=1}^{J} y_{Fj}\right) = \sum_{j=1}^{J} -c\bar{D}_j \frac{\partial y_{Fj}}{\partial r}\bigg|_R \tag{18}$$

$$\frac{d\theta_{Lj}}{dt} = \frac{3}{c_L R}\left[G\left(\theta_{Lj} - \theta_j y_{Fj}\right) + c\widetilde{D}_j \frac{\partial}{\partial r}\left(\theta_j y_{Fj}\right)\right]_R \tag{19}$$

$$\frac{d\Psi_{Lj}}{dt} = \frac{3}{c_L R}\left[G\left(\Psi_{Lj} - \Psi_j y_{Fj}\right) + c\widehat{D}_j \frac{\partial}{\partial r}\left(\Psi_j y_{Fj}\right)\right]_R \tag{20}$$

The recession rate of the droplet, as in the change in droplet radius R, is shown in Equation 21 and the change in droplet temperature, T_L, is shown in Equation 22. The terms q is the heat transfer to the droplet surface by conduction, q_{RAD} is the heat transfer to the droplet surface by radiation, and C_{PL} is the specific heat of the liquid phase.

$$\frac{dR}{dt} = -\frac{1}{c_L}\left(G + \frac{R}{3}\frac{dc_L}{dt}\right) \tag{21}$$

$$\frac{dT_L}{dt} = \frac{3}{c_L C_{PL} R}\left[q + q_{RAD} - Gh_{fg}\right] \quad (22)$$

The quasi-steady state model used within the well-mixed model does incorporates natural convection. It does this by multiplying Equations 13 and 22 with $Nu_0/2$ such that they become the Equations 23 and 24 below. Equations 16 and 17 remain unchanged but the calculation for Z then becomes Equation 25 below. Additionally, Nu_0 is calculated using a standard heat transfer correlation which uses the Prandtl number and the Grashof number as shown in Equation 26.

$$G = Nu_0 \frac{\lambda}{2C_{PF}R} \ln(1 + B_T) \quad (23)$$

$$\frac{dT_L}{dt} = \frac{Nu_0}{2}\frac{3}{c_L C_{PL} R}\left[q + q_{RAD} - Gh_{fg}\right] \quad (24)$$

$$Z = \frac{1}{1 + (Sh_0/2)[(R/r) - 1]} \quad (25)$$

$$Nu_0 = 2 + 0.43(GrPr)^{1/4} \quad (26)$$

3.2 Diffusion-Limited Continuous Thermodynamics Model

A previously developed diffusion-limited continuous thermodynamic model will also be used in this work [28], [38], and the calculations used within the model will be explained within this section. The diffusion-limited model assumes that the droplet's temperature is constant throughout the droplet but that the concentration of the components in the mixture changes along the radius depending on the diffusion process and some degree of internal mixing within the droplet. The diffusion-limited model uses a full transient numerical solution of Equations 6 to 9 for the vapour phase [28]. The diffusion-limited model assumes that diffusion in the radial direction is the only mixing mechanism in the liquid phase of the droplet. To take into account the small amount of internal mixing that still occurs in real-life droplet evaporation processes, an enhanced value of radial diffusivity will need to be used which is calculated from the diffusivity of a liquid component and a mixing factor χ as shown in Equation 27. Previous work suggests that the mixing factor of a droplet sits within the range of 2-4 [36], [42], [43]. In this work, a value of 3 will be used for the mixing factor.

$$\chi = D_{Leff}/D_L \quad (27)$$

The diffusion-limited continuous thermodynamics model solves for the composition of liquid components radially throughout the droplet. Therefore, the model uses the liquid phase transport process equations derived by Abdel-Qader and Hallett shown in Equations 28 to 30 [38].

$$\frac{\partial}{\partial t}\left(c_L x_{Fj}\right) + \nabla \cdot \left(c_L v^* x_{Fj}\right) = \nabla \cdot \left(c_L \chi \overline{D}_{Lj} \nabla x_{Fj}\right) \tag{28}$$

$$\frac{\partial}{\partial t}\left(c_L x_{Fj} \theta_{Lj}\right) + \nabla \cdot \left(c_L v^* x_{Fj} \theta_{Lj}\right) = \nabla \cdot \left(c_L \chi \widetilde{D}_{Lj} \nabla\left(x_{Fj} \theta_{Lj}\right)\right) \tag{29}$$

$$\frac{\partial}{\partial t}\left(c_L x_{Fj} \Psi_{Lj}\right) + \nabla \cdot \left(c_L v^* x_{Fj} \Psi_{Lj}\right) = \nabla \cdot \left(c_L \chi \widehat{D}_{Lj} \nabla\left(x_{Fj} \Psi_{Lj}\right)\right) \tag{30}$$

The diffusion limited model needs to incorporate new equations to represent the molar flux at the droplet surface with liquid diffusion, as shown in Equation 31, where x_{Fj} is the mol fraction of the continuous mixture j in the liquid phase and the subscript R refers to the properties at the droplet's surface. Additionally, liquid diffusion is also considered in new flux relation equations for the continuous mixture parameters, as shown in Equations 32 and 33.

$$G x_{FjR} - c_L \chi \overline{D}_{Lj} \left.\frac{\partial x_{Fj}}{\partial r}\right|_R = G y_{FjR} - c \overline{D}_j \left.\frac{\partial y_{Fj}}{\partial r}\right|_R \tag{31}$$

$$G x_{FjR} \theta_{LjR} - c_L \chi \widetilde{D}_{Lj} \left.\frac{\partial\left(x_{Fj} \theta_{Lj}\right)}{\partial r}\right|_R = G y_{FjR} \theta_{jR} - c \widetilde{D}_j \left.\frac{\partial\left(y_{Fj} \theta_j\right)}{\partial r}\right|_R \tag{32}$$

$$G x_{FjR} \Psi_{LjR} - c_L \chi \widehat{D}_{Lj} \left.\frac{\partial\left(x_{Fj} \Psi_{Lj}\right)}{\partial r}\right|_R = G y_{FjR} \Psi_{jR} - c \widehat{D}_j \left.\frac{\partial\left(y_{Fj} \Psi_j\right)}{\partial r}\right|_R \tag{33}$$

The diffusion-limited model was solved numerically using finite volume methods. In this work a time step of 0.005 s with 40 grid points in the liquid phase and 40 grid points in the vapour phase was used. The diffusion-limited model can handle only two separate component fractions in the droplet. The inputs used will be the alcohol component, and the FAME continuous mixture, which will represent all of the biodiesel components within the droplet.

The average liquid phase diffusivities of continuous mixture j shown in the above equations are calculated using Equations 34 to 36. Like the gas phase, $D_{Lj}(I)$ is the diffusivity of an individual species I in the continuous mixture fraction j as a function of I in the liquid phase. However, to preserve mol conservation, the liquid diffusivity must be the same for both fuel fractions, so that the diffusivity of the more volatile component is used to represent the liquid phase [38].

$$\bar{D}_{Lj} = \int_0^\infty D_{Lj}(I) f_{Lj}(I) dI \tag{34}$$

$$\widetilde{D}_{Lj}\theta_{Lj} = \int_0^\infty D_{Lj}(I) f_{Lj}(I) I dI \tag{35}$$

$$\widehat{D}_{Lj}\Psi_{Lj} = \int_0^\infty D_{Lj}(I) f_{Lj}(I) I^2 dI \tag{36}$$

However, this model currently does not consider gas phase convective heat transfer to the droplet. To model the effect of convection a relation will be developed by using film theory [44]. Film theory assumes that heat and mass transfer occur within a boundary layer or "film" of thickness δ that surrounds the droplet, and within this film the temperature changes from T_R to T_∞. The equation for heat transfer for an evaporating droplet then becomes Equation 37 given the boundary condition is that the temperature at a radius of R+δ is equal to T_∞.

$$q = \lambda \left[\frac{1}{\delta} + \frac{1}{R}\right] \frac{\ln(1 + B_T)}{B_T} (T_\infty - T_R) \tag{37}$$

The equation of heat transfer can also be thought as Equation 38 in which the heat transfer is the product of the heat transfer coefficient and the difference in temperature. Using the definition of Nusselt number in Equation 39, the equation of heat transfer then becomes Equation 40.

$$q = h_0 (T_\infty - T_R) \tag{38}$$

$$Nu_0 = \frac{h_0 d}{\lambda} \tag{39}$$

$$q = Nu_0 \frac{\lambda}{2R} (T_\infty - T_R) \tag{40}$$

Relating Equations 37 and 40 together, a relation can be developed, which is shown in Equation 41. Values of R and Nusselt number calculated in the well-mixed continuous thermodynamics model were used to determine an approximate film thickness to be used in the diffusion-limited model. Nusselt number was calculated using a correlation for natural convection, shown in Equation 42, within the well-mixed continuous thermodynamic model [28].

$$\frac{1}{\delta} = \frac{1}{R}\left(\frac{Nu_0}{2} - 1\right) \tag{41}$$

$$Nu_0 = 2 + 0.43(GrPr)^{1/4} \quad (42)$$

The diffusion-limited model uses a ratio of film thickness over droplet radius as an input, known as Z_N, which is used to set the coordinate of the outer boundary of the vapour phase calculation grid. The average of the calculated values of Z_N for the different ambient temperatures using the Nusselt numbers from the well-mixed model are shown in Table 3-1 below.

Table 3-1: Film thickness δ for diffusion-limited model at different ambient temperatures T_∞

Ambient Temperature, T_∞ (°C)	450	700
Ratio of Film Thickness and Droplet Radius, Z_N	3.6	2.2

3.3 Physical Property Correlations

The continuous thermodynamic models determine the mixture properties of the liquid phase and the vapour phase by integrating property correlations of an individual component, such as FAME, MGC, or an alcohol, with the gamma distribution function. The property correlations are linear or other simple functions of molecular weight and temperature. This section will cover the physical property correlations used in this work. They were developed in earlier work by estimating the properties for each fraction (e.g. alcohols, FAMEs) as a function of molecular mass and then fitting the correlating equations to these values [8], [39], [45].

Equation 43 shows how the critical pressure is calculated using the molecular weight I and the parameters a_p and b_p.

$$P_{cr} = a_p + b_p \cdot I \quad (43)$$

The critical temperature is calculated using the molecular weight I and the parameters a_T and b_T as shown in Equation 44.

$$T_{cr} = a_T + b_T \cdot I \quad (44)$$

The boiling temperature is calculated using the molecular weight I and the parameters a_b and b_b as shown in Equation 45. Since the boiling temperature is not exactly a linear function of

molecular mass for most compounds, the coefficients a_b and b_b must be fitted to best represent the range of species in the mixture.

$$T_B = a_b + b_b \cdot I \tag{45}$$

The mixture enthalpy of vaporization, h_{fg}, which is the average of the component's enthalpy of vaporization weighted by their mol fluxes, is determined using Equation 46 where a_{Hj}, b_{Hj}, and Φ_{Hj} are parameters specific to species j enthalpy of vaporization. The mixture enthalpy of vaporization calculation incorporates multiple distributions, which was derived by Abdel-Qader and Hallett [38].

$$h_{fg} = \sum_{j=1}^{J} \Phi_{Hj} \left\{ a_{Hj} \left[y_{Fj} - \frac{c\bar{D}_j}{N} \frac{\partial y_{Fj}}{\partial r} \right]_R + b_{Hj} \left[y_{Fj}\theta_j - \frac{c\widetilde{D}_j}{N} \frac{\partial \left(y_{Fj}\theta_j \right)}{\partial r} \right]_R \right\} \tag{46}$$

$$\Phi_H = \left[\frac{(T_{cr} - T)}{(T_{cr} - T_B)} \right]^{0.38} \tag{47}$$

The diffusivity can be calculated using the molecular weight I and the parameters a_D, b_D, and Φ_D using Equation 48. The parameter Φ_D is determined using the temperature and the parameter b_Φ as shown in Equation 49.

$$D_i = (a_D + b_D I)\Phi_D \tag{48}$$

$$\Phi_D = \frac{T^{5/2}}{(b_\Phi + T)} \tag{49}$$

The thermal conductivity is calculated using molecular weight I and the parameters a_K and b_K as shown in Equation 50. The parameters a_K and b_K is determine using the temperature and the parameters a_{KC}, a_{KT}, b_{KC}, and b_{KT} as shown in Equations 51 and 52.

$$\lambda = a_K(T) + b_K(T) \cdot I \tag{50}$$

$$a_K(T) = a_{KC} + a_{KT}T \tag{51}$$

$$b_K(T) = b_{KC} + b_{KT}T \tag{52}$$

The liquid specific heat is calculated using molecular weight I, temperature T, and the parameters a_L, b_L, and c_L as shown in Equation 53.

$$C_{PL} = (a_L + b_L T + c_L T^2) I \tag{53}$$

The vapour specific heat is calculated using molecular weight I and the parameters a_C and b_C as shown in Equation 54. The parameters a_C and b_C is determine using the temperature and the parameters a_0, a_1, a_2, a_3, b_0, b_1, b_2, and b_3 as shown in Equations 55 and 56.

$$C_P = a_C + b_C \cdot I \tag{54}$$

$$a_C = a_0 + a_1 \cdot T + a_2 \cdot T^2 + a_3 \cdot T^3 \tag{55}$$

$$b_C = b_0 + b_1 \cdot T + b_2 \cdot T^2 + b_3 \cdot T^3 \tag{56}$$

The specific volume is calculated using molecular weight I and the parameters a_v, b_v, and α_P as shown in Equation 58.

$$v = (a_v + b_v \cdot I)[1 + \alpha_P (T - 20℃)] \tag{57}$$

The parameters values used in this work can be found in Appendix A: Property Correlations Parameters Values.

3.4 UNIFAC Method

The UNIFAC method calculates the activity coefficient in terms of two parts, a combinational term and a residual term, which determine the activity coefficient of a component i as shown in Equation 58 below [46].

$$\ln \omega_i = \ln \omega_i^C + \ln \omega_i^R \tag{58}$$

The combinational term represents the contribution of the molecules size and area to the activity coefficient using Equation 59 where the area fraction Θ_i and the segment fraction φ_i of pure component i are calculated by Equations 60 and 61 respectively.

$$\text{Ln}\, \omega_i^C = \ln \frac{\varphi_i}{x_i} + \frac{z}{2} u_i \ln \frac{\Theta_i}{\varphi_i} + l_i - \frac{\varphi_i}{x_i} \sum_j x_j l_j \tag{59}$$

$$\Theta_i = \frac{u_i x_i}{\sum_j u_j x_j} \tag{60}$$

$$\varphi_i = \frac{w_i x_i}{\sum_j w_j x_j} \tag{61}$$

The molecular van der Waals volume w_i and surface area u_i of a pure component i are calculated from the sum of the volume and area parameters W_k and U_k of functional group k in pure component i, as shown in Equations 62 and 63. $N_k^{(i)}$ represents the number of functional groups k present in pure molecule i. Additionally, l_i is calculated from w_i and u_i as shown in Equation 64.

$$w_i = \sum_k N_k^{(i)} W_k \tag{62}$$

$$u_i = \sum_k N_k^{(i)} U_k \tag{63}$$

$$l_i = \frac{z}{2}(w_i - u_i) - (w_i - 1), \qquad z = 10 \tag{64}$$

The group parameters W_k and U_k are calculated from the van der Waals volume and surface areas of a functional group k using normalization factors 15.17 and 2.5×10^9, as shown in Equations 65 and 66.

$$W_k = \frac{V_{wk}}{15.17} \tag{65}$$

$$U_k = \frac{A_{wk}}{2.5 \times 10^9} \tag{66}$$

This work will only look at three different molecules which are alcohols, fatty acid methyl esters (FAME) and monoglycerides (MGC), and they only have six different functional groups present as shown in Table 3-2, which are CH_3, CH_2, CH, CH=CH, OH, and CH_2COO. The volume and area parameters of each functional group are listed in the table below [46], [47].

Table 3-2: UNIFAC functional group volume and area parameters [46], [47]

Functional Subgroup (k)	Functional Main Group	W_k	U_k
CH_3	CH_2	0.9011	0.848
CH_2	CH_2	0.6744	0.540
CH	CH_2	0.4469	0.228
CH=CH	C=C	1.1167	0.867
OH	OH	1.0000	1.200
CH_2COO	CCOO	1.6764	1.420

The residual component calculates the contribution of interactions between molecules to the activity coefficients, and is calculated using Equation 67.

$$\ln \omega_i^R = u_i \left[1 - \ln \left(\sum_j \Theta_j \tau_{ji} \right) - \sum_j \frac{\Theta_j \tau_{ij}}{\sum_k \Theta_k \tau_{kj}} \right] \tag{67}$$

The binary parameters τ_{ji} are calculated using experimental phase equilibrium data, as shown in Equation 68. Unfortunately, these data are not always available.

$$\tau_{ji} = exp\left(-\frac{e_{ji} - e_{ii}}{\bar{R}T} \right) \tag{68}$$

There is a second equation that can calculate the residual component of the activity coefficient by using functional groups, as shown in Equation 69, thus allowing the estimation of activity coefficient for substances for which one does not have VLE data. This equation takes into account the functional group's residual activity coefficient in a mixture, known as Π_k, which is calculated from Equation 70. $\Pi_k^{(i)}$ is the residual activity coefficient of a functional group k in a pure component i instead of in a mixture. Parameters used to calculate the residual activity coefficient $\Pi_k^{(i)}$ for functional group k are easily accessible and available online, and therefore Equation 69 will be used to calculate the residual activity coefficient ω_i^R.

$$\ln \omega_i^R = \sum_k N_k^{(i)} \left(\ln \Pi_k - \ln \Pi_k^{(i)} \right) \tag{69}$$

$$\ln \Pi_k = Q_k \left[1 - \ln\left(\sum_m \vartheta_m \Omega_{mk} \right) - \sum_m \frac{\Omega_m \Psi_{km}}{\sum_n \Omega_n \Psi_{nm}} \right] \tag{70}$$

The group interaction parameter Ω_{mn} is calculated from the energy of interaction E_{mn}, between the groups m and n, as shown in Equation 71. Alternatively, the group interaction parameter Ω_{mn} can also be calculated from group interaction parameter a_{mn} which is determined from experimental phase equilibrium data. The parameters for the group interaction parameters a_{mn} are easily accessible and available online, and therefore these parameters will be used to calculate the group interaction parameter Ω_{mn},

$$\Omega_{mn} = exp\left(-\frac{E_{mn} - E_{nn}}{\bar{R}T} \right) = exp\left(-\frac{a_{mn}}{T} \right) \tag{71}$$

The group interaction parameters a_{mn} have been determined and calculated from experimental phase equilibrium data and kept in a database [47]. Alternatively, the textbook, The Properties of Gases and Liquids, also has this data [46]. For this work, only the group interaction parameters listed in Table 3-3 are required.

Table 3-3: UNIFAC functional group interaction parameters, a_{mn}, in Kelvins [46], [47]

m \ n	CH_2	C=C	OH	CCOO
CH_2	0	86.02	986.5	232.1
C=C	-35.36	0	524.1	37.85
OH	156.4	457.0	0	101.1
CCOO	114.8	132.1	245.4	0

Equation 70 uses a different area fraction than the area fraction used in Equations 59 and 67: it uses the area fraction of a functional group which is calculated using Equation 72 using Q_m, the van der Waals surface areas for a functional group m, and X_m, the mole fraction of a functional group which is calculated using Equation 73.

$$\vartheta_m = \frac{Q_m X_m}{\sum_n Q_n X_n} \tag{72}$$

$$X_m = \frac{\sum_i x_i N_m^{(i)}}{\sum_n \sum_i x_i N_n^{(i)}} \tag{73}$$

4 Distillation Test of Biodiesel and Fitting of Model Biodiesel Composition

A distillation test was performed to determine the composition of the soybean biodiesel received from Innoltek. The distillation test that was performed was ASTM D86-20 [48], which is the standard test method to be used to perform a distillation test for petroleum fuels. Figure 4-1 shows the apparatus used for distillation tests, in which a 100 mL sample of fuel is distilled within the distillation flask, the evaporated fuel condenses as it passes through the cold bath, and the condensed liquid drops into the graduated cylinder. The measurements of the condensed liquid as percent recovered and the temperature of the fuel in the distillation flask is measured every 5% percent recovered. The ASTM D86-20 standard recommends that a vacuum distillation test should be performed for fuels that have a high boiling range such as biodiesel to prevent pyrolysis of the sample and formation of a solid residue at high temperatures. However, pyrolysis or residues were not observed, and thus in this work a normal distillation test with an ASTM D86-20 standard distillation flask was performed instead, since the equipment for a vacuum distillation test is much more complex. The fuel in the distillation flask was heated at a rate greater than the 5 mL of recovered condensed fuel per minute specified by the test. Additionally, this work used cold water instead of an ice bath to condense the evaporated fuel: since the boiling temperature of biodiesel is around 350 °C the difference between cold water and ice water is negligible [49], [50]. The apparatus used to perform the distillation test in this work did not have a shield around the burner, but did include a shield around the distillation flask, which is not shown in Figure 4-1.

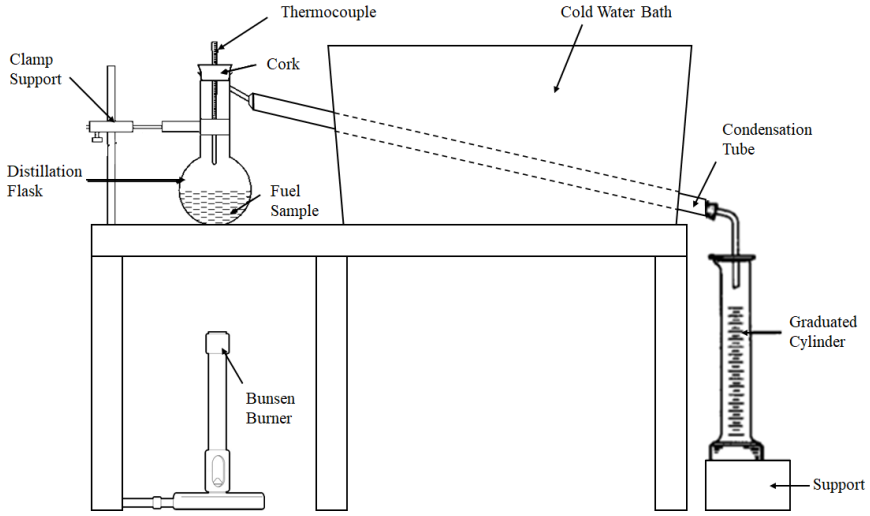

Figure 4-1: Apparatus for distillation test

Temperature measurements were taken at every 5% recovered fuel for a 100 mL sample, as shown in Figure 4-2. After the test was completed, there was not any solid residue leftover in the distillation flask, which would have been a sign that pyrolysis of biodiesel has occurred.

A numerical model was used to fit a mixture composed of two continuous mixtures, one FAME continuous mixture and one MGC continuous mixture, to the experimental data from the distillation test as shown in Figure 4-2. Five parameters have to be modified in order to fit the model to the experimental data: the mean θ and standard deviation σ of the FAME continuous mixture, the mean θ and standard deviation σ of the MGC continuous mixture, and the concentration of the FAME continuous mixture. The FAME continuous mixture will have boiling temperatures lower than the MGC fraction, and therefore the FAME continuous mixture will represent the experimental boiling temperatures up to about 80% recovered. The MGC continuous mixture with its higher boiling temperatures will represent the last few percent recovered during testing. Between 80% to 95% recovered is when the boiling temperatures transition from mainly the FAME components boiling to MGC components evaporating from the liquid. The mean θ of the continuous mixture can adjust the mean boiling temperature that the continuous mixture boils at on the distillation graph below, while the standard deviation σ can adjust the slope or the range of boiling temperatures that the continuous mixture boils at. The values for mean θ and standard deviation σ of the two continuous mixtures and the concentration of the FAME continuous mixtures were adjusted by trial and error such that the numerical model closely resembled the experimental results in Figure 4-2 below. This was done by visual inspection rather than numerical optimization. By using this curve fitting process, the composition of the biodiesel was assumed to be 93% FAME continuous mixture and 7% MGC continuous mixture, with the mean molecular weight, θ, and the standard deviation of the distribution, σ, shown in Table 4-1.

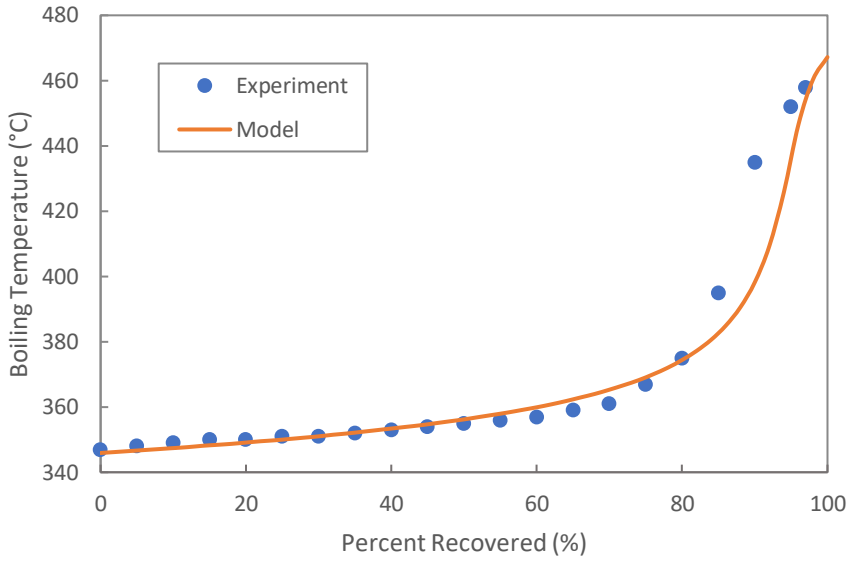

Figure 4-2: Distillation curve for biodiesel and distillation model using two continuous mixtures

Table 4-1: Composition of biodiesel as two continuous mixtures

Component	Mass Fraction (mass %)	Mean Molecular Weight, θ (g/mol)	Standard Deviation Molecular Weight, σ (g/mol)
Fatty Acid Methyl Esters	93	322	26
Monoglycerides	7	470	10

Additionally, a numerical model of the distillation test was used to fit a mixture of individual species to experimental data as shown in Figure 4-3, in which the individual species are composed of four FAME components and one MGC component. The concentration of FAME components and MGC components should be the same as the distillation results done above, in which the four FAME components will represent 93% of the mixture. The selection of the FAME components is done such that one component will represent the boiling temperatures at the lower end of the range of FAME boiling temperatures, another component will represent the higher end of the range, and two components will cover the middle of the range. Given that the inputs of the model are molecular weights, not boiling temperatures, two components will have a similar molecular weight as the FAME continuous mixture while the other two components will have molecular weights that are lower or higher than the molecular weight of the FAME continuous mixture will still remaining within the range of molecular weights for the continuous mixture.

FAME components were selected from a list of common FAMEs found in biodiesel provided by Hoekman et al. [51]. Previous work done by Hallett and Legault has shown that FAMEs with double bonds in its carbon chain behaves similarly to FAMEs without double bonds during distillation and droplet evaporation processes [8]. Due to the similar behaviour, property parameters of FAMEs without double bonds will be used in this work. Therefore, during the selection process of FAME components, whenever possible, a FAME that doesn't contain any double bonds is selected. If a second FAME component needs to be selected such that it has a similar molecular weight as a previously selected FAME component, a FAME component with one double bond can also be selected. The one MGC component is selected such that it would have a similar molecular weight as the MGC continuous mixture. Table 4-2 shows the assumed composition of biodiesel as individual components.

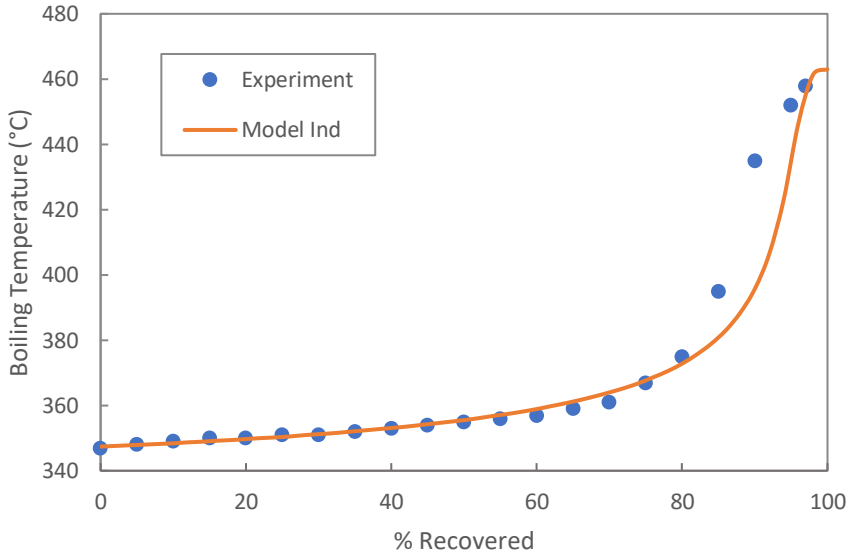

Figure 4-3: Distillation curve for biodiesel and distillation model using individual components

Table 4-2: Composition of biodiesel as individual components

FAME or MGC Component	Mass Fraction (mass %)	Molecular Weight (g/mol)
Methyl Arachidate	0.17	326.6
Methyl 11(Z)-Eicosenoate	0.12	324.5
Methyl Stearate	0.36	298.5
Methyl Behenate	0.28	354.6
Glycerol 1-Monohexacosanoate	0.07	470.8

5 Vapour-Liquid Equilibria of Alcohol-Biodiesel Blends

5.1 Determining the Representative Molecule for the UNIFAC Model of a Continuous Mixture

A continuous mixture is composed of multiple components, yet the UNIFAC method determines the activity coefficient of one component depending on the functional groups present within that one component. For this work, one activity coefficient will be used for each continuous mixture, and therefore a representative molecule will need to be selected to represent the continuous mixture in the UNIFAC calculation. This section looks into the importance of the selection of a representative molecule when using the UNIFAC method to represent a continuous mixture, and to also determine which representative molecule should be selected. To do this, vapour liquid equilibria (VLE) calculations for a mixture of individual components will be compared with the same calculations for a continuous mixture.

5.1.1 Continuous Alcohol Mixture with a Single FAME

Firstly, a continuous alcohol mixture with methyl oleate will be looked at. An alcohol continuous mixture mean molecular weight and standard deviation was determined by fitting the distillation numerical model of the alcohol continuous mixture with a distillation numerical model of a mixture of individual alcohol components, as shown in Figure 5-1. The alcohol continuous mixture was determined to have a mean molecular weight of 89.0 g/mol and a standard deviation of 20.0 g/mol, as shown in Table 5-1, when fitting the alcohol continuous mixture to the alcohol mixture with the composition shown in Table 5-2.

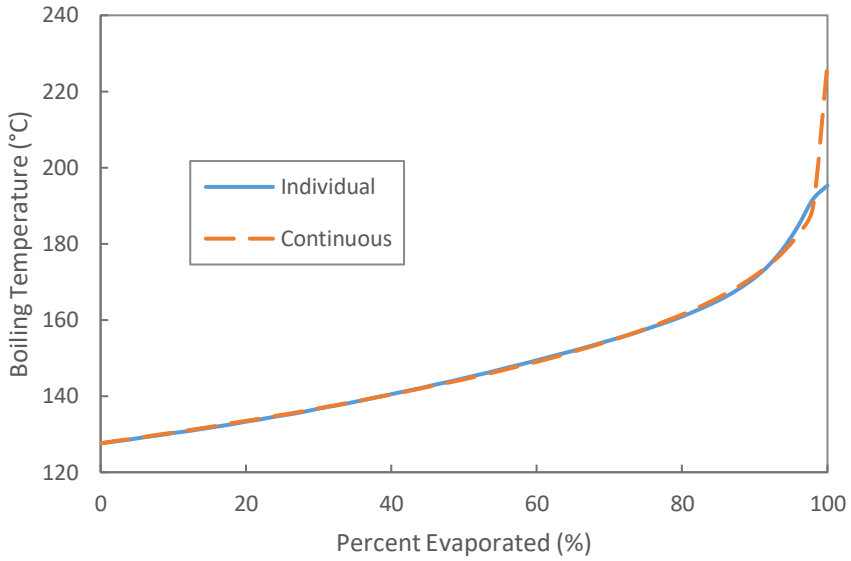

Figure 5-1: Numerical model of the distillation of an alcohol mixture with a composition of individual components or as a continuous mixture

Table 5-1: Composition of alcohol mixture as a continuous mixture

	Mean Molecular Weight, θ (g/mol)	Standard Deviation Molecular Weight, σ (g/mol)
Alcohol Mixture	89.0	20.0

Table 5-2: Composition of alcohol mixture as individual components

Alcohol Component	Mass Fraction (mass %)	Molecular Weight (g/mol)
Propanol	9	60.10
Butanol	20	74.12
Pentanol	25	88.15
Hexanol	33	102.17
Octanol	13	130.23

The components within the alcohol mixture only have three functional groups present, which are CH_3, CH_2, and OH. The quantities of the functional groups present in the alcohol mixture for each alcohol molecule are shown in Table 5-3.

Table 5-3: Number of each functional group k in each alcohol component i, $N_k^{(i)}$

Alcohol Component	$N_k^{(i)}$		
	CH_3	CH_2	OH
Propanol	1	2	1
Butanol	1	3	1
Pentanol	1	4	1
Hexanol	1	5	1
Octanol	1	7	1

There are four possible methods to pick a representative molecule to represent a continuous mixture when using the UNIFAC method. The first two methods use the molecule with the lowest or the highest molecular weight. As shown in Table 5-4, the functional groups of the representative molecule are used to represent the functional groups of a continuous mixture. For the molecule with the lowest molecular weight, propanol's functional groups are used to represent the alcohol mixture in the UNIFAC method. For the molecule with the highest molecular weight, octanol's functional groups are used. The other two possible methods use the mol average or the mass average, for which the mol fractions and the mass fractions of each molecule in Table 5-2 with the functional groups of each molecule listed in Table 5-3 are used to determine the functional groups to represent the continuous alcohol mixture in the UNIFAC method, with the numbers of functional groups listed in Table 5-4.

Table 5-4: Different methods to approximate the number of each functional group k in alcohol mixture i, $N_k^{(i)}$

Alcohol Mixture	$N_k^{(i)}$		
	CH_3	CH_2	OH
Lowest Molecular Weight	1	2	1
Highest Molecular Weight	1	7	1
Mol Average	1	4.0476	1
Mass Average	1	4.34	1

Figure 5-2 compares VLE calculations of continuous alcohol mixtures with methyl oleate using the four methods to determine the functional groups of the continuous mixture to a mixture of individual alcohol components with methyl oleate. As shown in the figure below, the continuous alcohol mixture underestimates the VLE for all four methods compared to the alcohol mixture of individual components when the alcohol mixture mol fraction is below 0.9. When the alcohol mol fraction is greater than 0.9, the continuous alcohol mixture overestimates the boiling temperature

when compared to the alcohol mixture of individual components. Both the continuous mixture of alcohol and the individual alcohol components are using the same boiling point correlation. A possible reason for this to occur is that when performing the VLE calculations between a continuous mixture and an individual component, the VLE calculation is unable to represent any non-ideal behaviour that is occurring between the individual components that are represented by the continuous mixture. In this case, there may be non-ideal behaviour that occurs between the alcohol components which is not represented when using a continuous mixture to represent all of the alcohol components, given that the UNIFAC method is applied to determine the activity coefficients between an alcohol continuous mixture and methyl oleate. Additionally, the method to choose a representative molecule and the number of functional groups to be used in UNIFAC method calculations appears to have an effect, as shown in Figure 5-2. Using the molecule with the highest molecular weight, octanol, to represent the continuous alcohol mixture gives the closest results to the VLE of an alcohol mixture with individual components with methyl oleate, while using the lowest molecular weight, propanol, to represent the continuous alcohol mixture deviates the most from the expected results. Using mass average and mol average to determine the number of functional groups to represent the continuous alcohol mixture gives very similar results for the VLE of an alcohol mixture with methyl oleate.

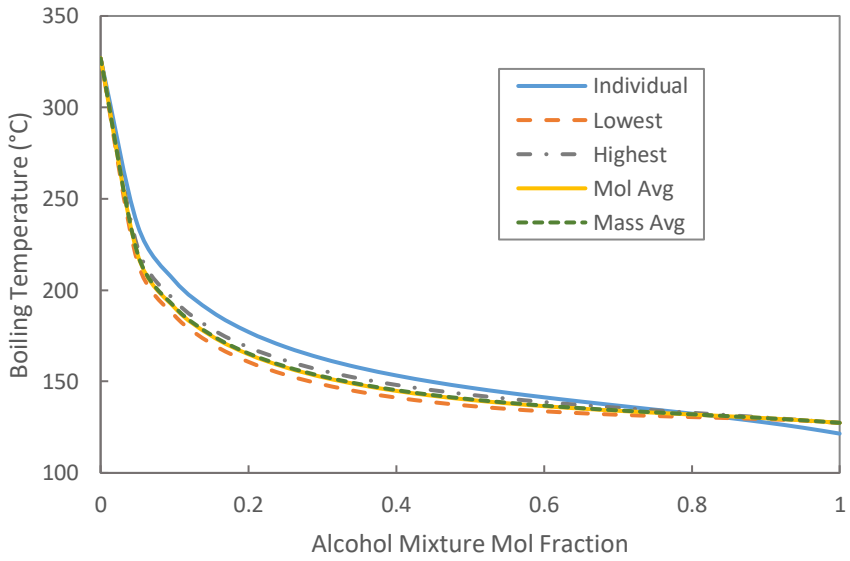

Figure 5-2: Vapour liquid equilibria of alcohol mixture with methyl oleate where the alcohol mixture is represented as individual components or as a continuous mixture with the functional groups represented by the molecule with the lowest molecular weight, highest molecular weight, mol average or mass average

5.1.2 Single Alcohol with a Continuous FAME Mixture

To see if the behaviour shown in Figure 5-2 between a continuous alcohol mixture with methyl oleate will occur for a continuous mixture of FAME components, calculations of VLE between a mixture of FAME components and propanol were done. The continuous FAME mixture determined in Section 4 during the distillation test of biodiesel will be used. The functional groups of the components found in the FAME mixture are shown in Table 5-5 below.

Table 5-5: Number of each functional group k in each fame component i, $N_k^{(i)}$

FAME Component	$N_k^{(i)}$			
	CH_3	CH_2	CH_2COO	CH=CH
Methyl Arachidate	2	17	1	0
Methyl 11(Z)-Eicosenoate	2	15	1	1
Methyl Stearate	2	15	1	0
Methyl Behanate	2	19	1	0

The four methods to determine the functional groups that will be used to determine the activity coefficient of a continuous FAME mixture in the UNIFAC method are shown in Table 5-6 below.

Table 5-6: Different methods to approximate the number of each functional group k in FAME mixture i, $N_k^{(i)}$

FAME Mixture	$N_k^{(i)}$			
	CH_3	CH_2	CH_2COO	CH=CH
Lowest Molecular Weight	2	15	1	0
Highest Molecular Weight	2	19	1	0
Mol Average	2	16.4552	1	0.1281
Mass Average	2	16.57	1	0.1290

As shown in Figure 5-3 below, the VLE behaviour of a continuous FAME mixture with propanol using the four methods got identical results to the VLE calculations of a FAME mixture of individual components with propanol. This shows that the slightly non-ideal behaviour between FAME components does not have an effect on the VLE given that FAME components are slightly polar, and that only the non-ideal interaction between a FAME component and propanol has an effect on the VLE of a FAME mixture and an alcohol. This goes to show that the VLE of a mixture of FAME components with an alcohol can be represented by a continuous FAME mixture with an alcohol. Additionally, Figure 5-3 shows that the selection of a representative molecule for a

continuous mixture does not have an effect for a continuous FAME mixture in VLE calculations. For this work, a mol average representation will be used to represent the number of functional groups of the continuous FAME mixture.

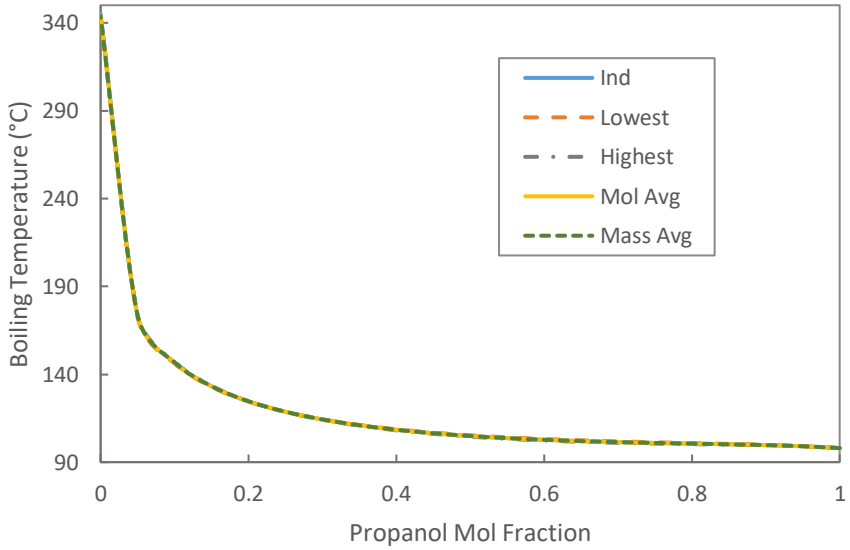

Figure 5-3: Vapour liquid equilibria of FAME mixture with propanol where the FAME mixture is represented as individual components or as a continuous mixture with the functional groups represented by the molecule with the lowest molecular weight, highest molecular weight, mol average or mass average

To see if the number of double bonds present in the representative FAME molecule has an effect on representing the VLE of alcohol-FAME mixtures, the VLE calculations were repeated for propanol and continuous FAME mixtures using different representative molecules. The different representative molecules are all FAME molecules with a carbon chain length of 17 carbons, similar to the mol average and the mass average representative molecule, but with a different number of double bonds present in the carbon chain, in which the number of functional groups are shown in Table 5-7 below.

Table 5-7: Number of functional groups present in FAME with a carbon chain length of 17 carbons with varying number of double bonds

# of Double Bonds	$N_k^{(i)}$			
	CH_3	CH_2	CH_2COO	CH=CH
0	2	16	1	0
1	2	14	1	1
2	2	12	1	2
3	2	10	1	3

Figure 5-4 shows the VLE calculations for a FAME continuous mixture with propanol in which the FAME continuous mixture is represented with a FAME molecule with varying number of double bonds present in the carbon chain. Additionally, the VLE calculations of the FAME mixture composed of individual FAME components with propanol are also shown for comparison. All VLE calculations got very similar results, in which there is some variance shown when the propanol mol fraction is between 0.05 and 0.25. By looking more closely at the calculated values, the addition of a double bond in the carbon chain increases the boiling temperature by 2-3°C when the propanol mol fraction is between 0.05 and 0.25. Additionally, the continuous FAME mixture that has the representative molecule with zero double bonds is the closest to the FAME mixture composed of individual FAME components. However, the difference between 2-3 C for boiling temperature has a negligible effect on droplet evaporation modelling, and thus the selection of the number of double bonds for the UNIFAC method is unimportant.

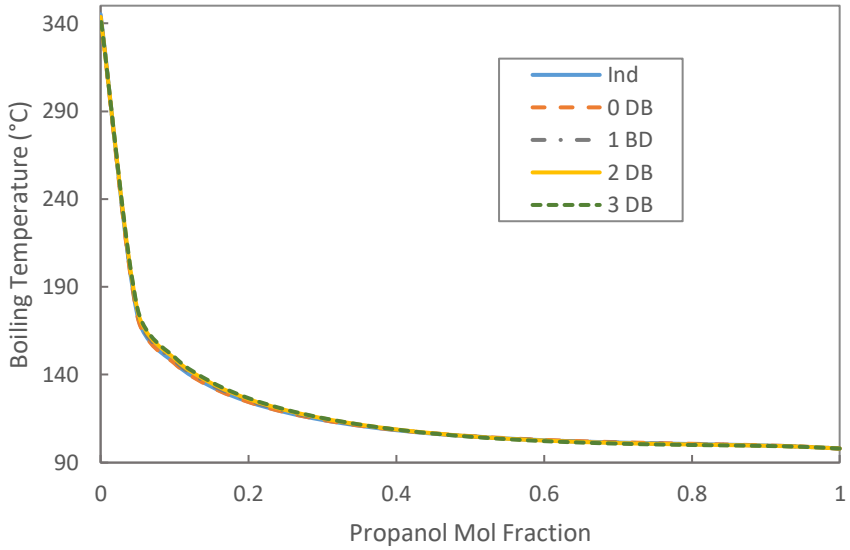

Figure 5-4: Vapour liquid equilibria of FAME mixture with propanol where the FAME mixture is represented as individual components or as a continuous mixture with the functional groups represented by a FAME molecule that has 0, 1, 2, or 3, double bonds

5.2 Comparing VLE Models with Experimental Data

To validate the UNIFAC model and its use to represent the VLE alcohol-biodiesel blends, experimental data for the VLE of some common methyl esters with ethanol [23] was compared with VLE calculations using both Raoult's Law and the UNIFAC method. The common methyl

esters that are examined in this work are methyl laurate, methyl myristate, and methyl oleate, with the chemical structure shown in Figure 5-5 below.

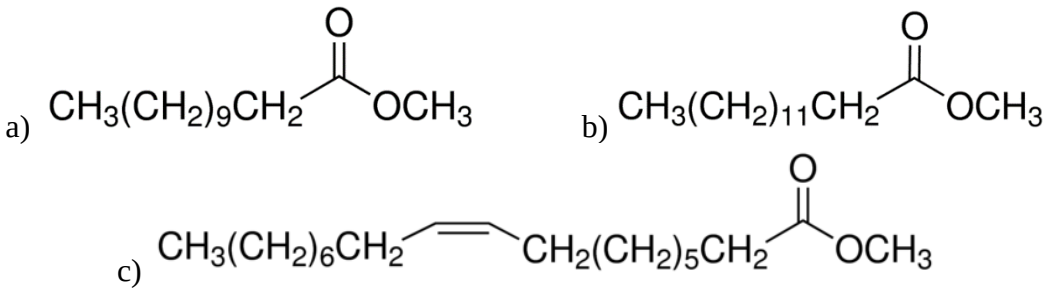

Figure 5-5: Chemical structures of a) methyl laurate, b) methyl myristate, and c) methyl oleate

The first set of experimental data is for a methyl laurate-ethanol system. As shown in Figure 5-6, the UNIFAC method agrees really well with the experimental data, whereas the VLE calculations that use Raoult's Law deviates from them with a difference of up to 30°C.

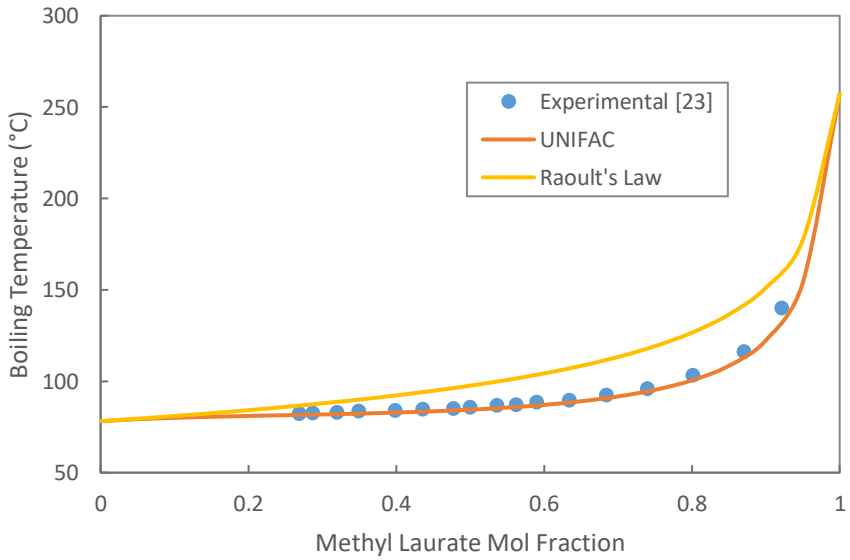

Figure 5-6: Comparison of vapour liquid equilibria modelling using the UNIFAC method and Raoult's Law with experimental data for methyl laurate-ethanol

The second set of experimental data is for methyl myristate-ethanol VLE [23]. As with methyl laurate-ethanol system, the UNIFAC method agrees well with the experimental data from the methyl myristate-ethanol system, as shown in Figure 5-7. The VLE calculations that use Raoult's Law overpredict the boiling temperatures by up to 26 °C.

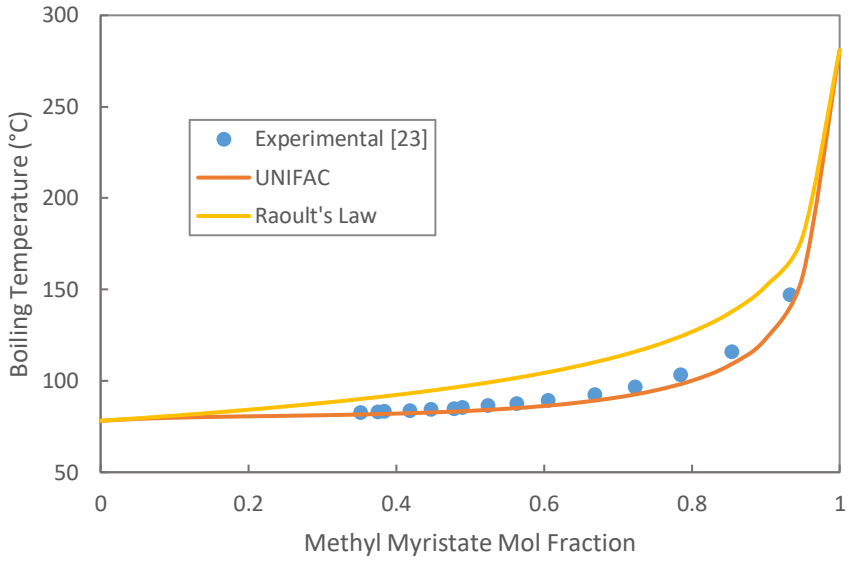

Figure 5-7: Comparison of vapour liquid equilibria modelling using the UNIFAC method and Raoult's Law with experimental data for methyl myristate-ethanol

Figure 5-8 show the VLE of methyl oleate and ethanol, which is the last set of methyl esters with ethanol. The UNIFAC method is again very close to the experimental results. Raoult's law produces boiling temperatures up to 20°C greater than the experimental VLE data. One of the experimental data points, specifically the value at the ethanol mol fraction of 0.91, was almost 25°C greater than with the UNIFAC method. This might be due to the double bonds present with methyl oleate, which are not present in methyl laurate and methyl myristate, as shown in Figure 5-5. The UNIFAC parameters between the double bond functional group and with other functional groups may not be as accurate as needed for representing the VLE of alcohol-methyl ester blends. The other possibility is an error in the experiment, specifically if the ethanol mol fraction for that data point was a few percent greater, that data point would be in line with the UNIFAC method. However, the UNIFAC method still produces VLE values that follow the experimental trend and agree well with majority of the data points, whereas Raoult's law still deviates widely from experimental data.

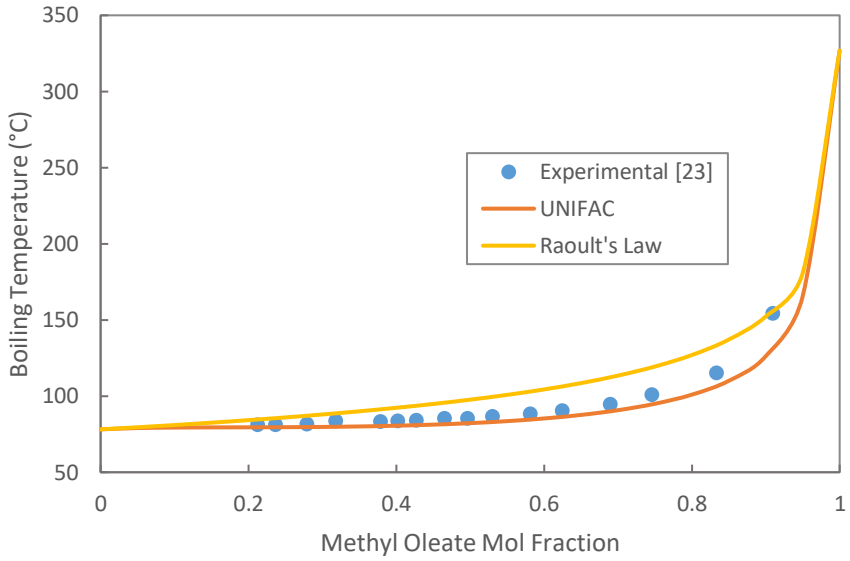

Figure 5-8: Comparison of vapour liquid equilibria modelling using the UNIFAC method and Raoult's Law with experimental data for methyl oleate-ethanol

To further test the UNIFAC method, the VLE of a biodiesel ethanol system using Raoult's Law and the UNIFAC method is compared with experimental VLE retrieved from Gou et al. [24], Silva et al. [25], and Kalvelage et al. [26]. The VLE calculations use the biodiesel composition of a FAME continuous mixture and a MGC continuous mixture that was determined in Section 4. Silva et al. used biodiesel with a FAME mass fraction of 96.6% [25] during VLE experiments whereas Kalvelage et al. used biodiesel with a FAME mass fraction of 96.5% [26]. Silva et al. also determined the fatty acid composition of the plant oil before transesterification as 53 wt% linoleic, 23 wt% oleic, 11 wt% palmitic, 4 wt% stearic, 8 wt% linolenic, and 1 wt% of other minor fatty acids [25]. Guo et al. did not provide information on how much ester was present in their biodiesel, but they did identify the fatty acids that were present in the plant oil before transesterification as palmitic, margaric, stearic, oleic, and linoleic [24]. As shown in Figure 5-9, the VLE calculations using the UNIFAC method agrees very well with the experimental data collected from Gou et al. and Kalvelage et al., whereas the VLE calculations using Raoult's Law do not. However, neither model agrees well for two points from the experimental data of Silva et al. [25], specifically when the ethanol mol fraction is equal to 0.1855 and 0.3422.

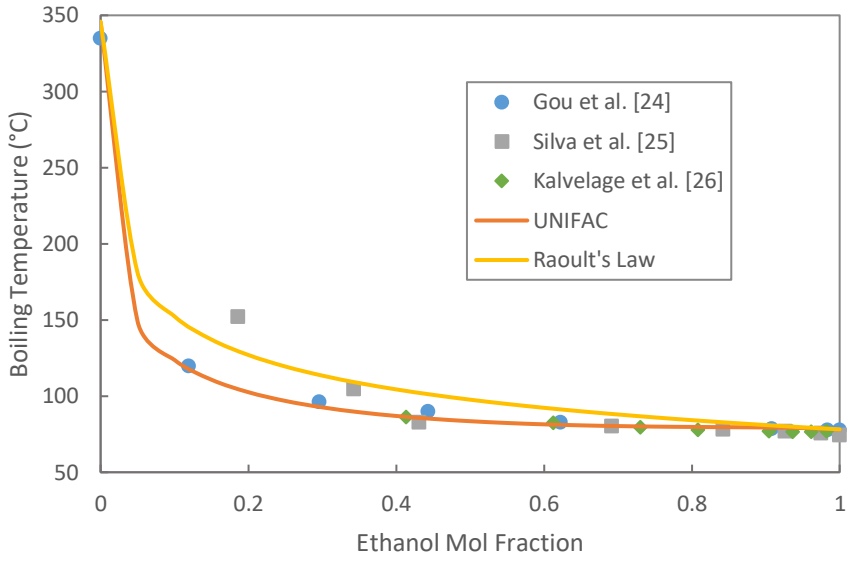

Figure 5-9: Comparison of vapour liquid equilibria modelling using the UNIFAC method and Raoult's Law with experimental data for biodiesel-ethanol

The experimental data of Silva et al. were measured at 91 kPa, whereas the present VLE calculations and the other experimental data were at 1 atm. However, the experimental work completed by Silva et al. also suggests that increasing the pressure by 10 kPa to 1 atm would only increase the temperature by 3-5°C [25], whereas Figure 5-9 shows that the boiling temperatures from Silva et al. are up to 50°C greater than the VLE calculations using UNIFAC method. In fact, this is probably not the cause for the discrepancy given that a lower atmosphere pressure should produce lower boiling temperatures, not higher boiling temperatures that Silva et al. produced during VLE experiments.

A possible cause of discrepancy is that biodiesel can have different composition depending on the plant oil used to produce the biodiesel or depending on the transesterification process. The composition of FAMEs within the biodiesel used by Silva et al., which was produced from soybean oil, was 53 wt% methyl linoleate, 23 wt% methyl oleate, 11 wt% methyl palmitate, 4 wt% methyl stearate, 8 wt% methyl linolenate, and 1 wt% of other minor FAMEs [25]. Methyl oleate, methyl linoleate, and methyl linolenate contain 1, 2, and 3 double bonds respectively, whereas the biodiesel used in this work is assumed, from curve fitting a numerical model to an experimental distillation test, to have only one FAME component with a double bond, which is methyl 11(z)-eicosenoate with a mass fraction of 12.9 %. The VLE and UNIFAC calculations were completed using the assumed composition of biodiesel from distillation tests. As mentioned earlier during the

comparison of VLE calculations for methyl oleate and ethanol in Figure 5-8, the UNIFAC method parameters for the double bond functional group may not be as accurate as desired for performing VLE calculations of alcohol-FAME blends that contain double bonds. For example in Section 5.1, the addition of the double bonds using the UNIFAC method only saw a temperature increase by 2-3° per double bond, which can't replicate the 50°C difference between the data from Silva et al. and the VLE calculations. Therefore, the large number of double bonds present in the biodiesel used by Silva et al. could be the cause of the discrepancy between the experimental VLE data of biodiesel-ethanol blends from Silva et al. and the VLE calculations of biodiesel-ethanol blends when using the UNIFAC method.

The second possible cause of the discrepancy is that the biodiesel used be Silva et al. is composed of 0.4 wt% diglycerides [25]. Most biodiesel composition measurements have shown that the diglyceride content of biodiesel is less than 0.1 wt % [9], [10], such that the present work did not consider diglycerides due to the typically very small amount present. The larger amount of diglycerides present could be the cause of the higher boiling temperatures reported by Silva et al. For example, glycerol 1-monostearate, a monoglyceride, has a molecular weight of 358.6 g/mol and a boiling point of 250°C [52], whereas 1,3-distearoylgycerol, a diglyceride, has a molecular weight of 625.03 g/mol and a boiling point of 579°C [53]. This could be the cause for the discrepancy between the VLE measurements of biodiesel-ethanol taken by Silva et al. and the boiling temperatures produced with the UNIFAC method.

As shown in this section of the report, the UNIFAC method was able to best represent the non-ideal VLE behaviours between FAME and alcohols, whereas Raoult's law was not able to reproduce the same behaviours. Therefore, the UNIFAC method was chosen to calculate the vapour pressures of components during droplet evaporation modelling.

5.3 Vapour-Liquid Equilibria of FAME-MGC-Alcohols

To get a better understanding of the evaporation process of biodiesel-alcohol droplets, VLE calculations performed used for the FAME-MGC-alcohol systems that will be tested during droplet evaporation experiments. Figure 5-10 shows the VLE behaviour of the FAME-MGC-propanol system. The boiling temperature does not rise above 150°C, which is ~50°C greater than the boiling temperature of propanol, as long as the propanol mol fraction within the mixtures

remains greater than 0.27 when the FAME mol fraction within the biodiesel is zero, or as long as the propanol mol fraction within the mixture remains greater than 0.09 when the FAME mol fraction within the biodiesel is one. Additionally, the boiling temperature doesn't get above 200°C as long as the propanol mol fraction within the mixtures is greater than 0.09 for a FAME mol fraction within biodiesel of zero and greater than 0.04 for then the FAME mol fraction within biodiesel is one. This goes to show that propanol will be the main component evaporating during droplet evaporation until the propanol concentration at the surface of the droplet becomes significantly small, especially since the initial composition of biodiesel is 0.93 (mol/mol) FAME and 0.07 (mol/mol) MGC.

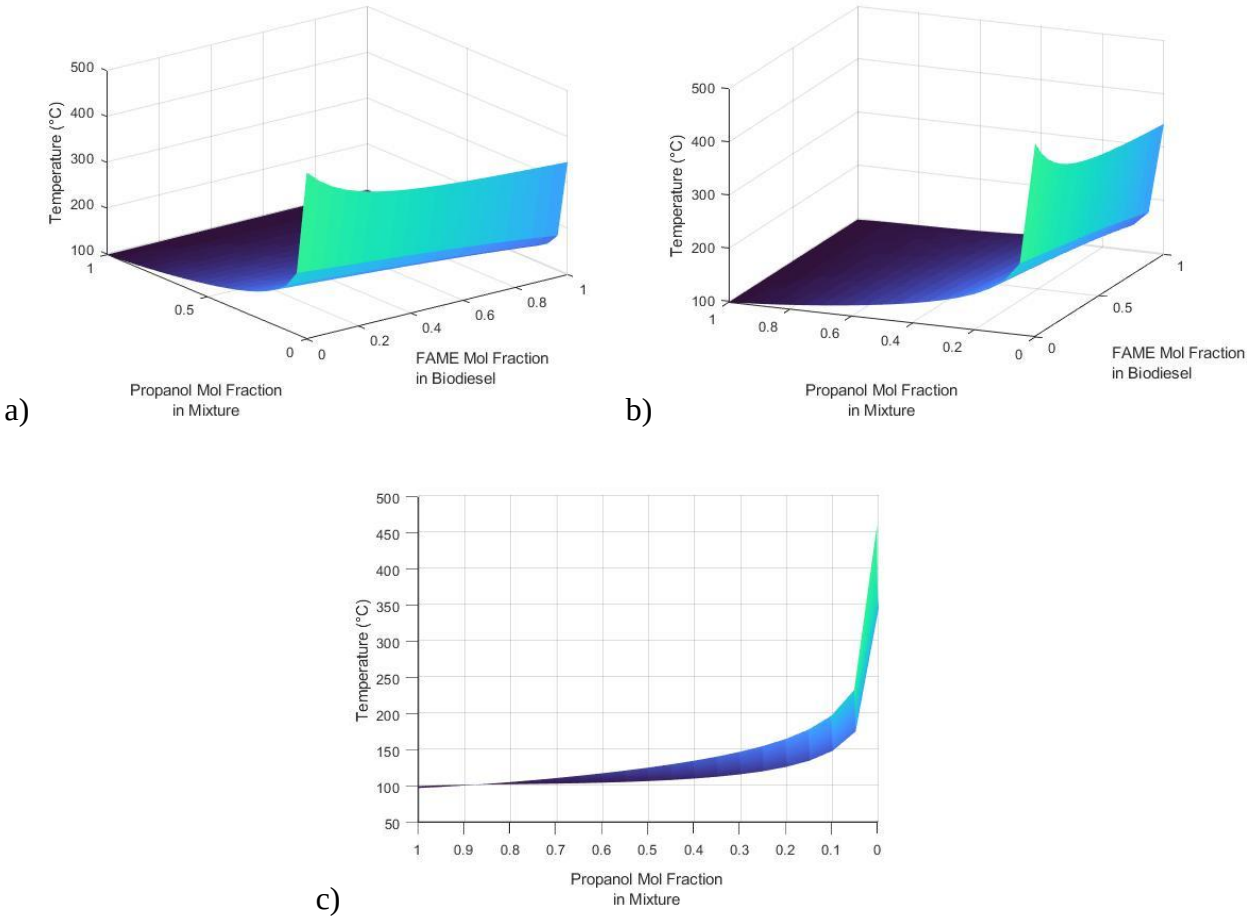

Figure 5-10: Vapour liquid equilibrium modelling using UNIFAC for FAME-MGC-propanol at 1 atm

Figure 5-11 shows the calculated VLE data for the FAME-MGC-pentanol system at 1 atm. As with the FAME-MGC-propanol system, the boiling temperature doesn't get above 200°C,

which is ~60°C greater than the boiling temperature of pentanol, as long as the pentanol mol fraction within the mixture remains greater than 0.26 when FAME mol fraction within biodiesel is zero, or as long as the pentanol mol fraction within the mixture remains greater than 0.10 when the FAME mol fraction within biodiesel is one. Additionally, the boiling temperature doesn't get above 250°C as long as the pentanol mol fraction within the mixture is greater than 0.09 for when the FAME mol fraction within the biodiesel is zero and greater than 0.04 for then the FAME mol fraction within the biodiesel is one. This again shows that for the droplet evaporation of biodiesel-pentanol droplets, pentanol will be the main component evaporating as long as the pentanol composition isn't significantly small at the droplet's surface.

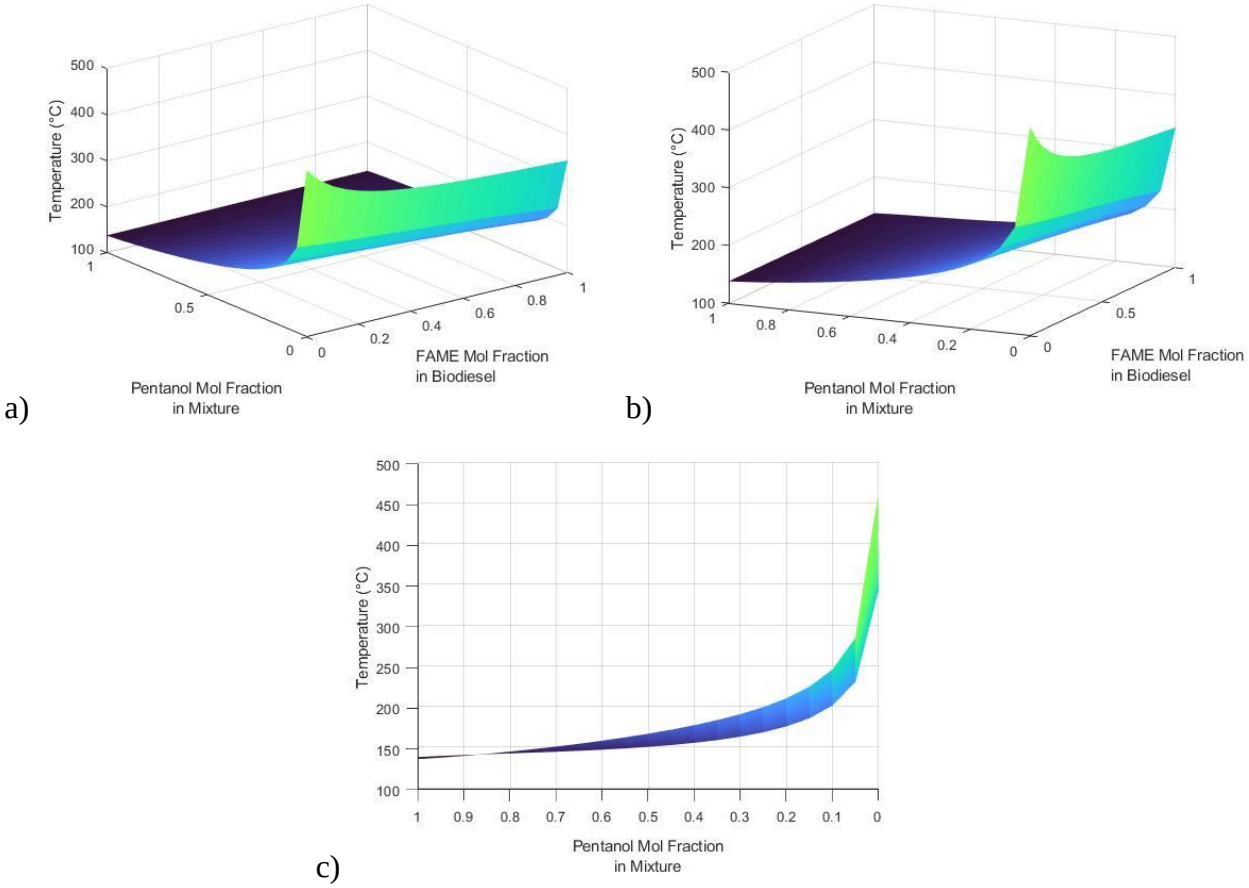

Figure 5-11: Vapour liquid equilibrium modelling using UNIFAC for FAME-MGC-pentanol at 1 atm

6 Droplet Evaporation Experiment Methodology

Droplet evaporation experiments were performed in which droplet diameters and droplet temperatures were measured throughout the evaporation process. The experiments were performed for environmental temperatures of 450°C and 700°C. Blends of biodiesel with 0%, 5%, 10%, 15%, and 20% of either propanol or pentanol were tested. The droplet evaporation experiments were performed for 6 to 8 trials, from which the average results will be used for analysis with the numerical models.

6.1 Experimental Setup

A moving furnace/suspended droplet technique is used to instantaneously increase the environmental temperature to either 450°C or 700°C. The experimental set-up of this furnace is shown in Figure 6-1. A 2μL droplet, generated and measured using a microliter syringe, is suspended on a thermocouple to measure the droplet temperature. The thermocouple is equipped with a bead of high temperature cement with a diameter of ~0.6 mm, to provide support for the liquid droplet to hang on. The furnace itself is heated with electric heaters, and an additional thermocouple shown in the Longitudinal Section view of Figure 6-1 measures the temperature at the center of the furnace. A Plexiglas enclosure surrounds the set-up shown in Figure 6-1, and it and the furnace are purged with nitrogen gas to maintain an inert atmosphere such that only droplet evaporation occurs, not combustion. Additional purging is used to remove the evaporated fuel from the furnace after each droplet is evaporated. Once the furnace has reached the steady state temperature of either 450°C or 700°C (steady state meaning that the environment temperature does not increase more than 2°C/min), the furnace is moved over the suspended droplet along rails by an air cylinder. Once the furnace moves over the droplet, a switch is triggered which triggers to a LabView program to start taking droplet photos, video, and droplet temperature measurements. The furnace itself is equipped with windows so that the optical system and camera can capture photos of the droplet during the evaporation process.

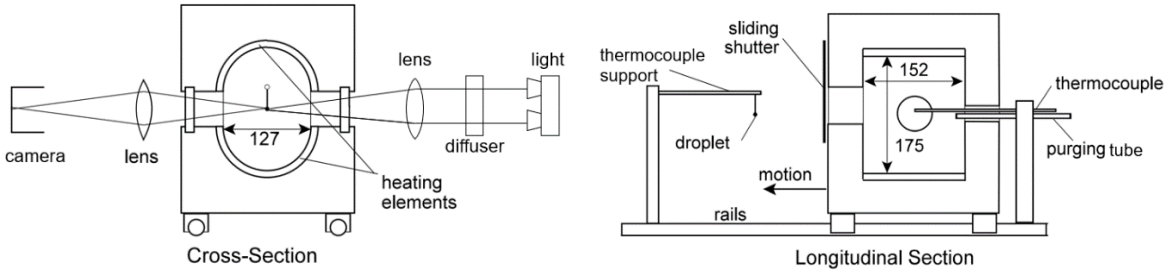

Figure 6-1: Cross-section and longitudinal section views of furnace and droplet setup

6.2 Droplet Diameter Measurements

Figure 6-1 also shows the optical and camera setup used to take photos of the droplets. The droplet is backlighted with a lighting system composed of two halogen bulbs, a light diffuser, and an 80 mm photographic lens. The image of the droplet is captured with a high-speed camera and a 150 mm photographic lens. The high-speed camera was a Chameleon3 USB3 camera from Teledyne FLIR with a resolution of 1280x1024 pixels and a frame rate of 149 fps. Photos were taken every 0.8 seconds for droplet evaporation at 450°C and every 0.2 seconds for droplet evaporation at 700°C. Additionally the camera took videos of the droplet evaporation process. The shape of the droplets in the photos was assumed to be a prolate spheroid, of which the major and minor diameters were measured from the photos and used to calculate a volume-equivalent diameter as shown in Equation 74 below.

$$d_{EQ} = \sqrt[3]{d_{MIN}^2 d_{MAJ}} \tag{74}$$

The droplet diameters were initially measured from the droplet images in units of pixels. A pixel to mm ratio needs to be determined by using the initial droplet pixel diameter and the initial droplet mm diameter. To determine the initial droplet diameter in mm, the volume of the thermocouple bead must be added to the initial liquid volume of the droplet, which is 2 μL, as in Equation 75.

$$d_{EQ} = \sqrt[3]{\frac{6}{\pi} V_{DROPLET} + d_{BEAD}^3} \tag{75}$$

The equivalent droplet diameters will be used in this work to represent the droplet diameter in modelling. Experimental droplet diameter measurements of each droplet evaporation trial can

be found in Appendix B: Experimental Droplet Diameter Data from Droplet Evaporation Experiments.

6.3 Droplet Temperature Measurements

Droplet temperature measurements are the second set of data collected from droplet evaporation experiments. A K-type thermocouple was used to measure the temperature of the droplet as the droplet hangs on the junction of the thermocouple. The thermocouple is composed of wires with a diameter of 0.002'' (0.05 mm), given that work completed by Tolonen has found that heat conduction through thermocouple wires of less than 0.005'' (0.13 mm) was negligible during droplet evaporation [54]. Due to the small diameters of the thermocouple wires, a bead of high temperature cement of about 0.6 mm diameter was added to the junction of the thermocouple to give support for the droplet to hang on. The thermocouple is connected to a National Instruments DAQ card, and with the help of a LABVIEW program, temperature measurements were taken from the thermocouples during droplet evaporation experiments. Experimental droplet temperature measurements of each droplet evaporation trial can be found in Appendix C: Experimental Droplet Temperature Data from Droplet Evaporation Experiments.

7 Droplet Evaporation Results

7.1 Biodiesel Droplets

Droplet evaporation experiments were first performed for biodiesel droplets before moving on to mixtures. Experimental results on biodiesel droplets were compared with the numerical model for the evaporation of a well-mixed droplet. The numerical model assumes that biodiesel is composed of a FAME continuous mixture and a MGC continuous mixture determined during the distillation test of the fuel while using the property parameters (listed in Appendix A: Property Correlations Parameters Values) that was determined by Hallett and Legault during previous droplet evaporation modelling of biodiesel fuels as continuous mixtures [8]. Non-ideal mixture behaviour is not expected to occur between the FAME and MGC components, therefore the model uses Raoult's Law to calculate the vapour pressure. All experiments were performed with droplet liquid volumes of 2 μL, and a thermocouple bead diameter of approximately 0.6 mm, giving an effective droplet diameter of 1.6 mm.

Figure 7-1 shows the droplet diameter history of biodiesel droplets at a furnace temperature of 450°C. Both the model and the experimental results agree quite well, with some small deviation between the experimental droplet diameter and the model between 6 and 10 seconds of the droplet's lifetime. The graph shows that the 2μL droplet has a lifetime of less than 14 seconds. (Note that both the model and experimental results stop when only the thermocouple bead remains.) The droplet initially experiences thermal expansion early in the droplet's lifetime. After 4 seconds the droplet's diameter starts decreasing due to the evaporation processes.

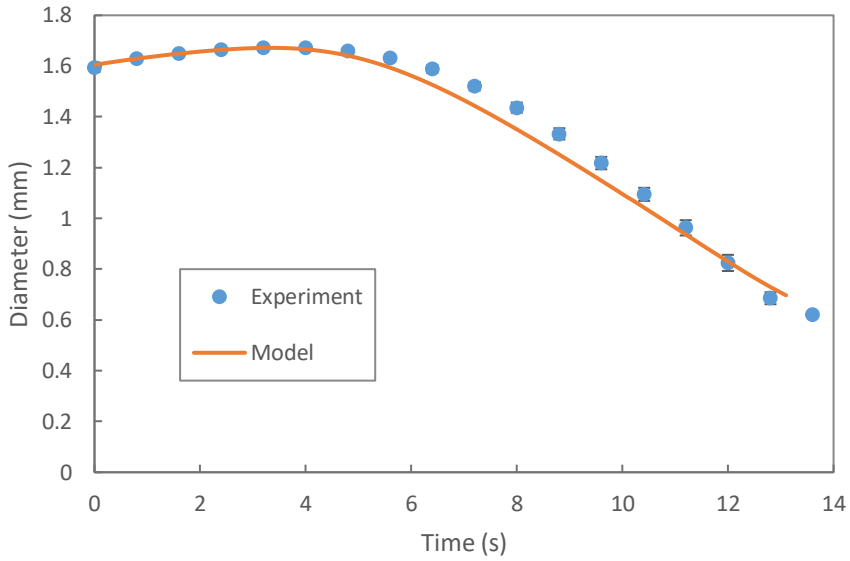

Figure 7-1: Droplet diameter of biodiesel during droplet evaporation at 450°C
Note: Experimental points give the mean and standard deviation of 8 individual measurements

Figure 7-2 shows the droplet's temperature for biodiesel droplet evaporation at a furnace temperature of 450°C. The model agrees quite well with the experimental results. The figure shows that the droplet undergoes heating between 0 and 5 seconds with a steady increase in temperature. After 5 seconds, the temperature curve flattens out to a temperature about 280-290°C, which is lower than the boiling temperatures of the FAME components observed during the distillation of biodiesel in Section 4 (345-365°C). The temperature starts to increase again at the end of the droplet's lifetime due to all of the FAME components being fully evaporated and the MGC, with higher boiling temperatures, are what is left over within the droplet.

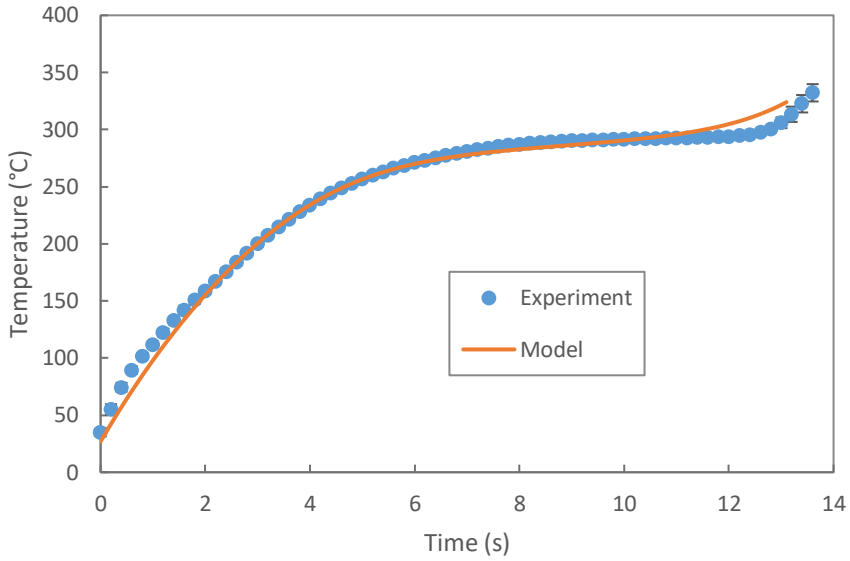

Figure 7-2: Droplet temperature of biodiesel during droplet evaporation at 450°C
Note: Experimental points give the mean and standard deviation of 8 individual measurements

Figure 7-3 shows droplet photos during the droplet evaporation of biodiesel at a furnace temperature of 450°C. The light at the center of the droplet is due to how the light reflects and refracts within the droplet when the droplet is lit with back-lighting. The lighting set-up is discussed in Section 6.2: Droplet Diameter Measurements. In the droplet photos shown below, the droplet evaporation process appears normal without any disturbances visible within the droplet.

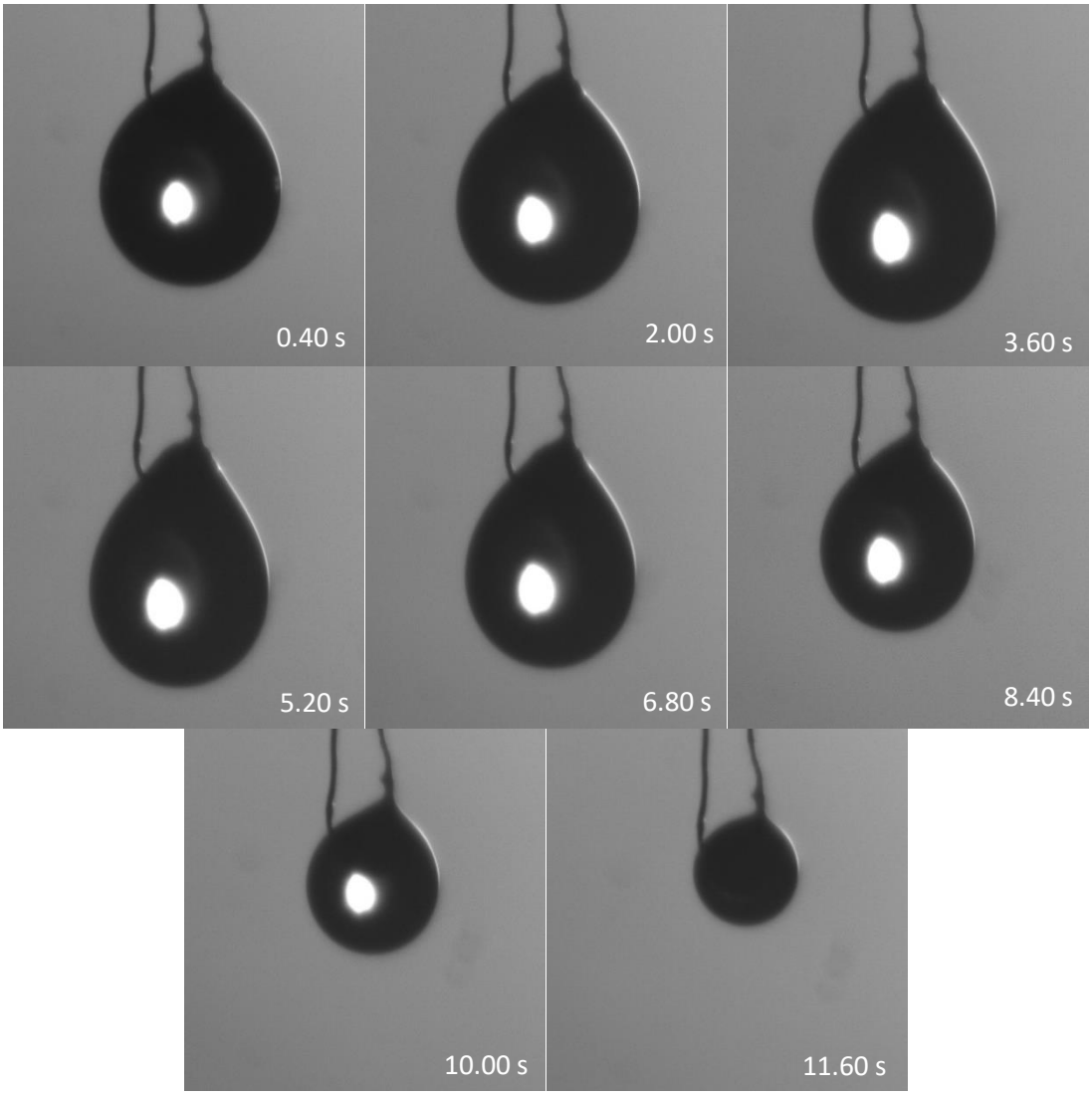

Figure 7-3: Droplet photos of biodiesel during droplet evaporation at 450°C

Figure 7-4 shows the droplet's diameter during biodiesel droplet evaporation at a furnace temperature of 700°C. The model and experimental results agree quite well, with some deviation between experimental droplet diameters and model's droplet diameters between 2.5 and 4.5 seconds. The droplet has a shorter lifetime at 700°C, about 4.6 seconds. As at 450°C, the droplet experiences thermal expansion, increasing the droplet's diameter from 0 to 2 seconds, after which it decreases.

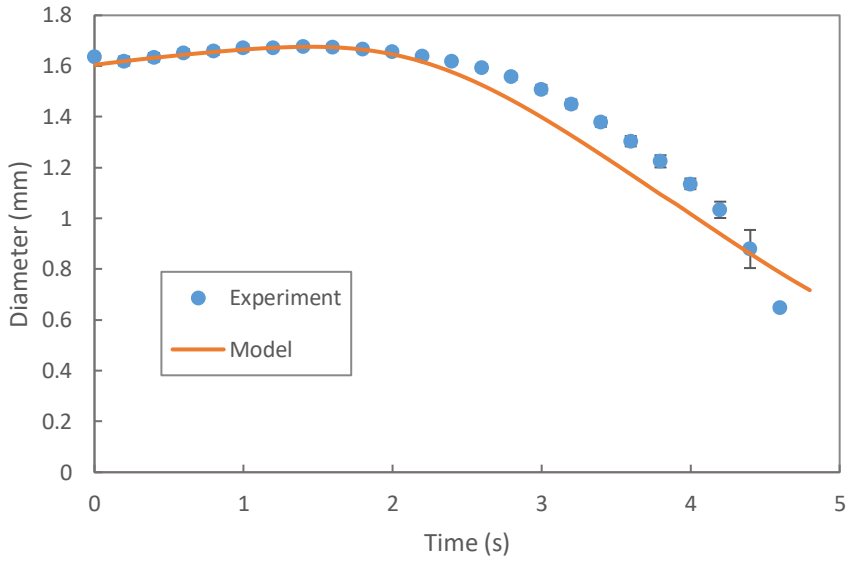

Figure 7-4: Droplet diameter of biodiesel during droplet evaporation at 700°C
Note: Experimental points give the mean and standard deviation of 8 individual measurements

Figure 7-5 shows the droplet photos during the droplet evaporation of biodiesel at a furnace temperature of 700°C. The images at 700°C are lighter than at 450°C because of the increased level of light radiation from the furnace walls. Small light flashes can be seen near the cement bead in photos at 1.60, 2.20, and 3.40 seconds with the photo at 4.00 seconds showing a lot of small light specks near the cement bead. These flashes appear to be caused by the light refracting through some small bubbles. The cement bead could act as a nucleation site for any bubbles to form. The distillation curves in Section 4 did not indicate the presence of any light components that could boil and produce bubbles. The other possibility is that the biodiesel could be undergoing pyrolysis and breaking down into light components that could form the bubbles that was observed during droplet evaporation experiments. Pyrolysis is not expected to occur given that the droplet temperatures observed in Figure 7-6 is lower than the measured temperatures during the distillation test in Section 4, and that solid residue was not observed during the distillation test. If leftover solid residue was observed, that would have been a sign that pyrolysis has occurred at the distillation temperatures. However, the larger bubbles seen at 3.40 seconds in Figure 7-5 appears to be responsible for the deviation between experiment and model in Figure 7-4.

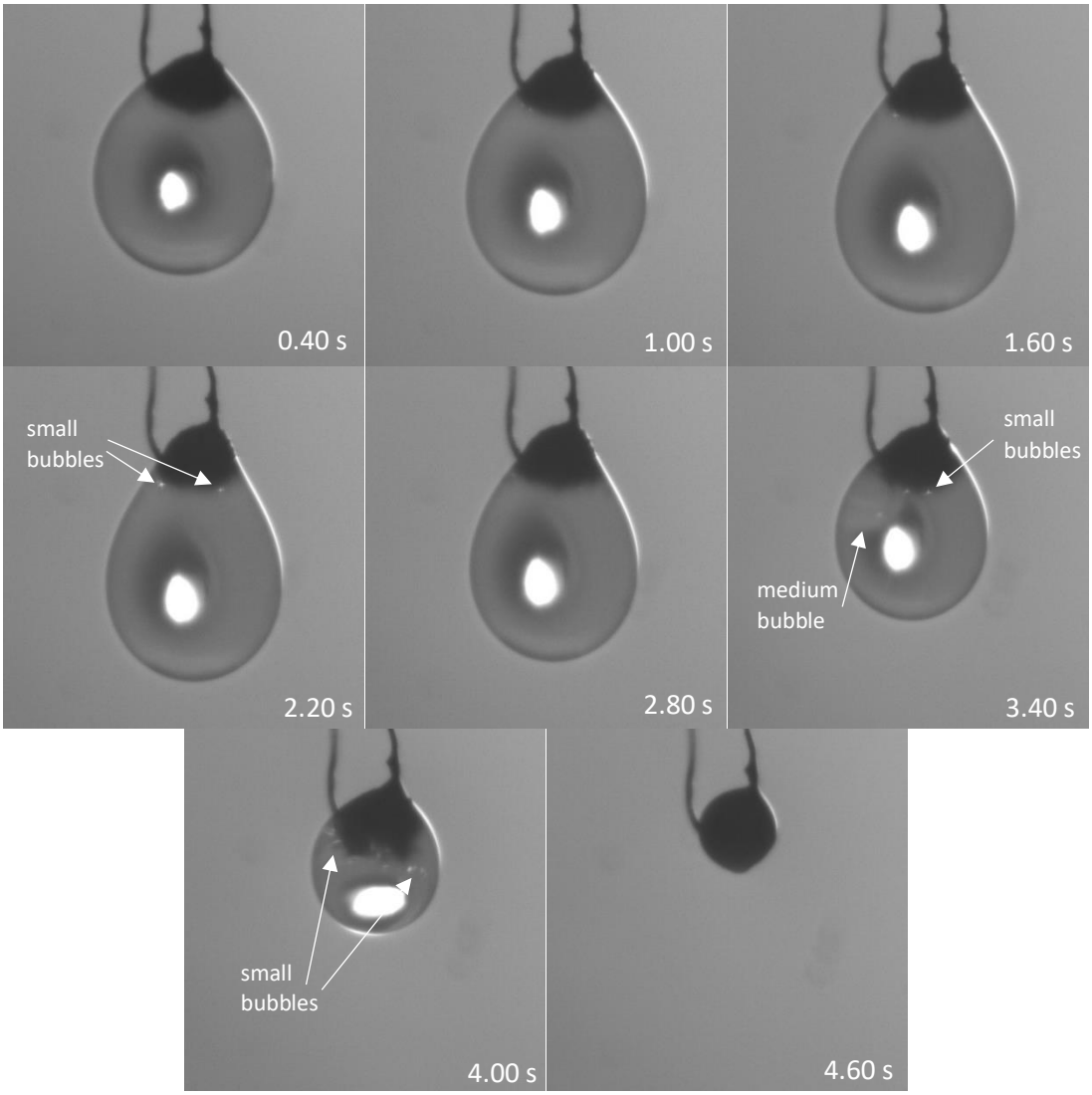

Figure 7-5: Droplet photos of biodiesel during droplet evaporation at 700°C

Figure 7-6 shows the droplet's temperature during biodiesel droplet evaporation at a furnace temperature of 700°C. As in Figure 7-2, the model agrees well with experimental droplet temperatures. The droplet undergoes steady increase in droplet temperature during 0 and 2 seconds. The droplet's temperature curve flattens slightly after 2 seconds. The temperatures shown in the figure below all remain below the boiling temperatures measured during the distillation test of biodiesel in Section 4. Since the boiling temperatures remain above the droplet temperatures, the bubble formation shown in the droplet photos above might be caused by a small amount of heat conduction through thermocouple wire, which could be providing the heat required to evaporate the components near the cement bead. Since the thermocouple wire is only 0.002'' (0.05

mm) in diameter, a more likely explanation is that the cement bead is absorbing some heat by radiation.

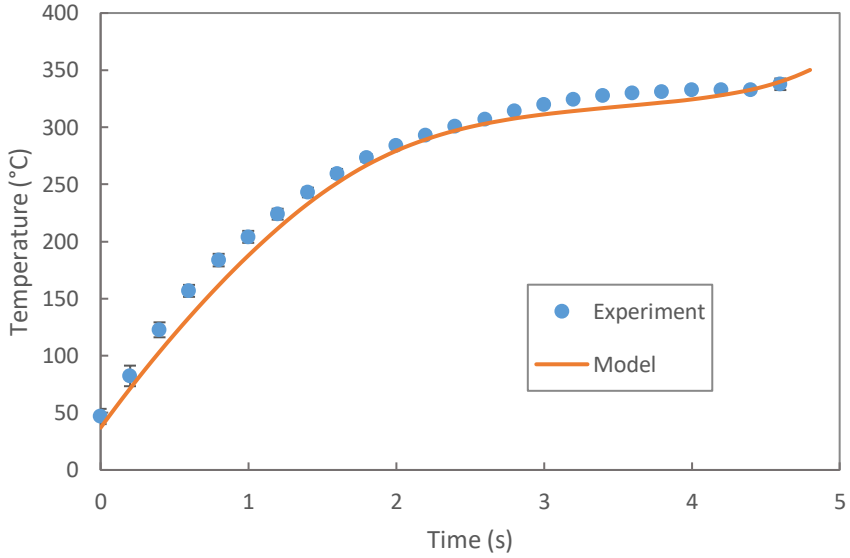

Figure 7-6: Droplet temperature of biodiesel during droplet evaporation at 700°C
Note: Experimental points give the mean and standard deviation of 8 individual measurements

The comparison of experimental droplet evaporation of biodiesel droplets with the numerical models shows that the distillation characteristics and properties used for the FAME and the MGC continuous mixtures give good predictions of the behaviour of the biodiesel sample used in this work. It should be noted that a significant part of the good agreement between the well-mixed model and the experiments is due to natural convection correlation that is incorporated within the well-mixed model, as mentioned in Section 3.1. Without this, predicted droplet lifetimes would be significantly longer.

7.2 Propanol-Biodiesel Droplets

The first droplet evaporation experiments with mixtures were performed for propanol-biodiesel blends. The experimental results will be compared with the well-mixed and the diffusion-limited models. Both models use the UNIFAC method to calculate vapour pressures and incorporate natural convection in which the diffusion-limited model uses the calculated value for the ratio of film thickness over droplet radius as shown in Section 3.2. As mentioned in Section 3.2, previous work has shown that the mixing factor should be between 2 and 4 to best represent the internal mixing that occurs within the droplet during droplet evaporation [36], [42], [43]. A

mixing factor in the middle of this range, specifically 3, was selected for this work. As for the biodiesel droplets, all experiments for alcohol-biodiesel droplets were performed with droplet liquid volumes of 2 µL, and a thermocouple bead diameter of approximately 0.6 mm, giving an effective droplet diameter of 1.6 mm. The results of these experiments are shown in the sections below.

7.2.1 Droplet Temperatures

Figure 7-7 shows the droplet temperature of biodiesel with 5% (v/v) propanol (PROP5) during droplet evaporation with the furnace temperatures at 450°C. As shown in the figure, the diffusion-limited model agrees well with experimental droplet temperatures, whereas the well-mixed model produces droplet temperature values that deviate from the experimental droplet temperatures between 1 and 3 seconds. As with the biodiesel droplets at 450°C, the rise of temperatures at the end of the droplet's lifetime could be caused by a combination of only the MGC components being left in the liquid to evaporate and the cement bead of the thermocouple being exposed to the environment as the remaining liquid evaporates. This rise is only predicted by the well-mixed model.

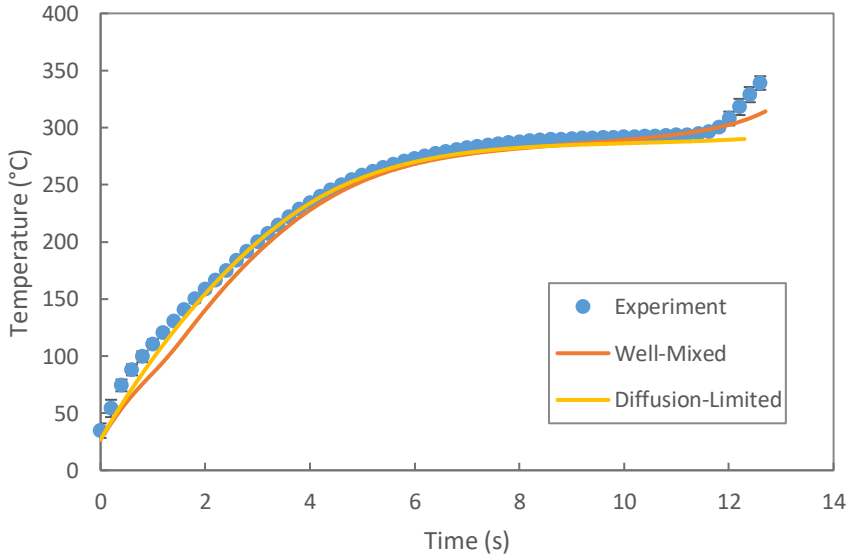

Figure 7-7: Droplet temperature of biodiesel with 5% propanol during droplet evaporation at 450°C

Note: Experimental points give the mean and standard deviation of 8 individual measurements

The experimental droplet temperatures for biodiesel droplets with 20% (v/v) propanol (PROP20) are shown in Figure 7-8 below along with the model predictions for droplet temperature.

As with the droplets of PROP5, the experimental droplet temperatures for droplets of PROP20 agree well with the diffusion-limited model. The droplet temperatures calculated using the well-mixed model did not agree as well with experimental droplet temperatures; in particular, the well-mixed model temperature curve flattens between 1 and 2 seconds. Experimental temperatures of PROP20 also shows the temperature increasing at the end of the droplet's lifetime, which could be the remaining MGC components evaporating and/or the thermocouple bead being exposed to the environment. The well-mixed model also shows the increase in droplet temperatures due to the remaining MGC components evaporating, whereas the diffusion-limited model does not show this behaviour given that this model only uses two fuel fractions, specifically the alcohol component and the FAME continuous mixture.

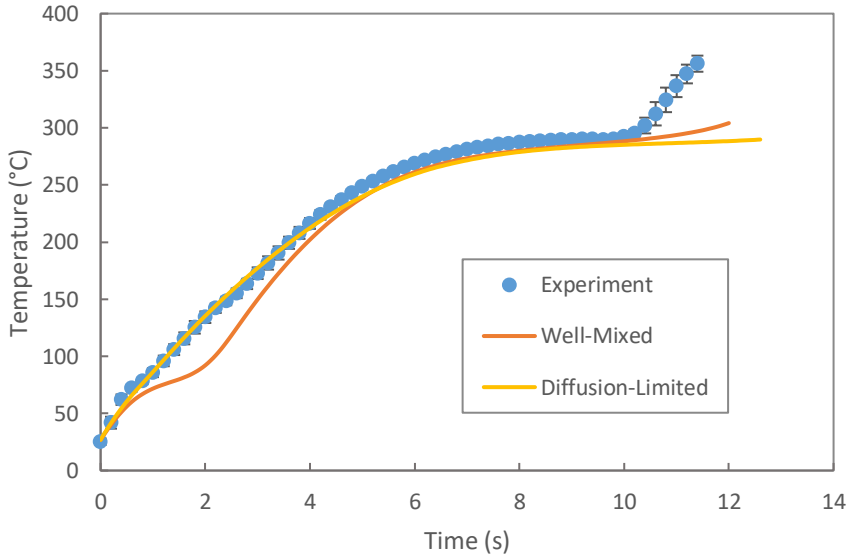

Figure 7-8: Droplet temperature of biodiesel with 20% propanol during droplet evaporation at 450°C

Note: Experimental points give the mean and standard deviation of 8 individual measurements

To understand better why the well-mixed model does not agree with experimental droplet temperatures, a graph of the calculated molar flux of evaporated fuel G, with the vapour mol fractions of the components at the surface of the droplet is shown in Figure 7-9. The mol fraction of the evaporated propanol component at the surface of the droplet peaks between 1 and 2 seconds due to the low boiling point of propanol compared to the FAMEs and MGCs. This causes the molar flux to peak significantly between 1 and 2 seconds.

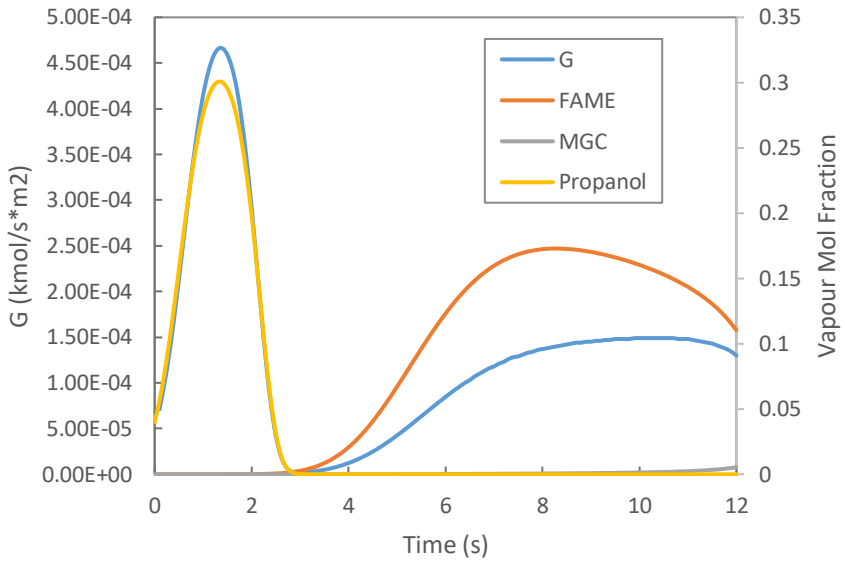

Figure 7-9: Calculated vapour molar flux and vapour mol fractions of well-mixed droplet of biodiesel with 20% during droplet evaporation at 450°C

When the molar flux peaks significantly, a large amount of heat is required to evaporate components. Equation 76 below gives the net heat transfer to the liquid Q_{liq} as the total heat transfer from the vapour phase Q_{net} minus the molar flux of evaporating components G multiplied by their enthalpy of vaporization h_{fg}. As the molar flux of vapour becomes large, the heat transfer to the liquid, which increases the droplet temperature, approaches zero, resulting in a pause in droplet heating due to the large molar flux of the evaporating propanol.

$$q_L = q_{net} - G * h_{fg} \tag{76}$$

For the diffusion-limited model, the propanol components have to slowly diffuse to the surface of the droplet before evaporating, causing the vapour mol fraction of the propanol to have a much lower and wider peak, and for the propanol components to slowly evaporate throughout the droplet's lifetime, as shown in Figure 7-10. This causes the molar flux of evaporating components to be less than with the well-mixed model and more constant throughout the droplet's lifetime. This results in a more nearly constant heat transfer to the droplet and a steadier temperature increase as shown in Figure 7-8. This also explains the lack of a sudden rise in temperature at the end of the droplet lifetime shown in Figure 7-7 and Figure 7-8, given that the heat transfer predicted by the model remains essentially constant and does not model the increase in heat transfer when the cement bead becomes exposed to the environment as the remaining liquid evaporates.

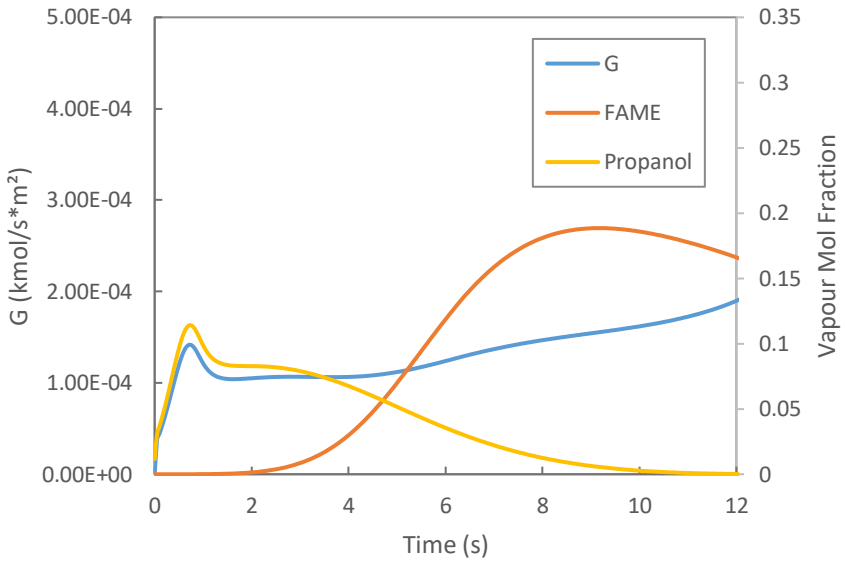

Figure 7-10: Calculated vapour molar flux and vapour mol fractions of diffusion-limited droplet of biodiesel with 20% during droplet evaporation at 450°C

The mixing factor χ models the effects of internal circulation within the droplet as an enhanced liquid diffusivity. Figure 7-11 shows the effect of the mixing factor on the diffusion-limited model for PROP20 at 450°C and Figure 7-12 shows the same thing but for the time range between 0 and 6 seconds. As shown in both figures, reducing the mixing factor to 1.35 causes the diffusion-limited model to move away from the well-mixed model, whereas increasing the mixing factor to 10 causes the diffusion-limited model to move towards the well-mixed model. As the mixing factor continues to increase, eventually the diffusion-limited model will behave exactly like the well-mixed model. However, previous work on internal mixing in the droplet during evaporation has shown that a mixing between 2 and 4 should be used [36], [42], [43]. For this work, a mixing factor of 3 was chosen.

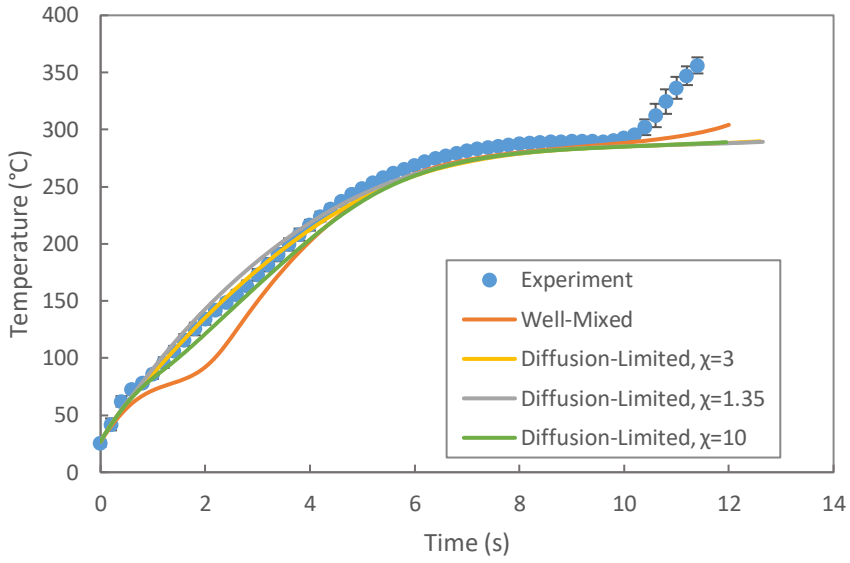

Figure 7-11: Droplet temperature of biodiesel with 20% propanol during droplet evaporation at 450°C with varying mixing factor, χ
Note: Experimental points give the mean and standard deviation of 8 individual measurements

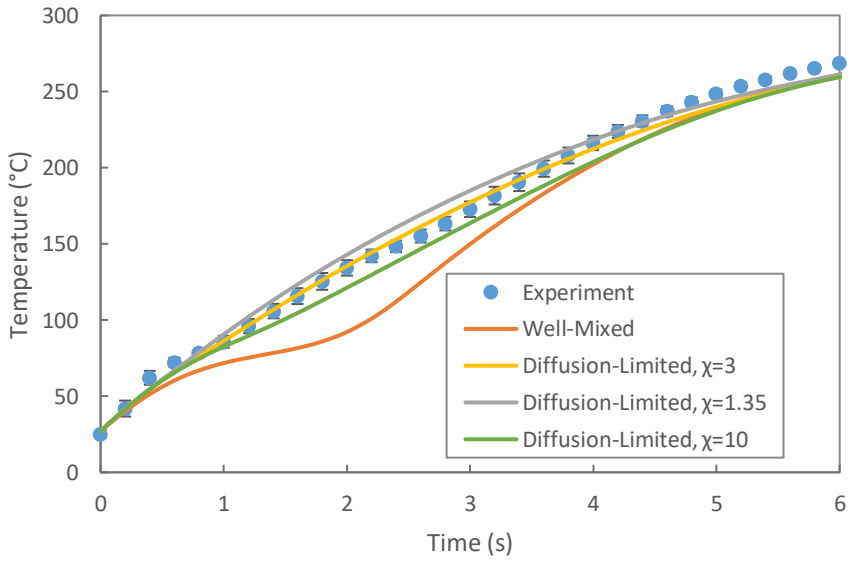

Figure 7-12: Droplet temperature of biodiesel with 20% propanol during droplet evaporation at 450°C with Varying Mixing Factor, χ, between 0 and 6 seconds
Note: Experimental points give the mean and standard deviation of 8 individual measurements

Figure 7-13 shows the droplet temperature during the droplet evaporation of PROP 5 at 700°C. Just as at 450°C, the diffusion-limited model agrees the best with experimental droplet temperatures, while the well-mixed model's temperatures do not increase at the same rate as the

experimental droplet temperatures. However, the diffusion-limited model does not reach as high a temperature as the experiments when the experimental droplet temperatures level off. Droplet photos shown in Section 7.2.2 show that the droplet becomes elongated in the vertical direction, exposing some of the thermocouple to the environment. This could possibly be the cause of high experimental droplet temperatures.

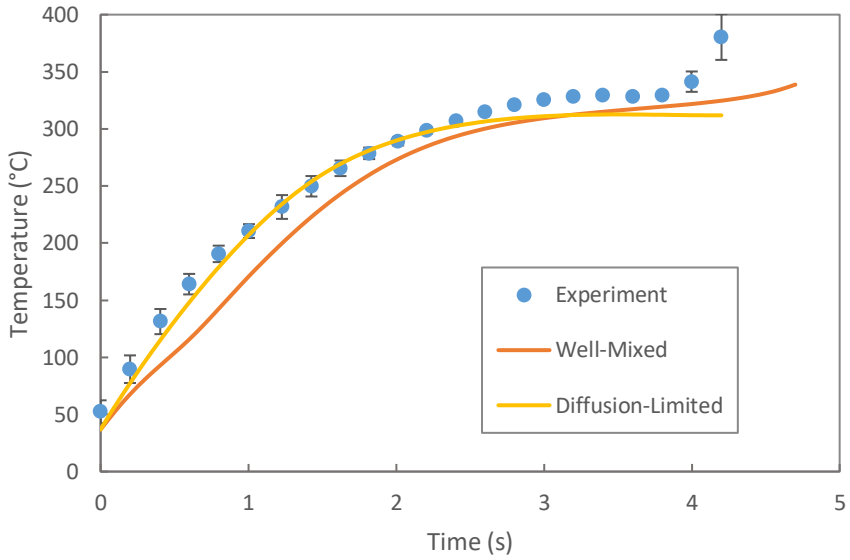

Figure 7-13: Droplet temperature of biodiesel with 5% propanol during droplet evaporation at 700°C

Note: Experimental points give the mean and standard deviation of 8 individual measurements

Figure 7-14 shows the droplet temperature during droplet evaporation of PROP20 at a furnace temperature of 700°C. Similar to previous droplet temperature results, the diffusion-limited model was best able to represent the experimental droplet temperature data, whereas the well-mixed model shows the temperature curve flattening between 0.5 and 1 seconds as all the propanol components evaporate. Additionally, similar to PROP5 at 700°C, the diffusion-limited model's temperature curve did not reach as high a temperature as the experimental droplet temperatures when the temperature curve flattens. Droplet photos shown in Section 7.2.2 do show that the droplet becomes vertically elongated, perhaps exposing some of the thermocouple to the environment, which could cause the higher measured temperatures.

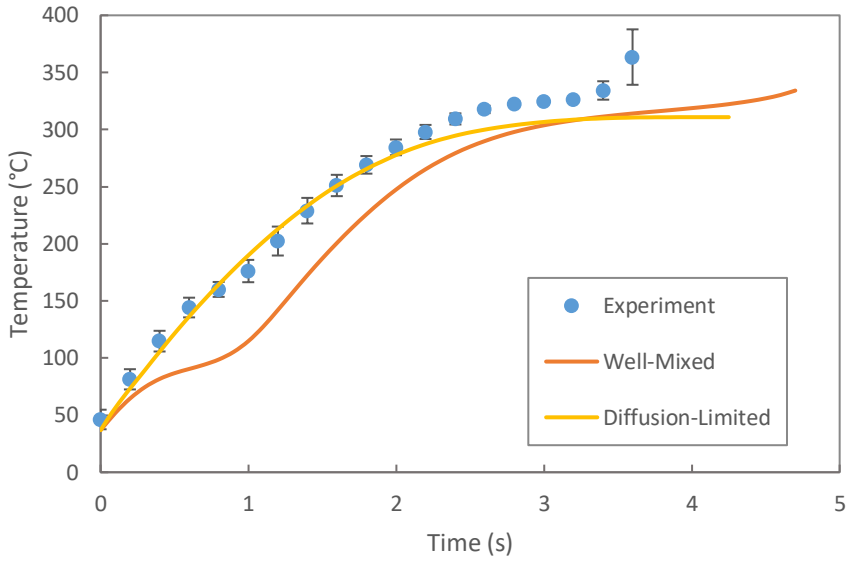

Figure 7-14: Droplet temperature of biodiesel with 20% propanol during droplet evaporation at 700°C

Note: Experimental points give the mean and standard deviation of 8 individual measurements

All droplet temperature figures have shown that the diffusion-limited model is the best model to represent droplet evaporation or propanol-biodiesel blends. This indicates that the movement of liquid components in the droplet caused by liquid diffusion has a significant effect, and that the evaporation of propanol components from the droplet will take longer than what is suggested by the well-mixed model. This also suggests that the composition of liquid components change radially throughout the droplet. These results indicate that the alcohol component remains in the center of the droplet longer throughout the droplet's lifetime, similar to what has been reported from previous droplet evaporation experiments with alcohol-biodiesel blends [17], [18], [19], [20].

7.2.2 Droplet Diameters

Figure 7-15 shows the droplet diameter of PROP5 droplet evaporation with a furnace temperature of 450°C. Both models, the well-mixed and the diffusion-limited models, agree quite well with the experimental droplet diameters. There is slight deviation between the experimental droplet diameters and the models between 6 and 10 seconds. The well-mixed model droplet diameter does decrease slightly just after 1 second. This behaviour is not seen with the diffusion-limited model, in which the diameter continues to increase due to thermal expansion. The diffusion-limited model saw thermal expansion of the droplet due to the higher temperatures (see

Figure 7-7), whereas the well-mixed model predicted lower temperatures and less thermal expansion occurring.

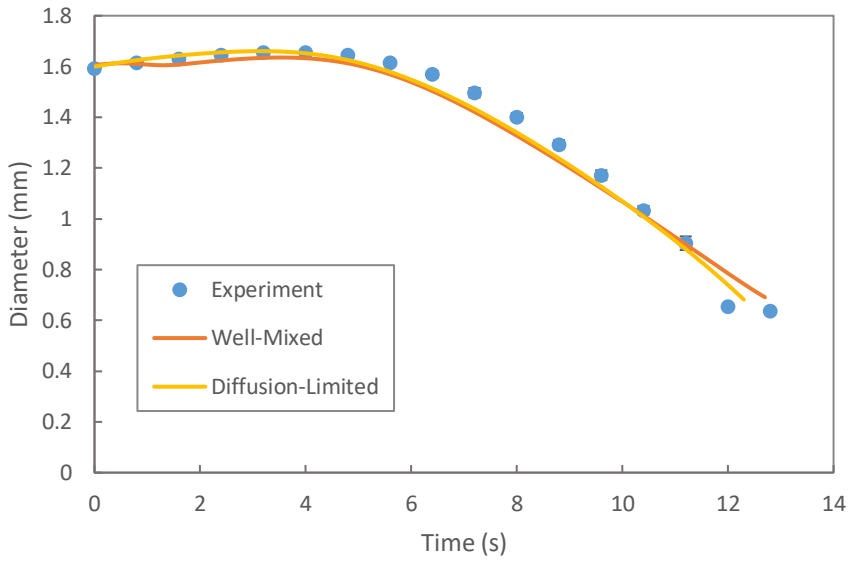

Figure 7-15: Droplet diameter of biodiesel with 5% propanol during droplet evaporation at 450°C

Note: Experimental points give the mean and standard deviation of 8 individual measurements

Figure 7-16 shows the droplet photos during droplet evaporation of PROP5 at a furnace temperature of 450°C. Small specks of light can be seen in the photos at 2.00 and 5.20 seconds. These are created when small bubbles form near the cement bead. The photos at 6.80 and 8.40 seconds show that a large bubble formed but did not reach the size the whole droplet. The bubble corresponds to the time period in which the experimental droplet diameter was greater than the diffusion-limited droplet diameter in Figure 7-15 above.

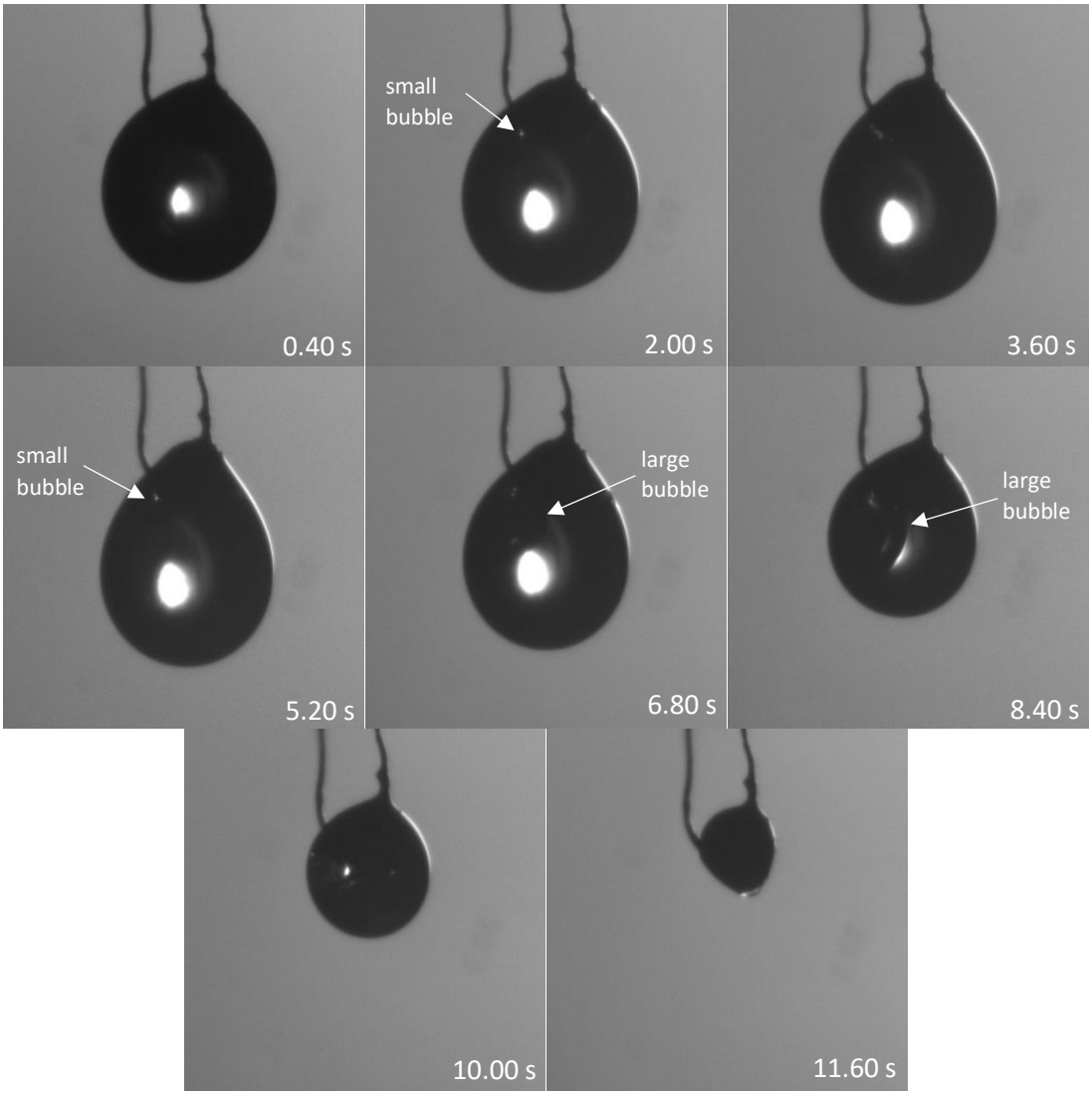

Figure 7-16: Droplet photos of biodiesel with 5% propanol during droplet evaporation at 450°C

Figure 7-17 shows droplet diameters at 450°C for PROP20. Similar to the droplet diameters for PROP5, the experimental values for PROP20 agree best with the diffusion-limited model. However, the deviation between the experimental data and the well-mixed model, specifically when the droplet diameters decrease at 2 seconds for the well-mixed model, is larger for PROP20 than it is PROP5. The experimental droplet diameters still deviates from the diffusion-limited model, in which the experimental droplet diameters were greater than the model between 5.7 and 8.8 seconds, and then the experimental droplet diameters showed a sharp drop to the diameter of the cement bead between 8.8 and 10.4 seconds.

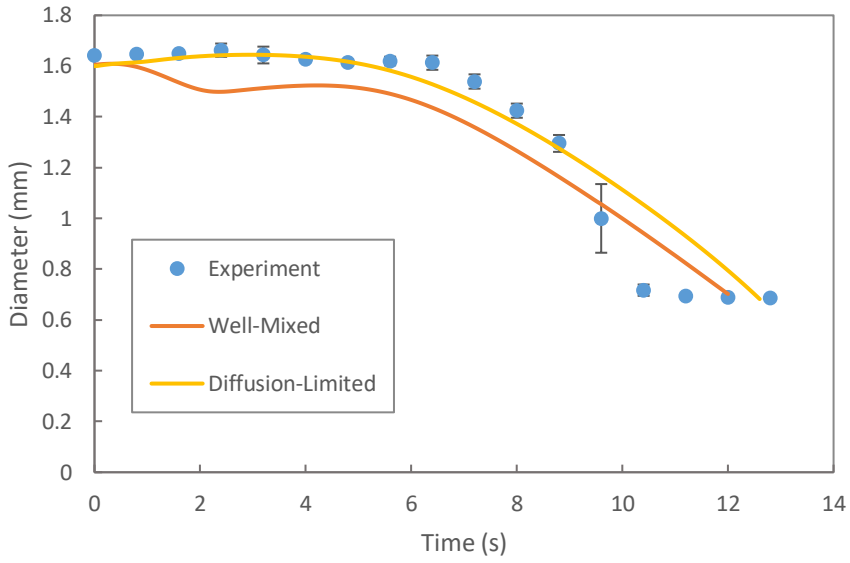

Figure 7-17: Droplet diameter of biodiesel with 20% propanol during droplet evaporation at 450°C

Note: Experimental points give the mean and standard deviation of 8 individual measurements

The droplet photos corresponding to the droplet evaporation of PROP20 at a furnace temperature of 450°C are shown in Figure 7-18. In the photos at 2.00 and 5.20 seconds, small specks of light can be seen near the cement bead, which is caused by the formation of small bubbles near the cement bead. Large bubbles can be seen in the photos at 6.80, 8.40, and 10.00 seconds. The large bubble at 10.00 seconds appears to escape the droplet. Those at 6.80 and 8.40 seconds correlate with the discrepancy between the experimental droplet diameter and the diffusion-limited model's droplet diameter shown in Figure 7-17 above. The droplet photos show the droplet becomes much smaller between 8.40 and 10.00 seconds corresponding to the drop in droplet diameters shown in Figure 7-17 above.

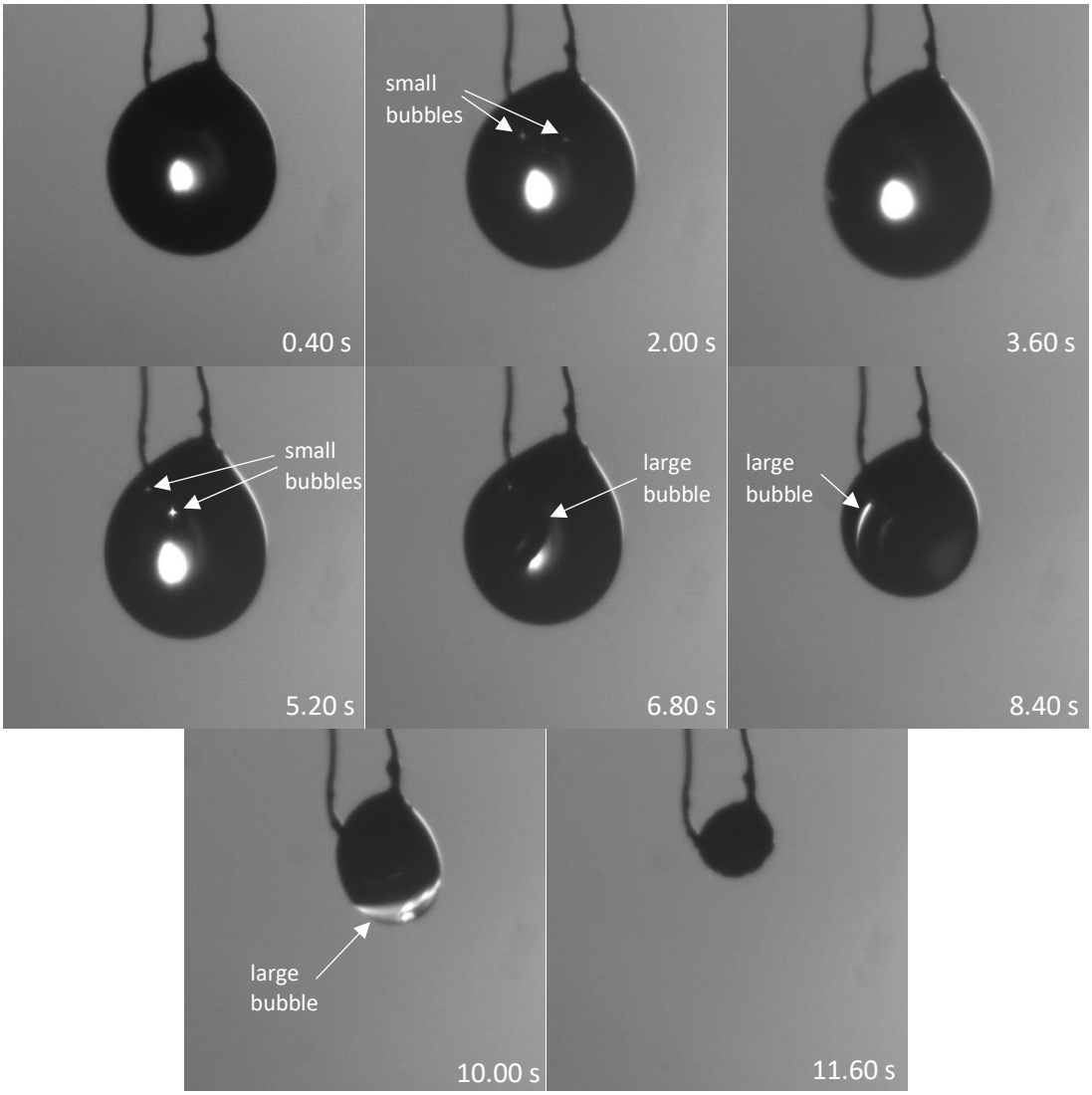

Figure 7-18: Droplet photos of biodiesel with 20% propanol during droplet evaporation at 450°C

Figure 7-19 shows the droplet diameter of PROP5 droplets during droplet evaporation in a furnace with a temperature of 700°C. As shown in the figure, the models deviate significantly from experimental droplet diameters between 2 and 4 seconds. The models both agree well with the experimental droplet diameters between 0 and 2 seconds, but the diffusion-limited model agrees the best.

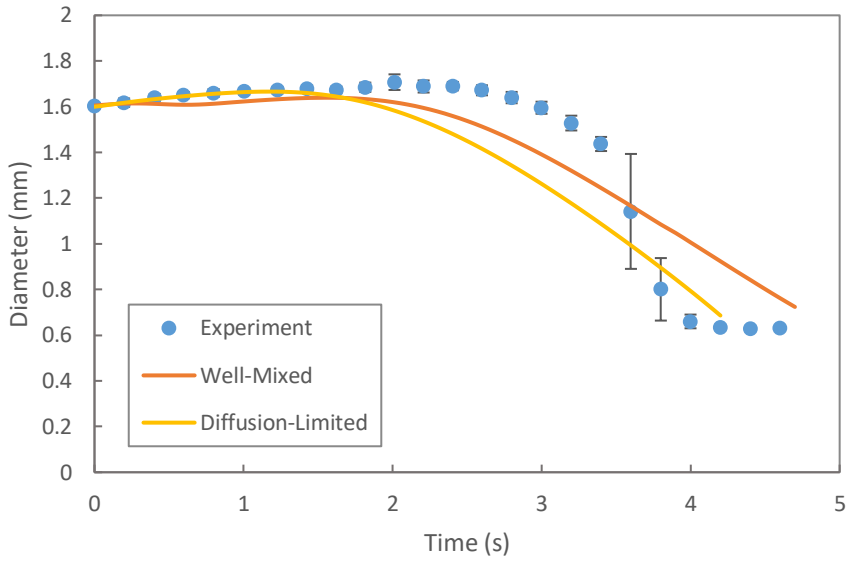

Figure 7-19: Droplet diameter of biodiesel with 5% propanol during droplet evaporation at 700°C

Note: Experimental points give the mean and standard deviation of 8 individual measurements

Figure 7-20 shows the droplet photos for PROP5 at a furnace temperature of 700°C. Droplet photos at 700°C appear more transparent due to radiation from the furnace walls that glow bright red when the furnace temperature is at 700°C. The photos at 0.80 and 1.40 seconds show small bubbles forming near the cement bead. The photos at 2.00, 2.60, and 3.20 seconds show a large bubble, which could have caused the increase in experimental droplet diameter in Figure 7-19. The large bubble shown at 3.20 seconds is large enough that the bubble's volume is close to the droplet's volume. The bubble must have burst after this, and the remaining unevaporated liquid forms a small droplet shown in the photo at 3.80 seconds. Additionally, the droplet photos of 2.00, 2.60, and 3.20 seconds do show the droplet becoming more elongated in the vertical direction and exposing some of the thermocouple to the environment. This could have explained the higher droplet temperatures shown in the last half of droplet evaporation at 700°C, shown in Section 7.2.1.

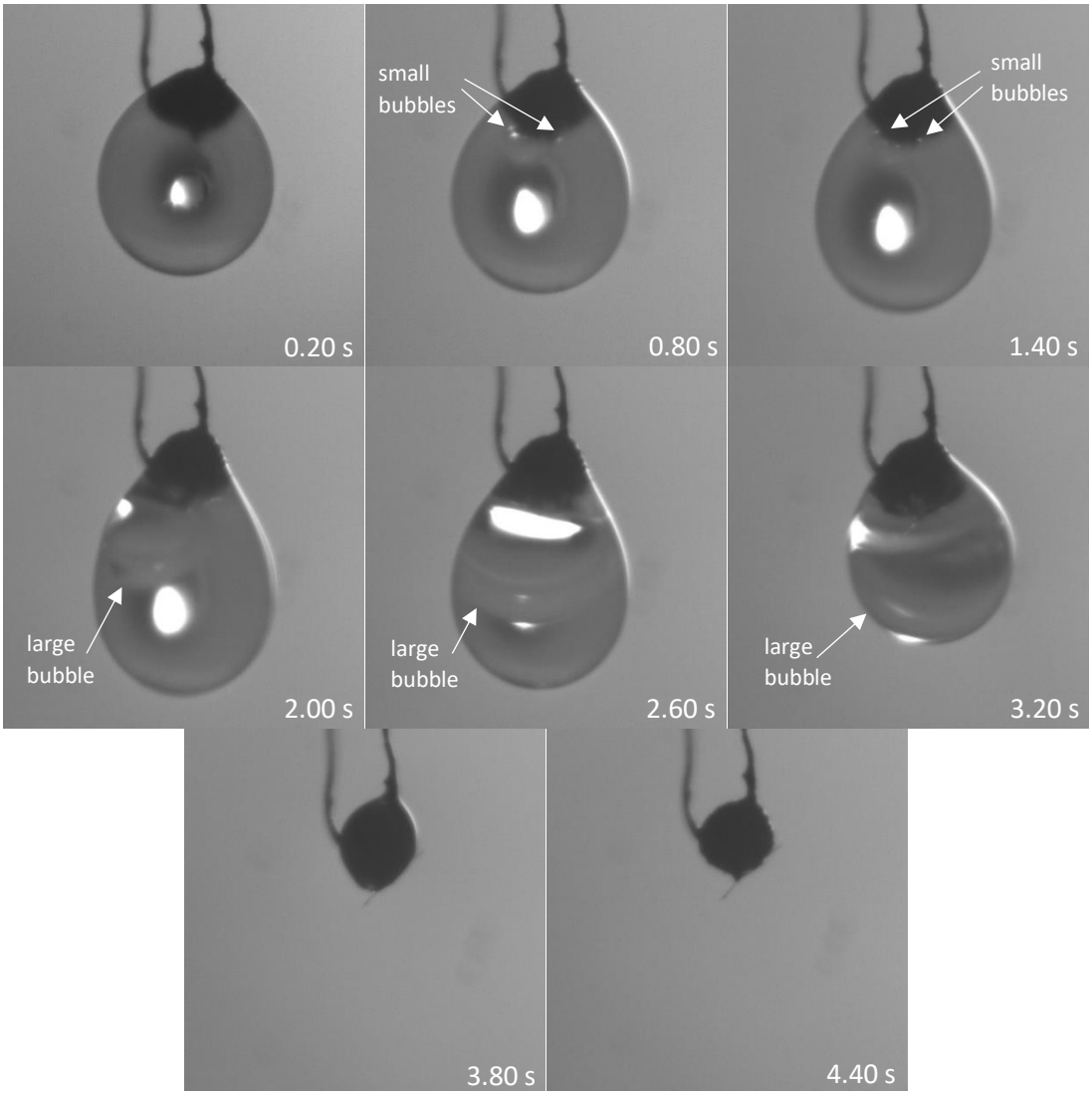

Figure 7-20: Droplet photos of biodiesel with 5% propanol during droplet evaporation at 700°C

The previous pictures have shown that the droplet evaporation of alcohol-biodiesel blends undergo different stages, which are shown in the diagram in Figure 7-21. Initially, the liquid droplet evaporates just at the surface of the droplet, as shown in Figure 7-21 part a). As previously shown, the diffusion-limited model agrees the best with experimental results, which suggests that alcohol components remain in the center of the droplet longer throughout the droplet's lifetime. This could cause the boiling temperature of the center of the droplet to remain low due to the propanol remaining in the center. The droplet temperature will continue to increase and exceed the boiling temperature, as the droplet is heated and if there is a nucleation site, such as the cement bead the droplet hangs on, bubbles will start to form, as shown in Figure 7-21 part b). As the droplet's temperature continue to increase above the boiling temperature of the center of the

droplet, more bubbles will form and merge together to form large bubbles, as shown in Figure 7-21 part c). More bubbles will continue to form during the droplet evaporation process, and these bubbles will merge with the large bubble to make the large bubble larger as shown in Figure 7-21 part d). The surface between the large bubble and the liquid droplet acts as a second surface for evaporation of components to occur, causing the large bubble to become larger. Eventually, the large bubble will become large enough such that it fills the majority of the volume within the droplet, shown in Figure 7-21 part e). In order for the gas in the large bubble to escape to the environment, the large bubble will have to break through the liquid film between the droplet's surface and the bubble's surface. Once the large bubble breaks through the liquid film, the remaining liquid, which has a boiling temperature greater than the droplet's temperature, just needs evaporate as shown in Figure 7-21 part f).

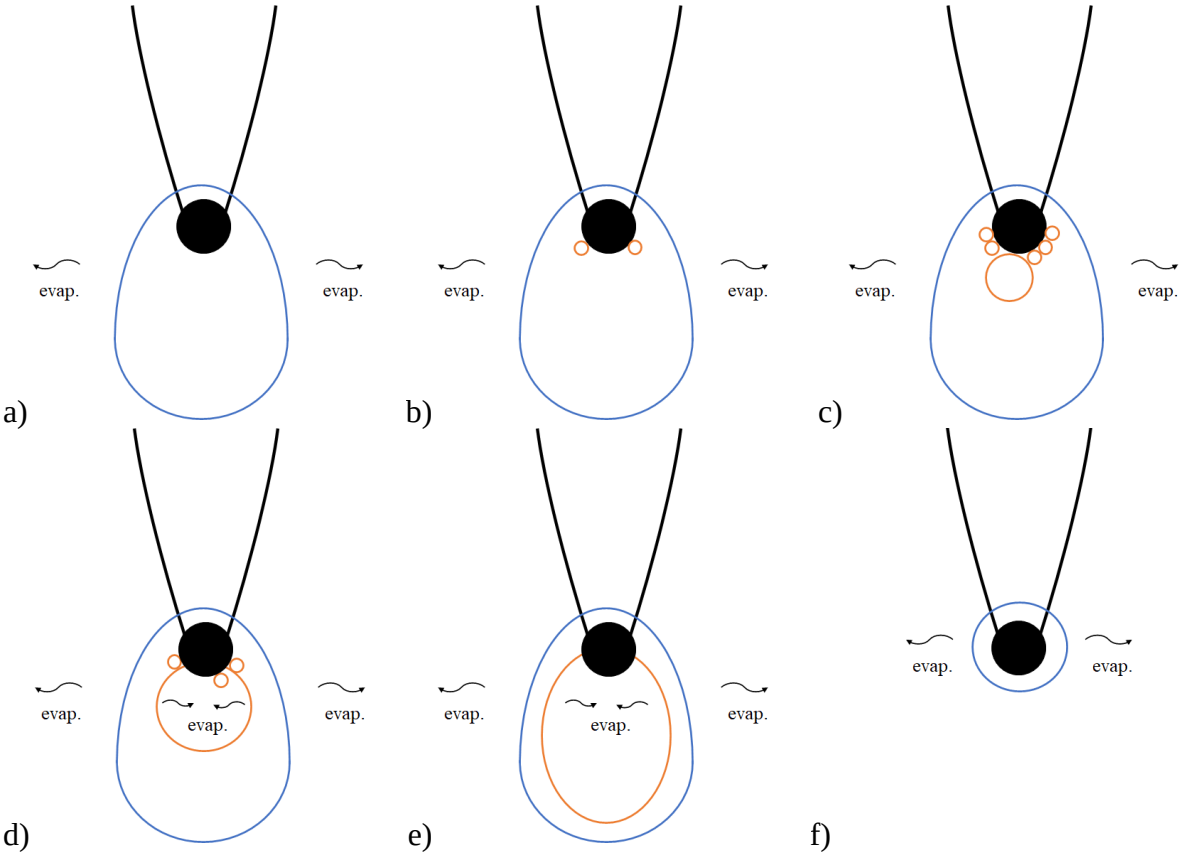

Figure 7-21: Stages of bubbling during droplet evaporation

Figure 7-22 shows the droplet diameter during evaporation of a droplet of PROP20 as well as droplet diameters calculated using the well-mixed and the diffusion-limited numerical models.

Droplet evaporation experiments of PROP20 showed more volatile bubbling, causing the diameter measurements to oscillate for the first 2.5 seconds. As in previous experiments, the well-mixed model did not agree well with experimental droplet diameters since it predicts that all of the propanol evaporates during the first second, causing the droplet diameter to drop. The diffusion-model best represents experimental data, except when large bubbles form, causing the experimental droplet diameter to increase, as shown in the figure below between 0.6 and 1 seconds, and 1.8 and 3 seconds.

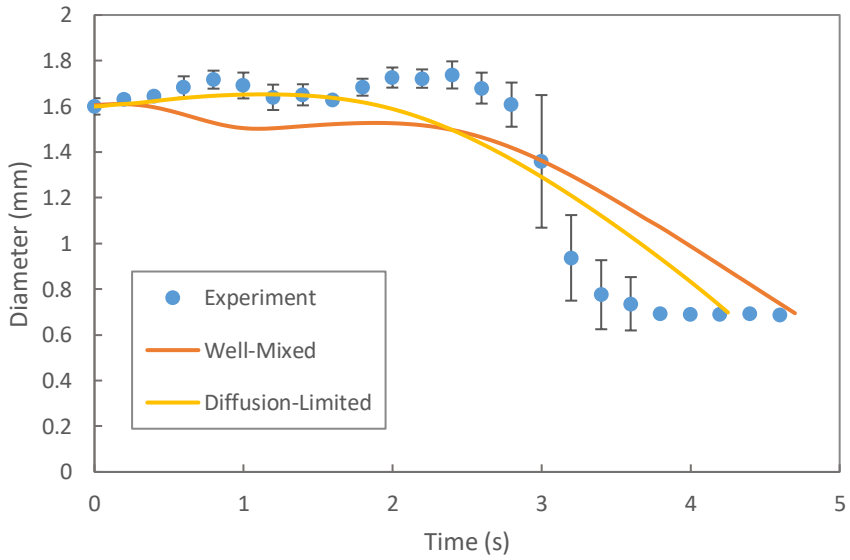

Figure 7-22: Droplet diameter of biodiesel with 20% propanol during droplet evaporation at 700°C

Note: Experimental points give the mean and standard deviation of 8 individual measurements

Figure 7-23 shows the droplet photos during evaporation of PROP20 at a furnace temperature of 700°C. The shaky photos at 0.80 and 2.00 seconds show how volatile the droplet evaporation process can be when the droplet has a large alcohol content such as 20% and is evaporating at a high temperature of 700°C. Theses shaky photos indicate that the droplet is rapidly expanding and contracting due to bubbles forming and escaping the droplet, and it correlates with the peaks of droplet diameters shown at 0.8 and 2 seconds in Figure 7-22. For example, the bubbles near the cement bead at 0.80 seconds could have caused the rapid expanding and contracting. In the photos at 2.00, 2.60, and 3.20 seconds, large bubbles can be seen in the droplet. The photos at 2.00 and 2.60 seconds can correlate with the increased experimental droplet diameters shown in Figure 7-22. The large increase in droplet diameter can cause a higher rate of droplet evaporation.

However, it is the large bubbles escaping the droplet that causes the drastic decrease in droplet diameter between 2.8 and 3.4 seconds, and could be the reason why the droplet diameter at 3.2 seconds is less than the diffusion-limited model's droplet diameter when the photo of 3.20 seconds still shows a bubble present in the droplet. Additionally, the photos at 2.00, 2.60, and 3.20 seconds show that droplet become more vertically elongated and the thermocouple partially exposing itself to the environment. This could have resulted in the higher droplet temperatures shown in Section 7.2.1 for droplet evaporation of PROP20 at 700°C.

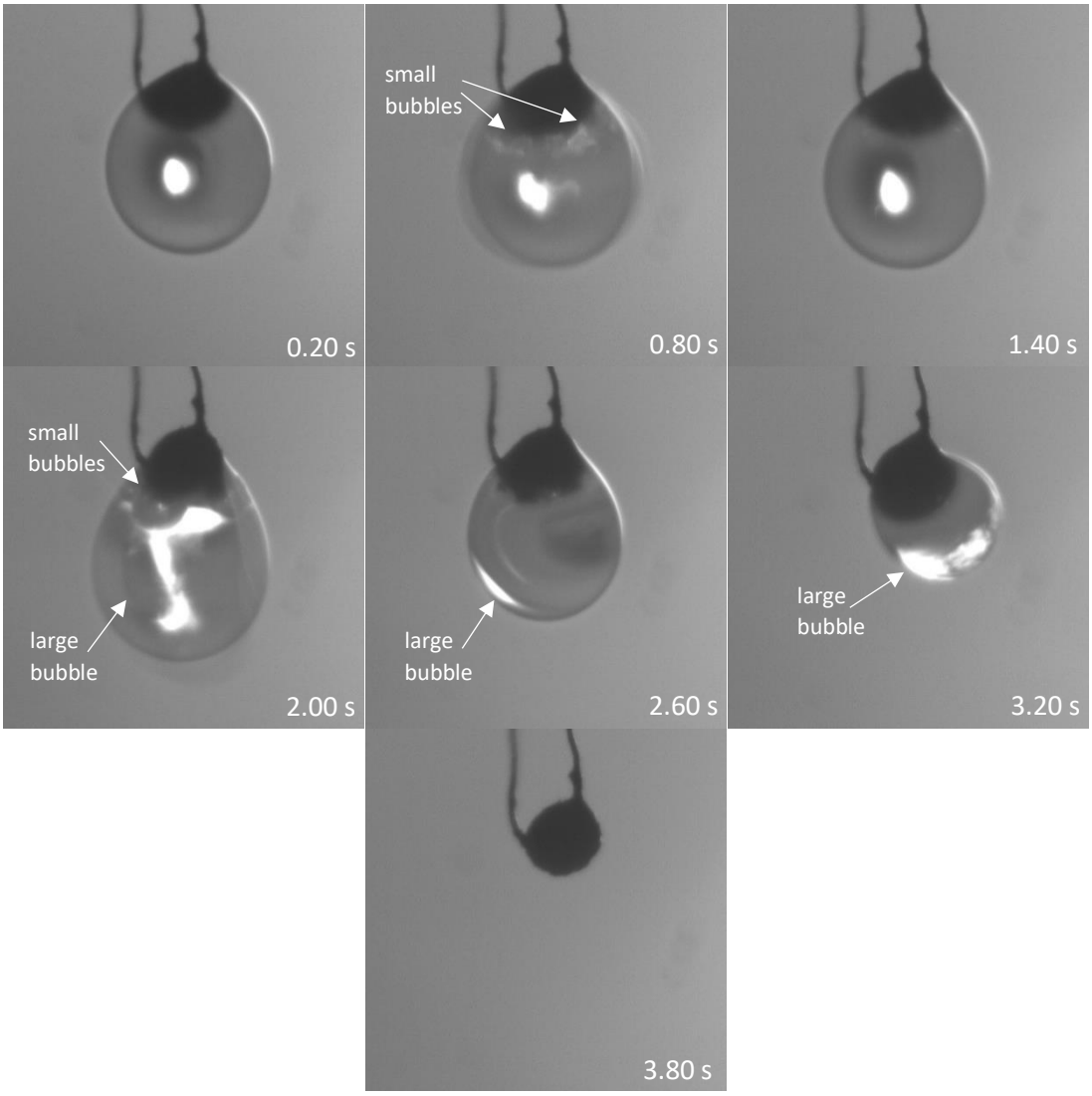

Figure 7-23: Droplet photos of biodiesel with 20% propanol during droplet evaporation at 700°C

As shown in the previous pictures, bubbling does occur within the droplet during the droplet evaporation of PROP5 and PROP20. However, bubbling is not modelled by the numerical

models. To see if the bubbling, specifically the formation of the large bubbles, has an effect on the experimental droplet diameters, the estimated volume of the large bubbles was removed from the experimental droplet volumes and the results are shown as "Adjusted Experiment" in the figures below. This was only done to the droplet evaporation experiments at a furnace temperature of 450°C given that it was easier to identify the perimeter of the large bubbles in photos at 450°C. However, the perimeters of the large bubbles were estimates, even at 450°C, given that the refraction of the light through the droplet and the bubbles can distort the size of the bubbles.

Figure 7-24 shows the adjusted experimental droplet diameters and experimental droplet diameters produce fairly similar results. This suggests that the formation of large bubbles doesn't have an effect on the droplet diameter for PROP5 droplets during evaporation at 450°C.

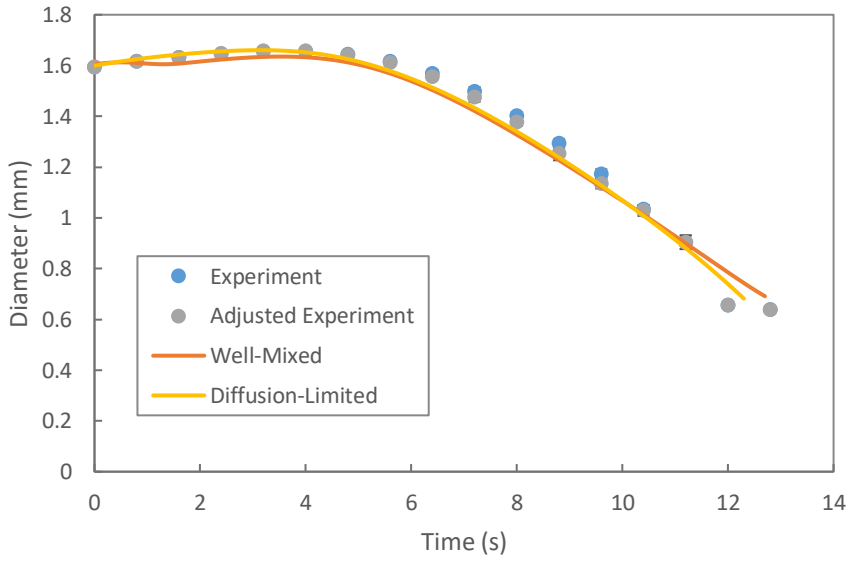

Figure 7-24: Droplet diameter, with adjusted experimental droplet diameter, of biodiesel with 5% propanol during droplet evaporation at 450°C
Note: Experimental points give the mean and standard deviation of 8 individual measurements

Figure 7-25 shows the adjusted experimental diameters for PROP20 in which the experimental diameters are corrected for the volume of the large bubbles. The adjusted experimental results are similar to the diffusion-limited model, but cannot compensate for the effect of the sudden decrease in diameter caused by the bubble bursting.

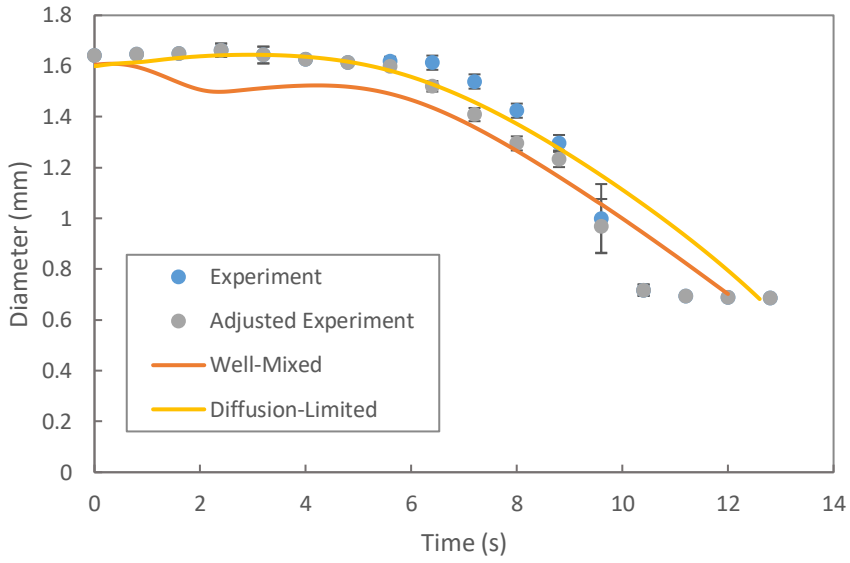

Figure 7-25: Droplet diameter, with adjusted experimental droplet diameter, of biodiesel with 20% propanol during droplet evaporation at 450°C
Note: Experimental points give the mean and standard deviation of 8 individual measurements

The comparison of experimental droplet diameters of propanol-biodiesel blends with the numerical models have shown that the diffusion-limited model was the best model to represent the droplet diameters. Droplet photos have shown that bubbles form within the droplet, usually starting at the thermocouple bead and become more frequent throughout the droplet's lifetime. There was some deviation between the experimental droplet diameters and the droplet diameters calculated using the diffusion-limited model in the last half of the droplet's lifetime, in which the experimental droplet diameters were larger than the model. Droplet photos have shown that the formation of large bubbles causes the increase in experimental droplet diameters. If the approximate volume of the large bubbles is removed from the experimental droplet diameters, the adjusted experimental droplet diameters behave similarly to the model. Additionally, the process of the large bubble escaping the droplet causes a sharp drop in droplet diameters.

7.2.3 Droplet Boiling Temperatures

Boiling and bubbling have been observed within the droplet during droplet evaporation of propanol-biodiesel blends. In order to confirm that boiling and bubbling can occur, the boiling temperatures at different radial position within the droplet are compared with the droplet temperature. Boiling and bubbling can occur as long as the boiling temperature of the liquid is less than the droplet temperature. However, a nucleation site also needs to be present in order for

bubbles to form and the cement bead that the droplet hangs on can act as a nucleation site. (Without a nucleation site, the liquid could superheat beyond its boiling temperature.) The boiling temperatures of the liquid are determined using the concentrations of components at different radial positions as predicted by the diffusion-limited model. Z is the dimensionless radial position within the droplet, where Z is equal to the ratio of the radius at that radial position over the radius of the droplet. For example, Z=0 is the center of the droplet and Z=1 is the surface of the droplet.

Figure 7-26 shows the propanol mol fractions at different radial positions calculated by the diffusion-limited model for droplet evaporation of PROP5 at 450°C. As shown in the figure, the propanol concentration at the center of the droplet (Z=0) remains unchanged for the first 3.2 seconds of the evaporation process. However, at the surface of the droplet (Z=1), the propanol concentration decreases rapidly and is close to zero at 3.2 seconds. At any time during the droplet's lifetime, the propanol concentration increases, up to the initial propanol concentration, as the radial position moves from the surface to the center of the droplet. These concentrations from the diffusion-limited model are used to determine the boiling temperatures.

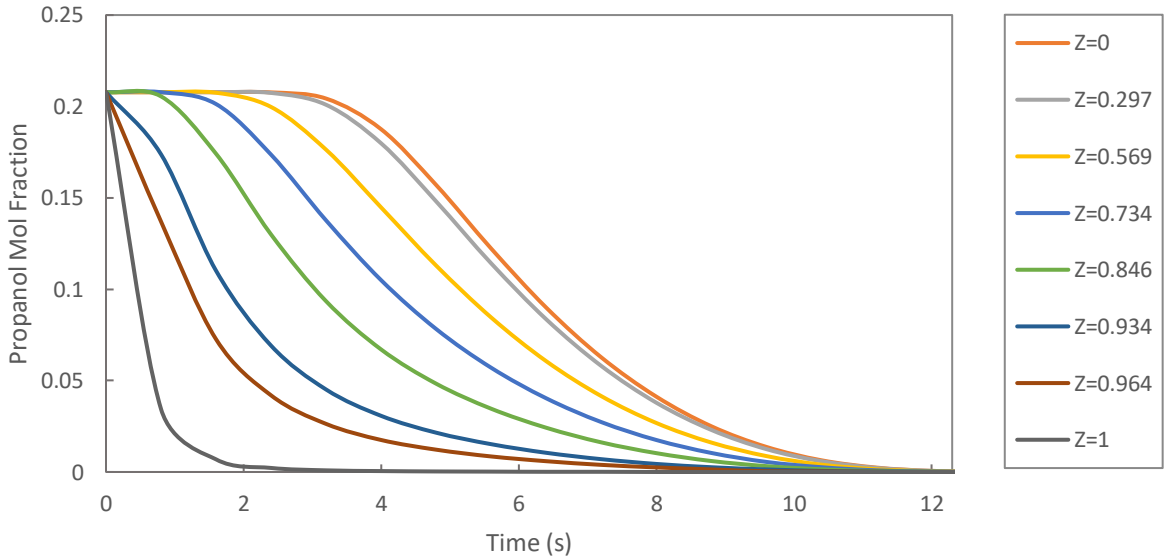

Figure 7-26: Propanol mol fractions at different radial positions for biodiesel with 5% propanol during droplet evaporation at 450°C, where Z=r/R

Figure 7-27 shows the droplet temperature with the boiling temperatures at different radial positions within the droplet during droplet evaporation of PROP5 at a furnace temperature of 450°C. As shown in the figure below, for most of the droplet, i.e. for Z=0 to 0.964, the boiling

temperature falls below the droplet's temperature between roughly 2 and 8 seconds. Therefore, this suggests that internal boiling can occur for the PROP5 droplet through most of the droplet lifetime. At the surface, evaporation occurs below the boiling point, since the surface is exposed to the atmosphere, but the inside of the droplet must reach the bubble point in order to boil or form bubbles.

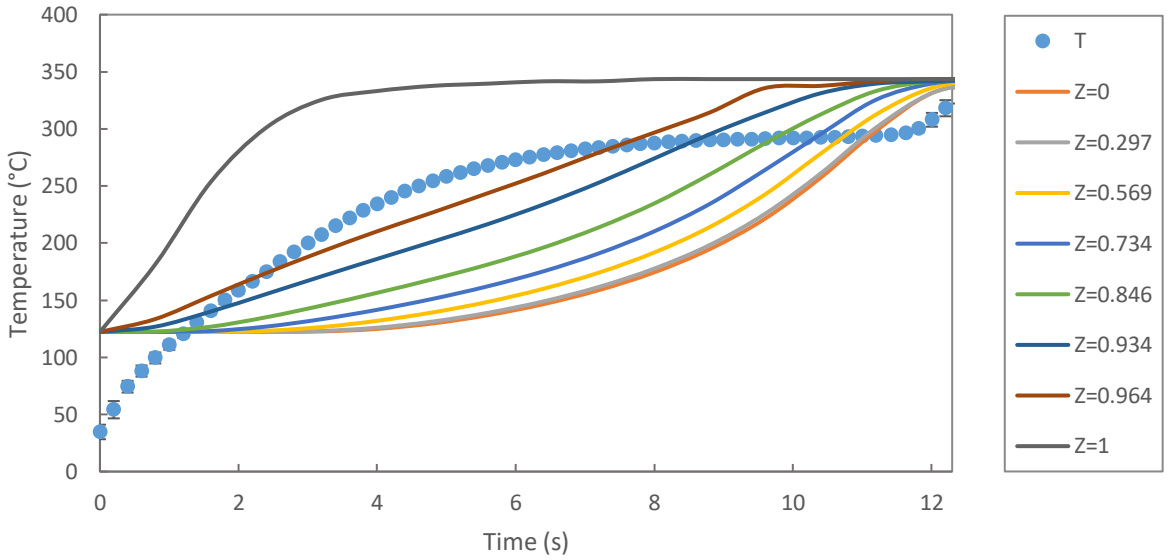

Figure 7-27: Droplet temperature and boiling temperature at different radial positions for biodiesel with 5% propanol during droplet evaporation at 450°C, where Z=r/R
Note: Experimental points give the mean and standard deviation of 8 individual measurements

Figure 7-28 shows the temperature of a droplet of PROP20 and the boiling temperature curves at different radial positions in the droplet. Compared to the droplet of PROP5 the boiling temperatures in the PROP20 droplets are lower and fall below the droplet's temperature for a longer period of time. This indicates more vigorous internal boiling, which is indeed what was observed.

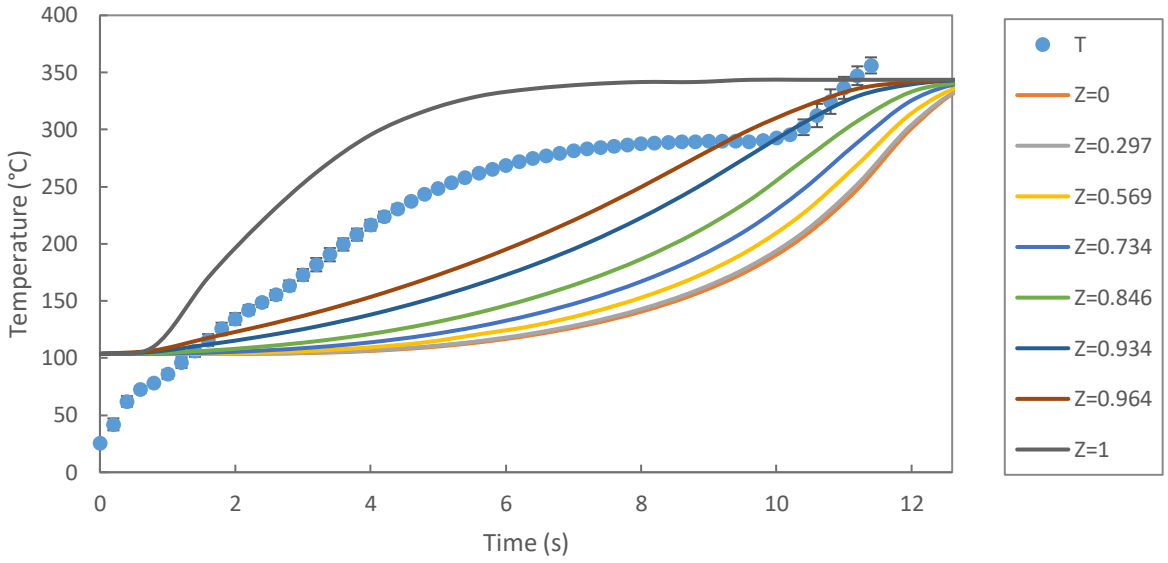

Figure 7-28: Droplet temperature and boiling temperature at different radial positions for biodiesel with 20% propanol during droplet evaporation at 450°C, where Z=r/R
Note: Experimental points give the mean and standard deviation of 8 individual measurements

Figure 7-29 shows the droplet temperature and the boiling temperature at different radial positions within the droplet for a droplet of PROP5 at a furnace temperature of 700°C. The boiling temperature at radial positions of Z=0 to 0.982 becomes less than the droplet temperature starting roughly at 0.75 seconds, and then the boiling temperatures remain below the droplet temperatures for the remainder of the droplet's lifetime, whereas the surface boiling temperatures always remain above the droplet temperature since the mixture at the surface can evaporate into the atmosphere without reaching the boiling temperature. The increase of the droplet temperatures at the end of the droplet's lifetime is not reproduced by the diffusion-limited model, since this model could only include two fuel fractions, the alcohol component and the FAME continuous mixture. Therefore, boiling or the formation of bubbles can start to occur at about 0.75 seconds for a droplet of PROP5 as long as there is a nucleation site present, such as the cement bead that the droplet hangs on.

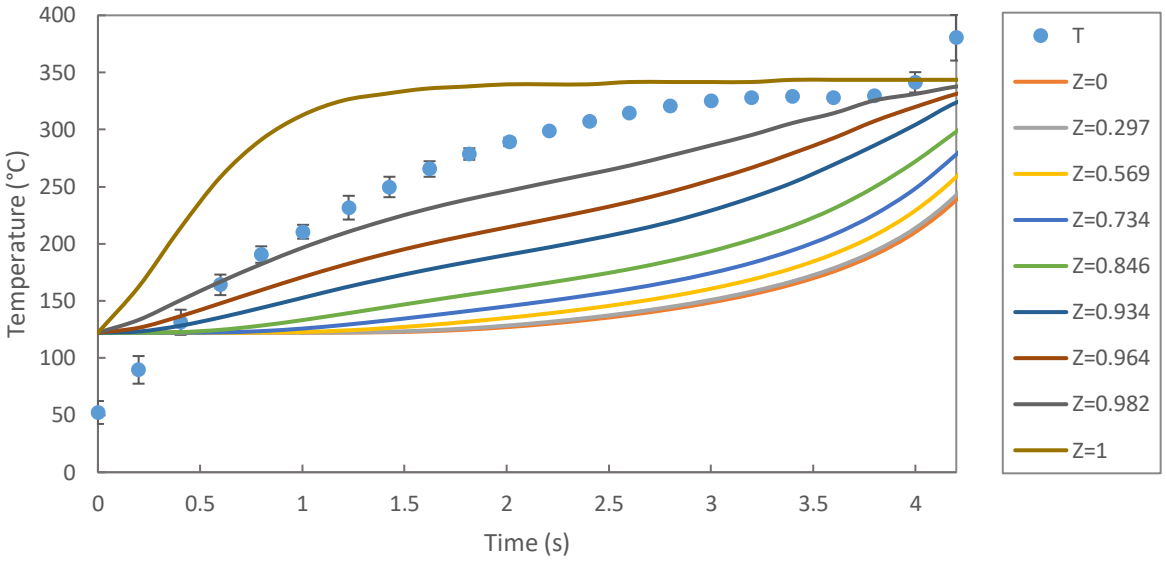

Figure 7-29: Droplet temperature and boiling temperature at different radial positions for biodiesel with 5% propanol during droplet evaporation at 700°C, where Z=r/R
Note: Experimental points give the mean and standard deviation of 8 individual measurements

Figure 7-30 shows the droplet temperature with the boiling temperatures at different radial positions for droplet evaporation of PROP20 at 700°C. The boiling temperature drops below the droplet's temperature at 0.4 seconds for Z=0 to 0.982, whereas the boiling temperature of the surface remains above the droplet temperature up to the end of the droplet's lifetime. This again shows that boiling and bubble formation can start to occur at 0.4 seconds as long as there is a nucleation site present.

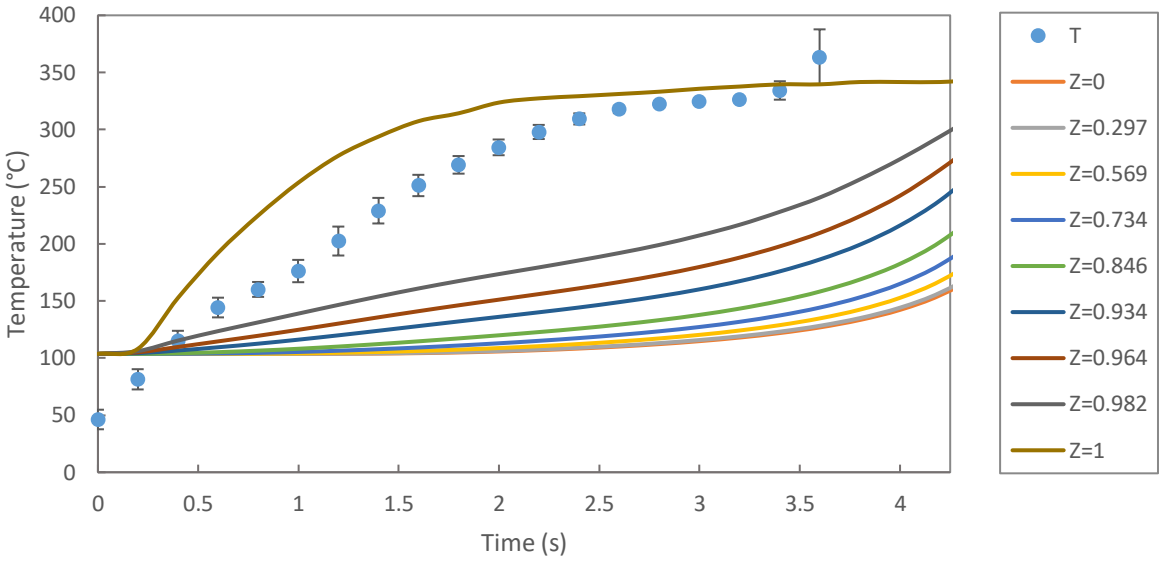

Figure 7-30: Droplet temperature and boiling temperature at different radial positions for biodiesel with 20% propanol during droplet evaporation at 700°C, where Z=r/R
Note: Experimental points give the mean and standard deviation of 8 individual measurements

This section has confirmed that the radial variation of the liquid composition of propanol-biodiesel droplets does allow internal boiling and bubble formation to occur, given that most of the droplet's boiling temperature is less than the droplet's temperature. In fact, the boiling temperature of the droplet reaches below the droplet's temperature during the first quarter of the droplet's lifetime. However, the boiling temperature of the surface of the droplet remains above the droplet's temperature throughout the droplet's lifetime. These calculations were unable to determine when the formation of large bubbles starts to occur, as in when the experimental results will start to deviate from the diffusion-limited model. Additionally, the models assume a uniform liquid temperature, but some radial temperature change is expected to occur, such that the temperature at the center of the droplet will be lower than the temperature at the surface of the droplet. This might slightly reduce the range in which boiling and bubble formation can start to occur within the droplet. The experimental temperatures represent some sort of average liquid temperature and are probably slightly less than the surface temperatures.

7.2.4 Summary of Results for Propanol-Biodiesel

Droplet evaporation experiments of propanol-biodiesel droplets have confirmed that the liquid phase of alcohol-biodiesel droplets is not uniformly mixed but depends to some extent on liquid diffusion processes. Because of this, the diffusion-limited model was best able represent droplet temperature data. The model was also best able to represent the droplet diameter data

during the first half of the droplet's lifetime. The formation of large bubbles causes the experimental droplet diameters to become larger than expected for the last half of the droplet's lifetime. The formation of bubbles occur due to the large propanol concentration that remains in the center of the droplet longer throughout the droplet's lifetime, causing the boiling temperature of the inner portion of the droplet to reach below the droplet's temperature. Experiments and calculations were also performed with biodiesel with 10% (v/v) and 15% (v/v) propanol, the results of which can be found in Appendix D: Additional Results for Biodiesel Propanol Mixtures.

7.3 Pentanol-Biodiesel Mixtures

Droplet evaporation experiments were also performed for pentanol-biodiesel blends to see if the trends shown for propanol-biodiesel blends also occur for them. The droplet evaporation experiments for pentanol-biodiesel blends were performed similarly to the propanol-biodiesel blends in which liquid droplets with the volume of 2 μL was hanged onto a thermocouple bead of ~0.6 mm, giving an effective initial droplet diameter of 1.6 mm. Additionally, experiments were performed at furnace temperatures of 450°C and 700°C. The results of these experiments are shown in the sections below.

7.3.1 Droplet Temperatures

Figure 7-31 shows the droplet temperature for the droplet evaporation of biodiesel with 5% (v/v) pentanol (PENT5) at a furnace temperature of 450°C. The well-mixed model and the diffusion-limited model both agree quite well with the experimental droplet temperature data. The well-mixed model does still show a little deviation from experimental droplet temperature; however, this is less obvious for the PENT5 blend than it is for the PROP5 blend. The experimental droplet temperature does increase at the end due to the transitions from mainly FAME components evaporating to MGC components evaporation and the thermocouple bead starts to become exposed to the environment at the end of the droplet's lifetime.

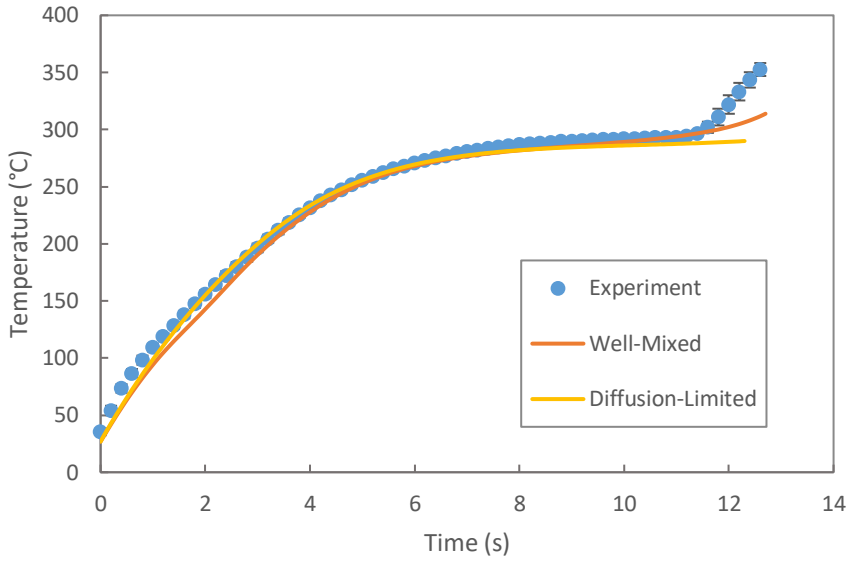

Figure 7-31: Droplet temperature of biodiesel with 5% pentanol during droplet evaporation at 450°C

Note: Experimental points give the mean and standard deviation of 8 individual measurements

Figure 7-32 shows the droplet temperatures for the droplet evaporation of biodiesel with 20% (v/v) pentanol (PENT20) blends at a furnace temperature of 450°C. The diffusion-limited model was best able to represent the droplet temperatures for PENT20 blends. At 20% (v/v) pentanol concentration, the deviation between the well-mixed model and the experimental droplet temperatures are more pronounced. The flattening of the well-mixed temperature curve for the PENT20 blends occurs later in the droplet's lifetime, between 2 and 4 seconds, and at higher temperatures, between 100°C and 200°C, than for PROP20 blends, for which this occurred between 0 and 2 seconds and between 50°C and 150°C (see Figure 7-8 and Figure 7-14). This makes sense, since pentanol has a higher boiling point (specifically 136°C [55]) than propanol (97°C [56]), and the well-mixed temperature curve flattens when all of the alcohol component is evaporating.

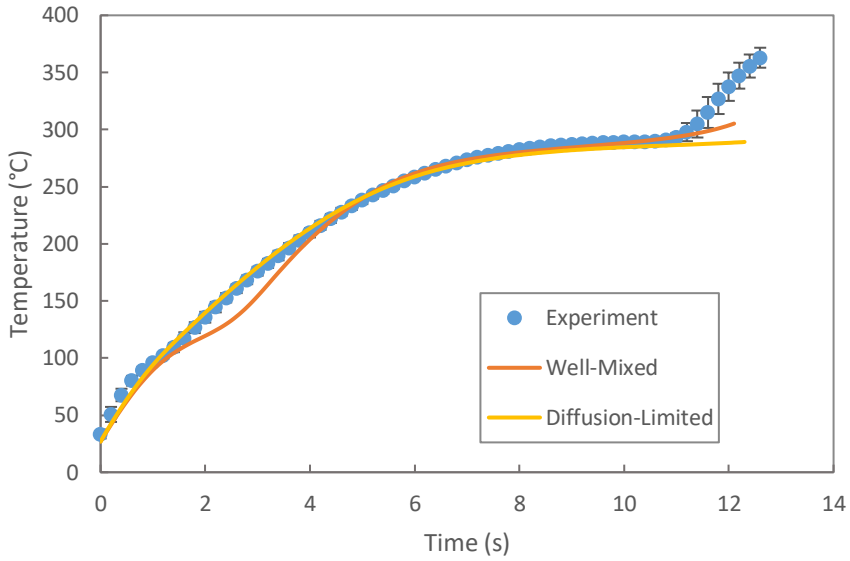

Figure 7-32: Droplet temperature of biodiesel with 20% pentanol during droplet evaporation at 450°C

Note: Experimental points give the mean and standard deviation of 8 individual measurements

Figure 7-33 shows the effect of the mixing factor on the diffusion-limited model for PENT20 at 450°C and Figure 7-34 shows the same thing but for the time range between 0 and 6 seconds. As shown in both figures, reducing the mixing factor to 1 causes the diffusion-limited model to move away from the well-mixed model, whereas increasing the mixing factor to 10 cause the diffusion-limited model to move towards the well-mixed model. As the mixing factor continues to increase, eventually the diffusion-limited model will behave exactly like the well-mixed model. However, previous work on internal mixing in the droplet during evaporation has shown that a mixing between 2 and 4 should be used [36], [42], [43]. For this work, a mixing factor of 3 was chosen.

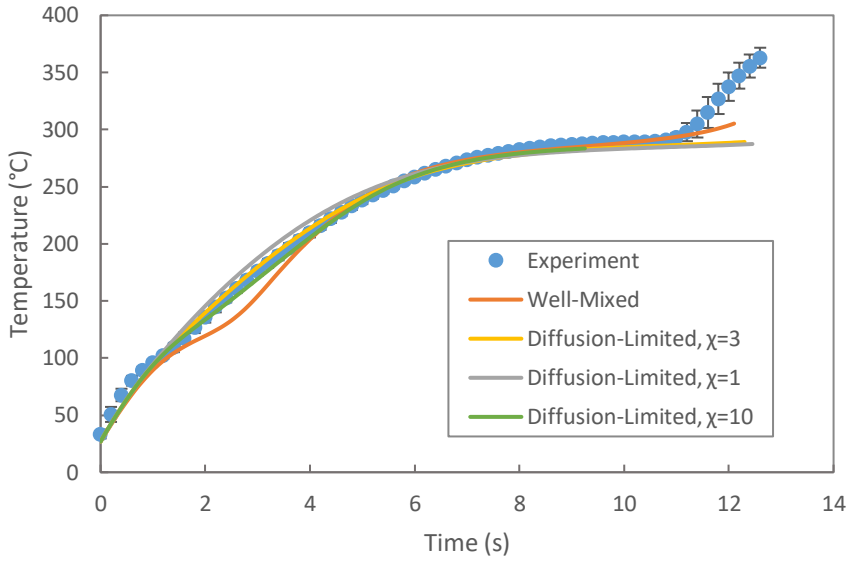

Figure 7-33: Droplet temperature of biodiesel with 20% pentanol during droplet evaporation at 450°C with varying mixing factor, χ
Note: Experimental points give the mean and standard deviation of 8 individual measurements

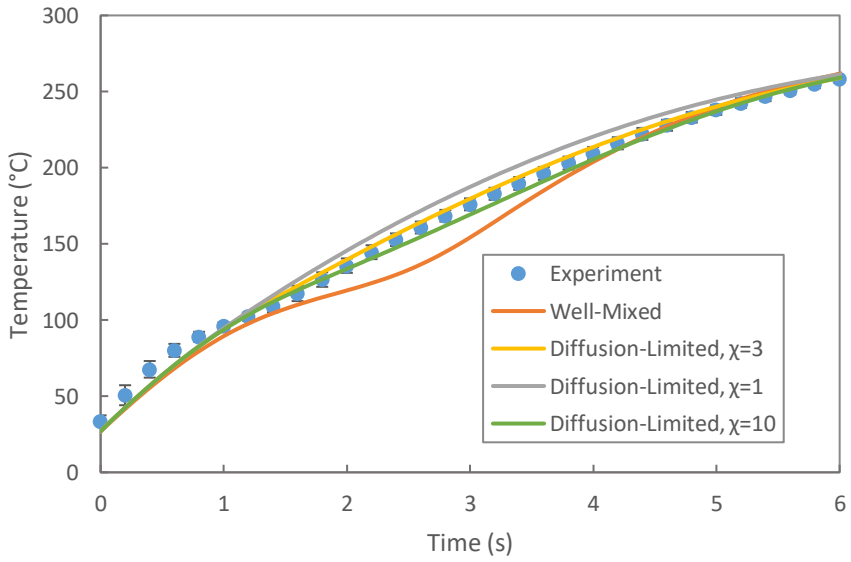

Figure 7-34: Droplet temperature of biodiesel with 20% pentanol during droplet evaporation at 450°C with Varying Mixing Factor, χ, between 0 and 6 seconds
Note: Experimental points give the mean and standard deviation of 8 individual measurements

Figure 7-35 shows the droplet temperature for the droplet evaporation of PENT5 at a furnace temperature of 700°C. The diffusion-limited model was best able to represent the droplet temperatures. Again, the well-mixed model deviates from the experimental data as most of the

liquid pentanol evaporates in the first 1 to 2 seconds of the droplet evaporation lifetime, reducing droplet temperatures. The experimental droplet temperatures are about 15°C greater than the diffusion-limited model when the droplet temperature curve flattens between 2.8 and 4 seconds. Droplet photos in Section 7.3.2 do show the droplet become more vertically elongated during this time period, thus exposing some of the thermocouple to the environment and increasing the measured temperature.

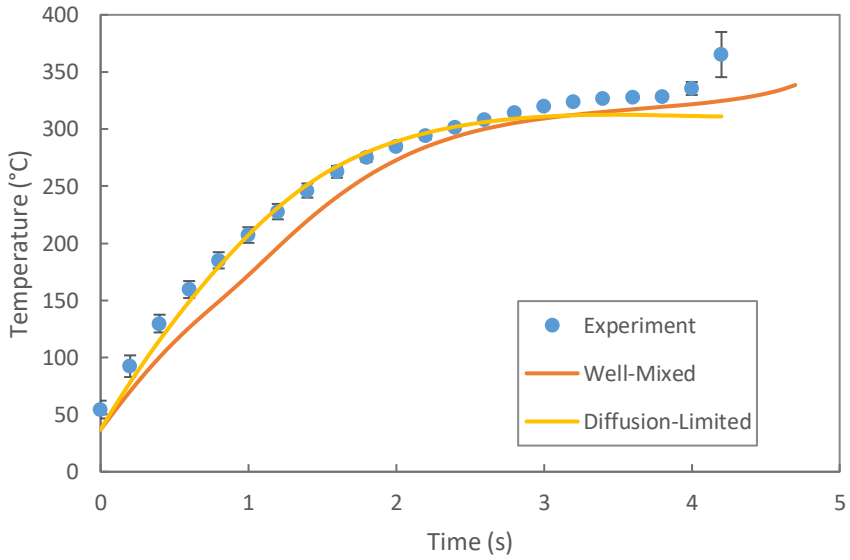

Figure 7-35: Droplet temperature of biodiesel with 5% pentanol during droplet evaporation at 700°C

Note: Experimental points give the mean and standard deviation of 7 individual measurements

Figure 7-36 shows the droplet evaporation of PENT20 at a furnace temperature of 700°C. The diffusion-limited model was best able to represent the droplet temperatures, whereas the well-mixed model still shows the temperature curve flattening in the first second as the pentanol evaporates from the droplet. The experimental droplet temperatures do drop slightly lower than the diffusion-limited model between 1 and 2 seconds, suggesting that a different mixing factor, possibly a larger mixing factor should be used when modelling droplet evaporation of pentanol-biodiesel blends at high temperatures. However, this is unlikely given that previous work has suggested that the mixing factor should be between 2 and 4 [36], [42], [43].

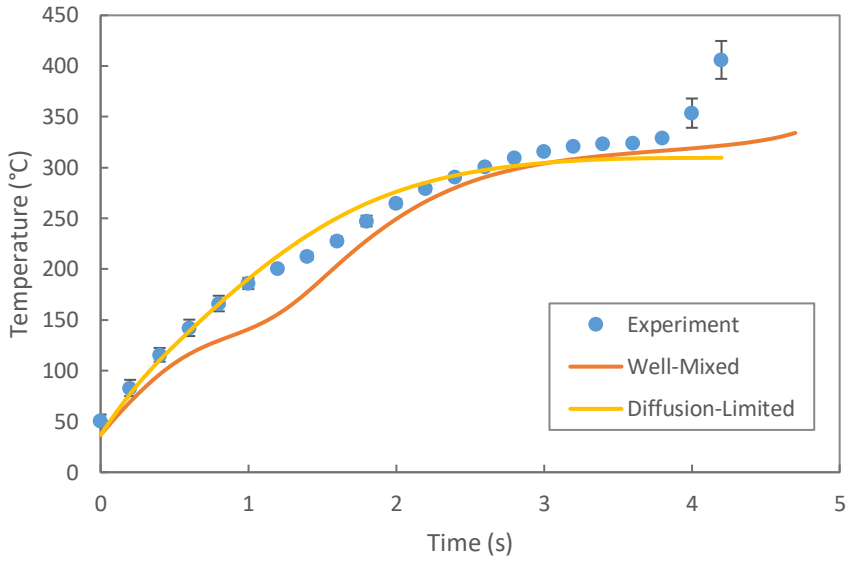

Figure 7-36: Droplet temperature of biodiesel with 20% pentanol during droplet evaporation at 700°C

Note: Experimental points give the mean and standard deviation of 7 individual measurements

Figure 7-37 shows the same results as Figure 7-36 but also include droplet temperatures calculated from the diffusion-limited model that use a higher mixing factor of 10. These results show how a high mixing factor affects the diffusion-limited model, in which the calculated droplet temperatures for χ=10 is lower for χ=3 between 0.6 and 2 seconds. Further increasing the mixing factor should make the results of the diffusion-limited model to approach the results of the well-mixed model. However, the figure shows that the difference between the experimental droplet temperatures and the diffusion-limited model with χ=3 occurs later than the difference between χ=10 and χ=3, which suggests something else is the more probable cause and a higher mixing factor is not required to be used in this case.

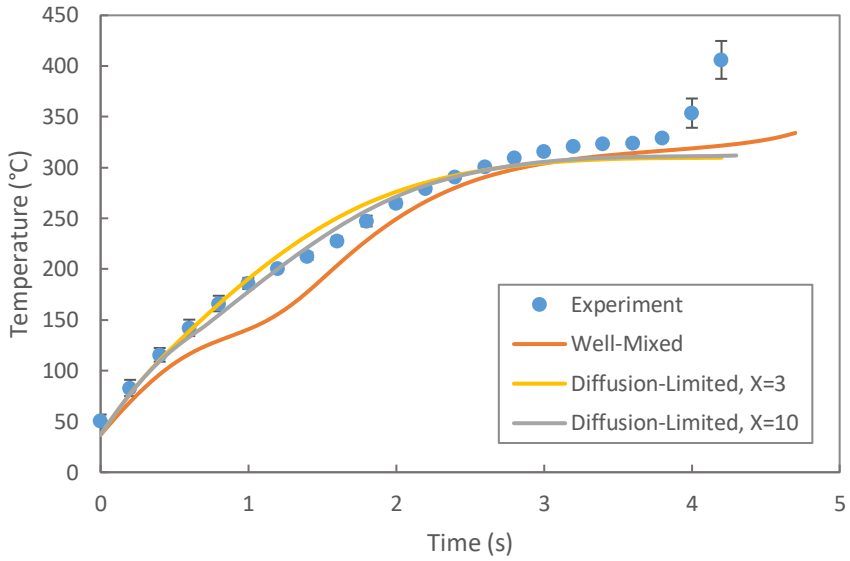

Figure 7-37: Droplet temperature of biodiesel with 20% pentanol during droplet evaporation at 700°C with diffusion-limited model using χ=10
Note: Experimental points give the mean and standard deviation of 7 individual measurements

The more probable cause of the dip in droplet temperatures shown in Figure 7-36 is that some large bubbles escaping the droplet between 1 and 2 seconds, causing a high molar flux of evaporated components away from the droplet and decreasing the heat sent to the droplet for droplet heating. Figure 7-44 in Section 7.3.2 shows a drop in droplet diameter at ~1.5 seconds, suggesting bubbles have escaped, causing the sudden decrease in diameters. This bubbles escaping would result in a higher molar flux of evaporated components and thus causing the droplet temperature to increase at a slower rate. The experimental droplet temperatures also remain about 10°C above the diffusion-limited model's droplet temperature when the temperature curves flatten, between 2.6 and 3.8 seconds, a similar behaviour that was observed for other mixtures at 700°C, in which droplet becomes vertically elongated and exposing some of the thermocouple to the environment and caused the higher droplet temperatures.

The droplet temperature figures have shown that the diffusion-limited model is best able to represent pentanol-biodiesel blends. The well-mixed model continues to show all of the pentanol components evaporating early in the droplet's lifetime, but at higher temperatures due to pentanol's higher boiling point. Additionally, the droplet evaporation of pentanol-biodiesel blends shows the same characteristics as propanol-biodiesel blends, in which the liquid phase of the

droplet depends on diffusion processes such that a high alcohol concentration remains in the center of the droplet longer in the droplet's lifetime.

7.3.2 Droplet Diameters

Figure 7-38 shows the droplet diameters during droplet evaporation of PENT5 at a furnace temperature of 450°C. The figure also includes the droplet diameters calculated using the well-mixed model and the diffusion-limited model. The two models actually produce similar results, in which the decrease in droplet diameter at 2 seconds due to most of the pentanol evaporating for the well-mixed model is not as visible as previous alcohol-biodiesel mixtures. This is expected given that previous work with well-mixed and diffusion-limited models shows that the difference between the two models decrease when the boiling points between the components in the mixture is reduced [38], [57]. The models were able to reproduce experimental droplet diameters for the first 5 seconds, after which the experimental droplet diameters were greater than the models, which could be due to the formation of large bubbles within the droplet.

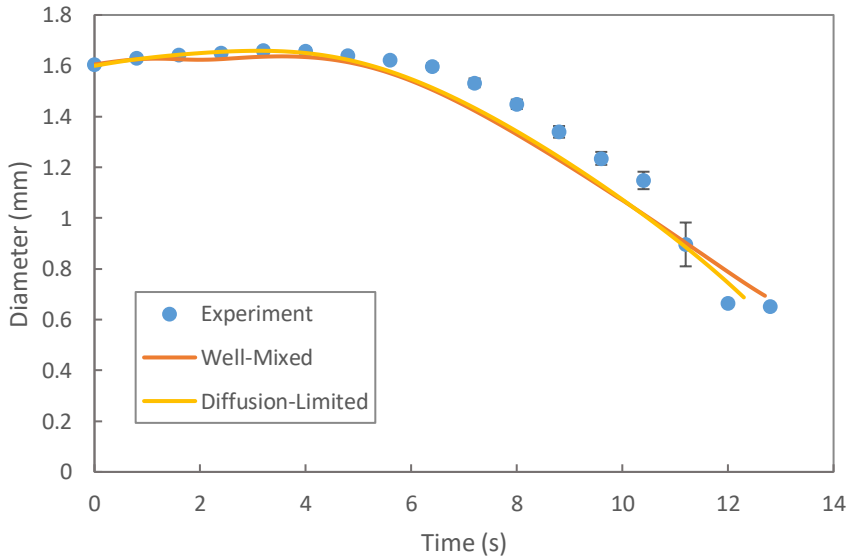

Figure 7-38: Droplet diameter of biodiesel with 5% pentanol during droplet evaporation at 450°C

Note: Experimental points give the mean and standard deviation of 8 individual measurements

Figure 7-39 shows droplet photos during the droplet evaporation of PENT5 at a furnace temperature of 450°C. A small light speck can be seen at 2.00 seconds, which could be the formation of a small bubble near the cement bead. The photos at 6.80 and 8.40 seconds show large bubbles in the droplet, which correlates with the increase in experimental droplet diameters in

Figure 7-38 above. Additionally, a small bubble can be seen present alongside the large bubble at 8.40 seconds, which shows that small bubbles continue to form even when a large bubble is present.

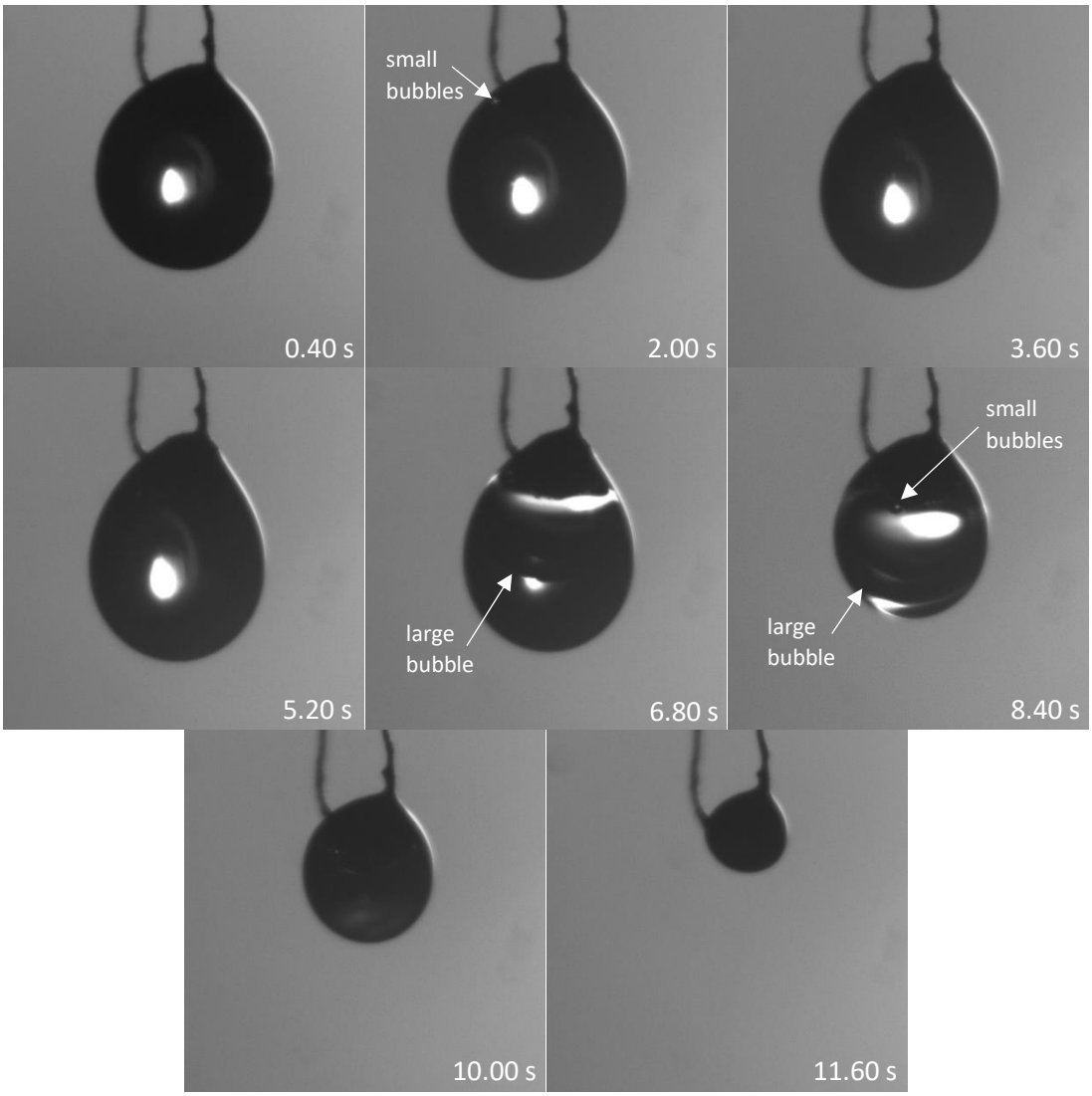

Figure 7-39: Droplet photos of biodiesel with 5% pentanol during droplet evaporation at 450°C

Figure 7-40 shows the droplet diameters during droplet evaporation of PENT20 at a furnace temperature of 450°C. The diffusion-limited model was best able to represent experimental droplet diameters whereas the well-mixed model shows the droplet diameter decreasing at 2 seconds due to most of the pentanol component evaporating. The diffusion-limited model was able to predict experimental droplet diameters for the first 5 seconds. Afterwards, the experimental droplet diameters were larger than the calculated droplet diameters from the diffusion-limited model, probably due to the formation of large bubbles.

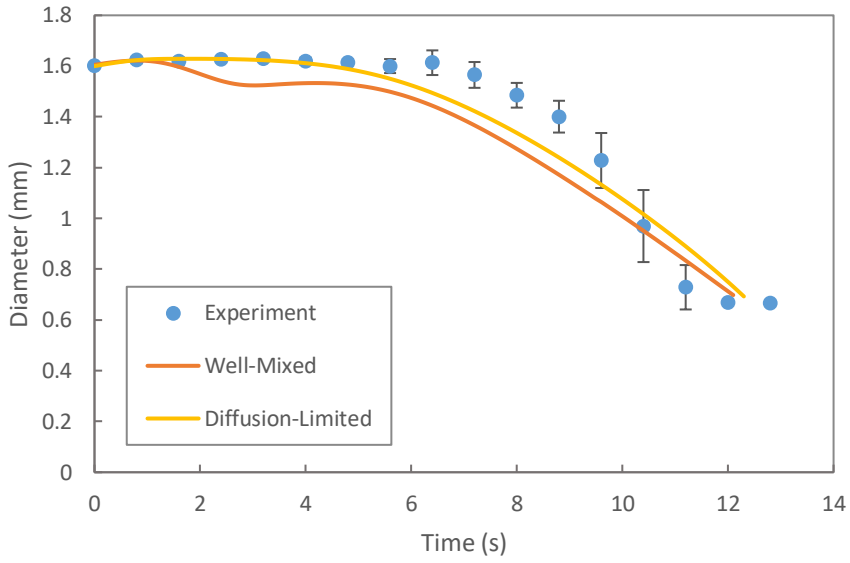

Figure 7-40: Droplet diameter of biodiesel with 20% pentanol during droplet evaporation at 450°C

Note: Experimental points give the mean and standard deviation of 8 individual measurements

Figure 7-41 shows the droplet photos during the evaporation of PENT20 at 700°C. Small flashes of light can be seen near the cement bead in the photos at 2.00, 3.60, and 5.20 seconds, which represent small bubbles forming near the cement bead. Large bubbles can be seen in droplet photos at 6.80, 8.40, and 10.00 seconds, which correlates with the increase in experimental droplet diameters in Figure 7-40 above. A small bubble, which is shown as a small flash of light, can also be seen alongside the large bubble at 6.80 seconds.

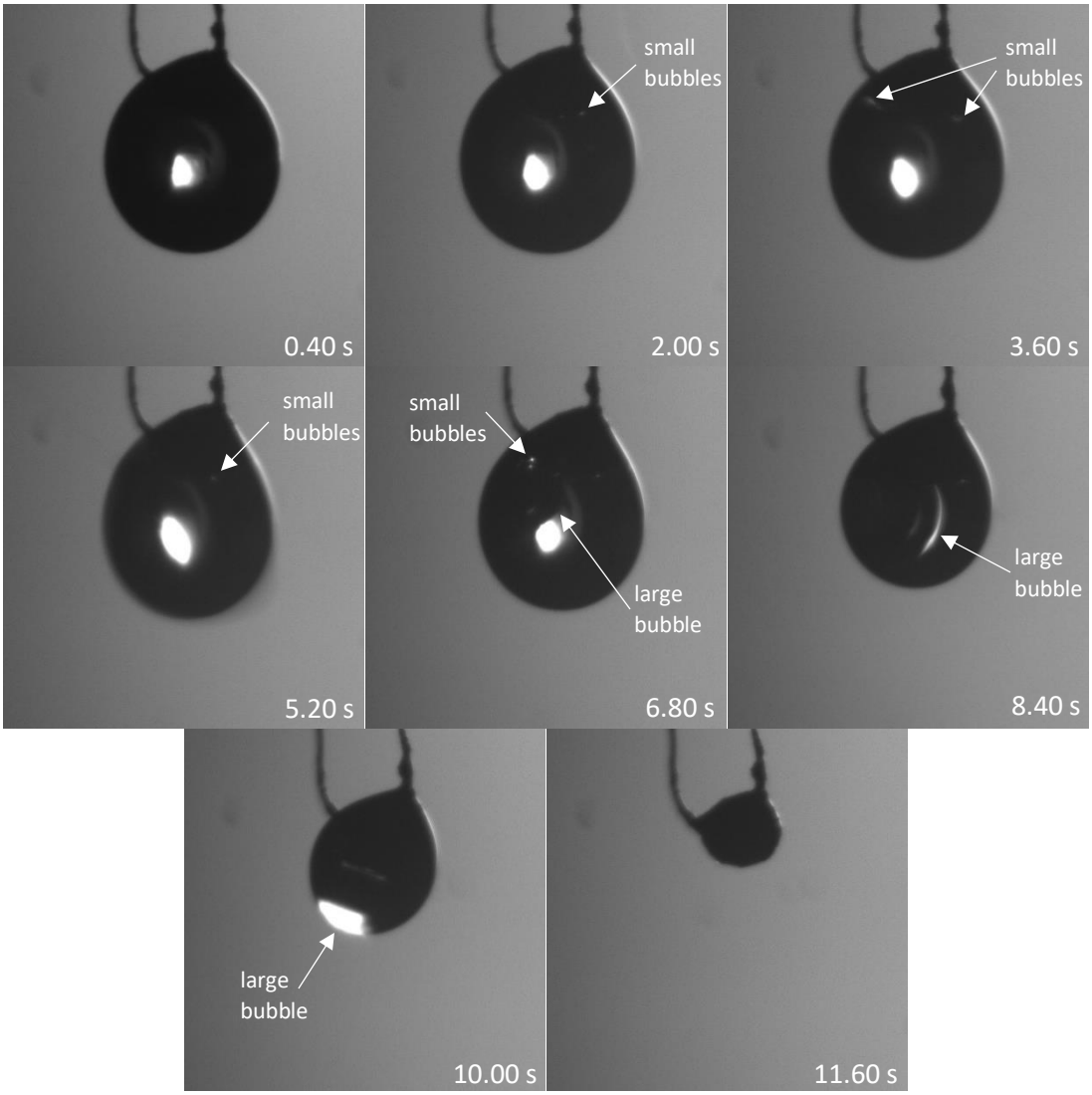

Figure 7-41: Droplet photos of biodiesel with 20% pentanol during droplet evaporation at 450°C

Figure 7-42 shows droplet diameters during droplet evaporation of PENT5 at 700°C. As with the droplet diameters for PENT5 at 450°C, the well-mixed model doesn't show much decrease in droplet diameter at 1 second when all of the pentanol component has evaporated. However, the diffusion-limited model was the best model to reproduce experimental droplet diameters, giving droplet diameters similar to experimental values for the first 1.5 seconds before dropping below the experimental diameters between 2 and 3.5 seconds.

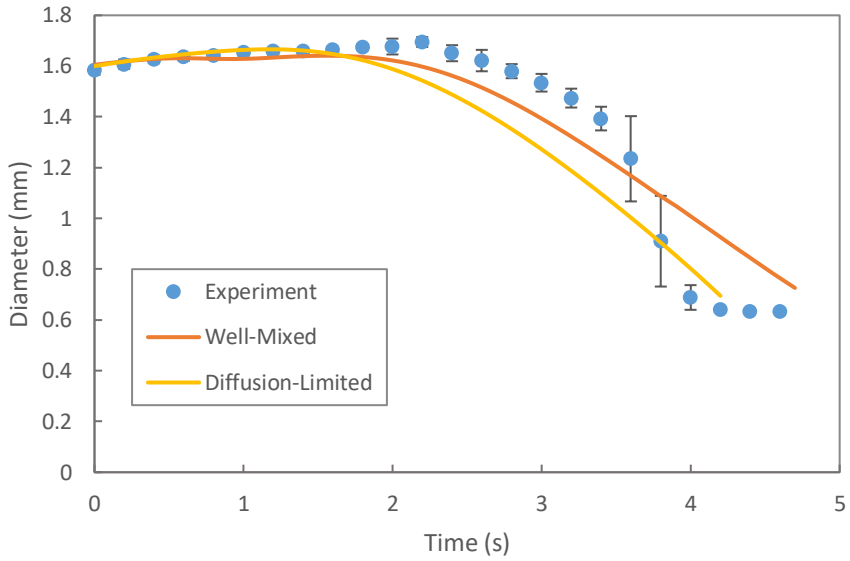

Figure 7-42: Droplet diameter of biodiesel with 5% pentanol during droplet evaporation at 700°C

Note: Experimental points give the mean and standard deviation of 7 individual measurements

Figure 7-43 shows droplet photos during the evaporation of PENT5 at a furnace temperature of 700°C. Small bubbles, on their own, are hard to see in this set of photos. However, a large bubble did form in the droplet in the photos at 2.60 and 3.20 seconds, which correlates with the increased droplet diameters seen in Figure 7-42 above. Additionally, small bubbles can be seen alongside the large bubble at 2.60 seconds. The photos at 2.60 and 3.20 seconds also show the droplet becoming more vertically elongated and exposing some of the thermocouple to the environment.

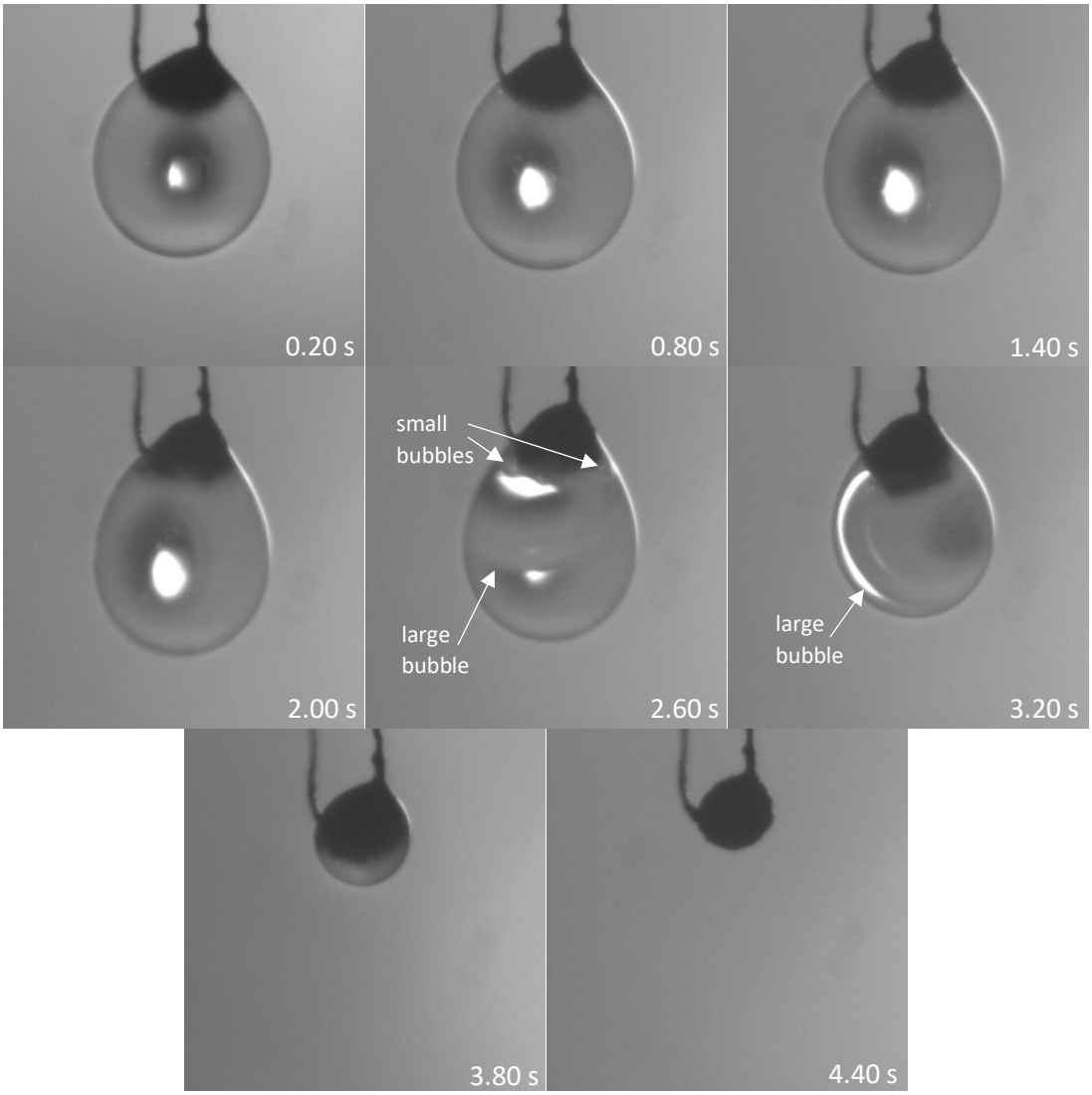

Figure 7-43: Droplet photos of biodiesel with 5% pentanol during droplet evaporation at 700°C

Figure 7-44 shows droplet diameters during the evaporation of PENT20 at a furnace temperature of 700°C. The well-mixed model shows a drop in droplet diameters between 1 and 1.5 seconds due to all of the pentanol components evaporating. For the first two seconds, the diffusion-limited model produces droplet diameters that are very similar to the experimental droplet diameters. Afterwards, between 2 and 3.5 seconds, the experimental droplet diameters are larger than the droplet diameters calculated by the diffusion-limited model.

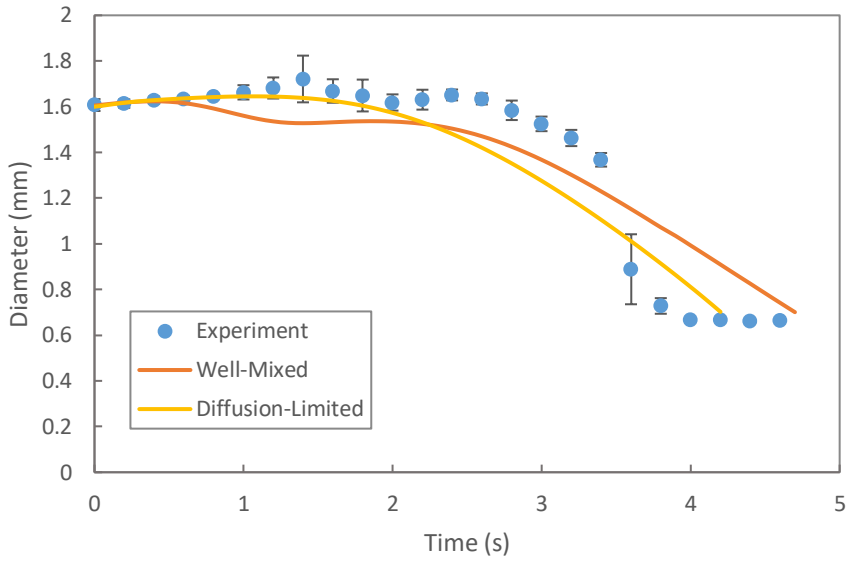

Figure 7-44: Droplet diameter of biodiesel with 20% pentanol during droplet evaporation at 700°C

Note: Experimental points give the mean and standard deviation of 7 individual measurements

Figure 7-45 shows droplet photos during evaporation of PENT20 at a furnace temperature of 700°C. The evaporation of a droplet with a high alcohol content, such as 20% (v/v), and at a high temperature of 700°C causes bubbles to rapidly form and escape the droplet, causing rapid expansion and contraction of droplet diameter, as shown by the shaky photos at 1.40 and 2.00 seconds, which correlate with the increase and decrease in experimental droplet diameter shown between 1 and 2 seconds in Figure 7-44 above. The shaky photo at 1.40 seconds shows multiple small bubbles formed. A large bubble can be seen in the photos at 2.60 and 3.20 seconds, which correlates with the increased droplet diameters shown in Figure 7-44. Additionally, a medium sized bubble can also be seen alongside the large bubble in the photo at 2.60 seconds. The photos at 2.60 and 3.20 seconds do show the droplet become vertically elongated, such that some of the thermocouple is exposed to the environment.

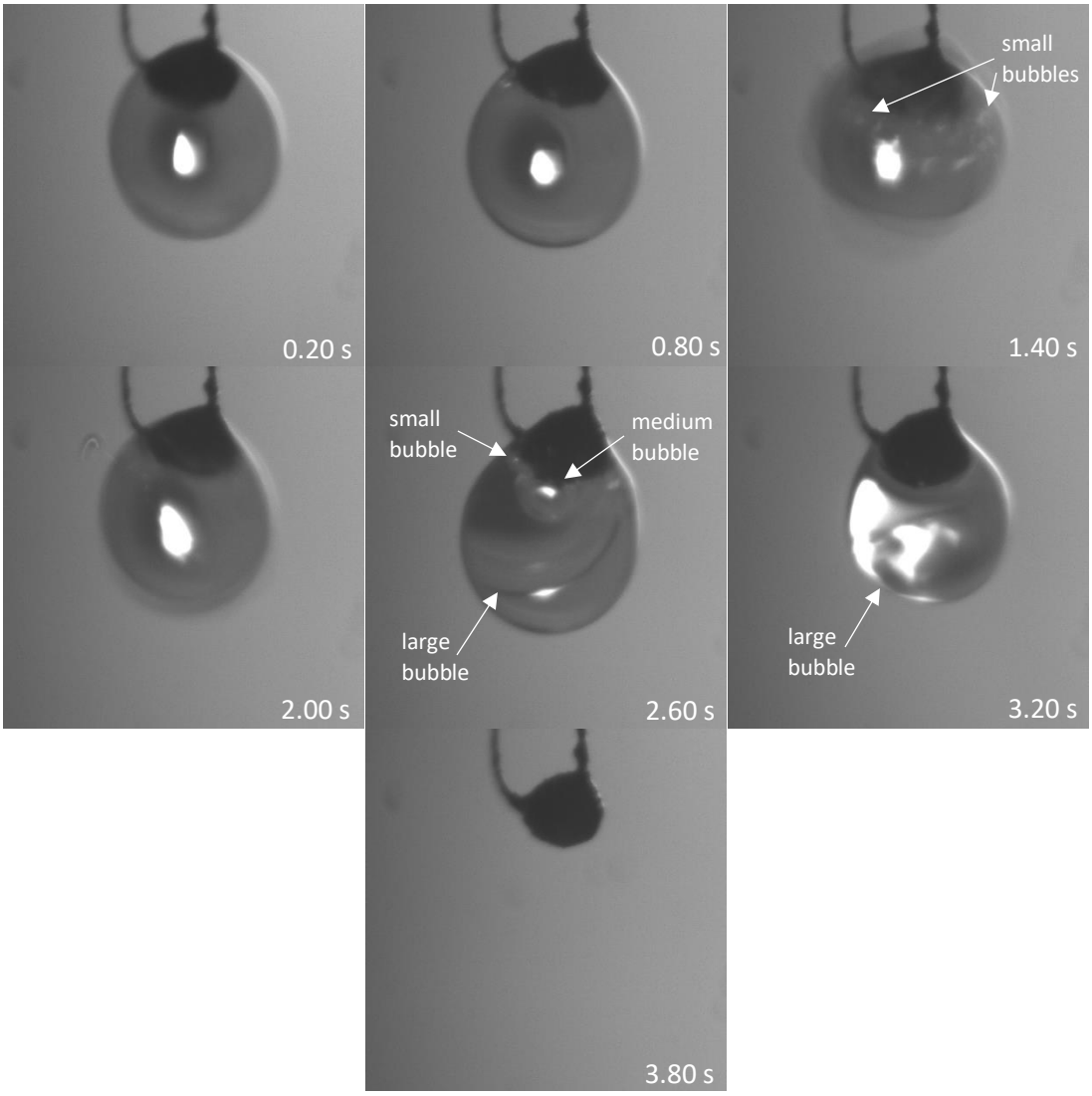

Figure 7-45: Droplet photos of biodiesel with 20% pentanol during droplet evaporation at 700°C

As shown in the previous pictures, bubbling does occur within the droplet during the droplet evaporation of PENT5 and PENT20. However, bubbling is not modelled by the numerical models. To see if the bubbling, specifically the formation of the large bubbles, has an effect on the experimental droplet diameters, the volume of the large bubbles was removed from the experimental droplet diameters and the results are shown as "Adjusted Experiment" in the figures below. This was only done to droplet evaporation experiments at a furnace temperature of 450°C, since it was easier to identify the perimeter of the large bubbles in photos from the droplet evaporation experiments at 450°C.

Figure 7-46 shows the adjusted experimental diameters for the droplet evaporation of PENT5 at a furnace temperature of 450°C, in which the adjusted experimental diameters has the volume of the large bubbles removed. The adjusted experimental diameters for PENT5 show very similar results to the diffusion-limited model.

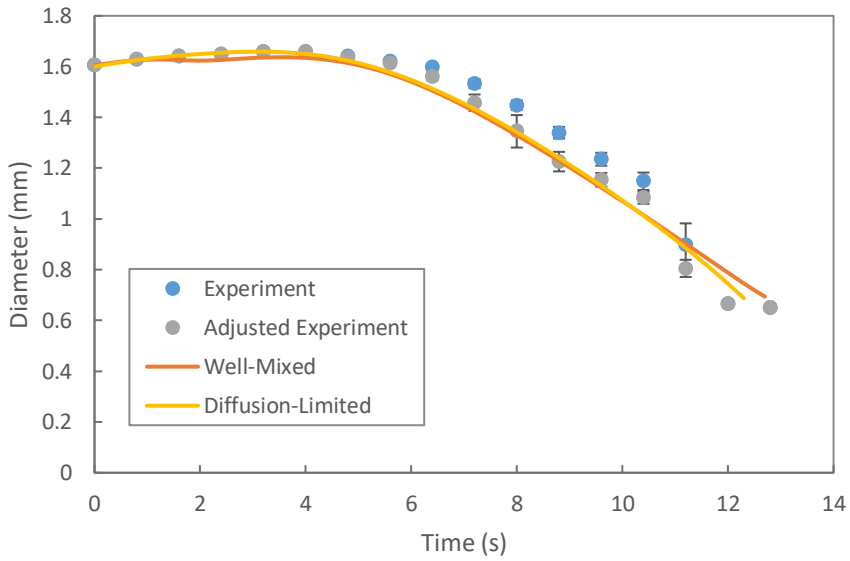

Figure 7-46: Droplet diameter, with adjusted experimental droplet diameter, of biodiesel with 5% pentanol during droplet evaporation at 450°C
Note: Experimental points give the mean and standard deviation of 8 individual measurements

Figure 7-47 shows the adjusted experimental diameters for the droplet evaporation of PENT20 at a furnace temperature of 450°C, in which the adjusted experimental diameters have the volume of the large bubbles removed. As with the experimental diameters for PENT5, the adjusted experimental diameters are very similar to those from the diffusion-limited model, and the large discrepancy in Figure 7-40 is removed.

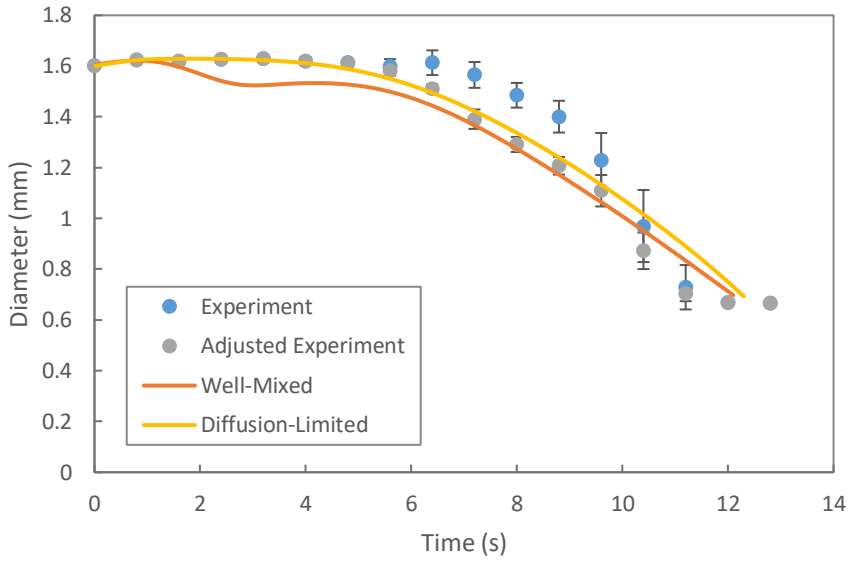

Figure 7-47: Droplet diameter, with adjusted experimental droplet diameter, of biodiesel with 20% pentanol during droplet evaporation at 450°C
Note: Experimental points give the mean and standard deviation of 8 individual measurements

In this section, experimental droplet diameters of pentanol-biodiesel blends were compared to droplet diameters calculated using numerical models. The diffusion-limited model is the best model to represent the droplet diameters of pentanol-biodiesel blends. The experimental diameters were sometimes larger than the calculated droplet diameters from the models. However, the droplet photos have shown that the formation of large bubbles causes the increase in experimental droplet diameters. Additionally, the droplet photos have shown the formation of many, small bubbles before the formation of large bubbles. By removing the approximate volume of the large bubbles, the experimental droplet diameters behave similarly to the droplet diameters calculated by the diffusion-limited model.

7.3.3 Droplet Boiling Temperatures

Bubbles have been observed to form in the droplet during the droplet evaporation of pentanol-biodiesel blends. To confirm that boiling and bubble formation can occur, the boiling temperature at different portions of the droplet is compared with the droplet temperature. As with the propanol-biodiesel blends, the boiling temperatures were determined by the concentration of components at different radial positions using the diffusion-limited model. The radial position in the droplet is identified by Z, which is equal to the ratio of the radius at the current position over

the radius of the droplet. For example, Z=0 represents the center of the droplet and Z=1 represents the surface of the droplet.

Figure 7-48 shows the droplet temperatures and the boiling temperatures at different radial positions for the droplet evaporation of PENT5 at a furnace temperature of 450°C. The portion of the droplet where the boiling temperature falls below the droplet temperatures is smaller for PENT5 than it was for PROP5: this only occurs for Z=0 to 0.846 owing to pentanol's higher boiling point. A large portion, Z=0.934 to 1, has the boiling temperature remain above the droplet temperature. This means that bubble formation can occur for a smaller portion of the PENT5 droplet and for a shorter time than for PROP5. Boiling and bubble formation can start between 2.4 to 3.2 seconds at temperatures of 188°C to 201°C for PENT5 droplets. This is later in the droplet's lifetime and at higher temperatures than for PROP5 droplets.

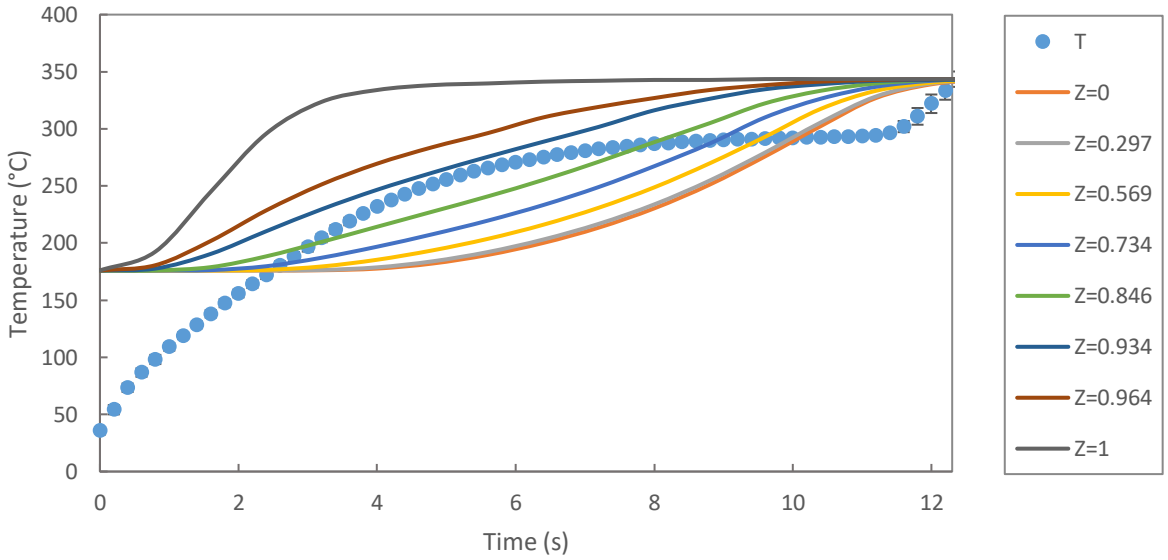

Figure 7-48: Droplet temperature and boiling temperature at different radial positions for biodiesel with 5% pentanol during droplet evaporation at 450°C, where Z=r/R
Note: Experimental points give the mean and standard deviation of 8 individual measurements

Figure 7-49 shows the droplet temperature and the boiling temperature at different radial positions for PENT20 at a furnace temperature of 450°C. For most of the droplet, from Z=0 to 0.964, the droplet temperature was greater than the boiling temperature between 3 and 9 seconds. This starts later than for PROP20, for which the start of boiling occurred at around 1.6 seconds, and PENT20 shows a more gradual transition. The surface's boiling temperature remains greater than the droplet's temperature.

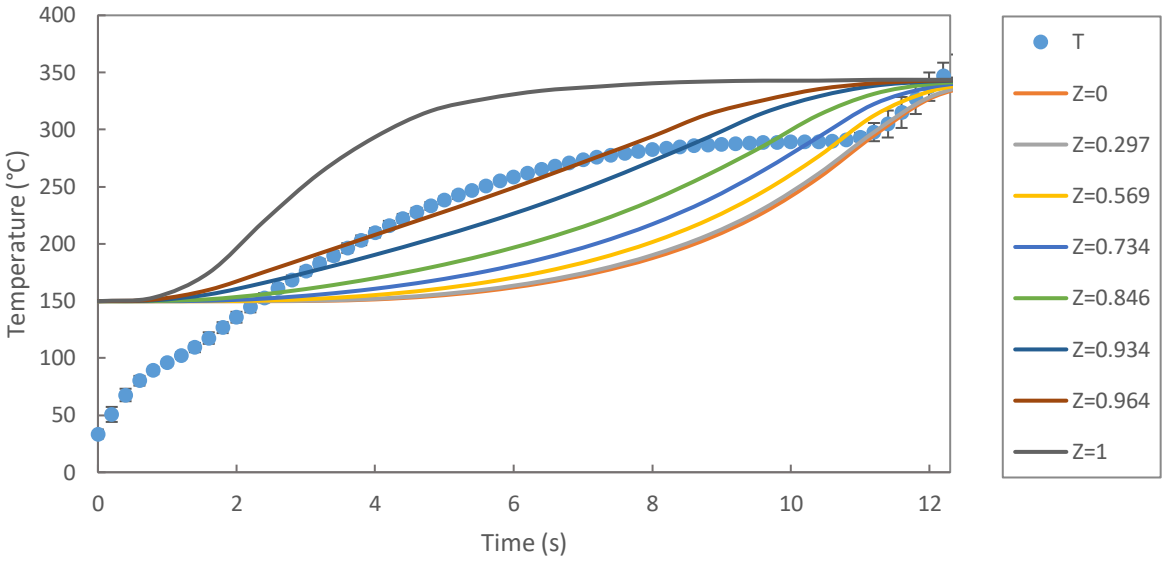

Figure 7-49: Droplet temperature and boiling temperature at different radial positions for biodiesel with 20% pentanol during droplet evaporation at 450°C, where Z=r/R
Note: Experimental points give the mean and standard deviation of 8 individual measurements

Figure 7-50 shows the droplet temperature and the boiling temperature at different radial positions for droplet evaporation of PENT5 at a furnace temperature of 700°C. The droplet temperature was larger than the boiling temperature for most of the droplet, Z=0 to Z=0.982, from roughly 1 second to the end of the droplet's lifetime. Again, these results show a more gradual transition from not boiling to boiling than what was observed for PROP5 at 700°C. The boiling temperature for the droplet surface remains above the droplet temperature until near the end of the droplet's lifetime, when the boiling temperature becomes less than the droplet temperature at the end of the droplet's lifetime. The droplet temperature increases above the boiling temperature at the surface of the droplet because the droplet transitions to mainly evaporating the remaining MGC components. The boiling temperature at the surface calculated by the diffusion-limited model did not consider the higher concentration of MGC at the end of the droplet's lifetime, since the diffusion-limited model cannot accommodate a third (MGC) fuel fraction.

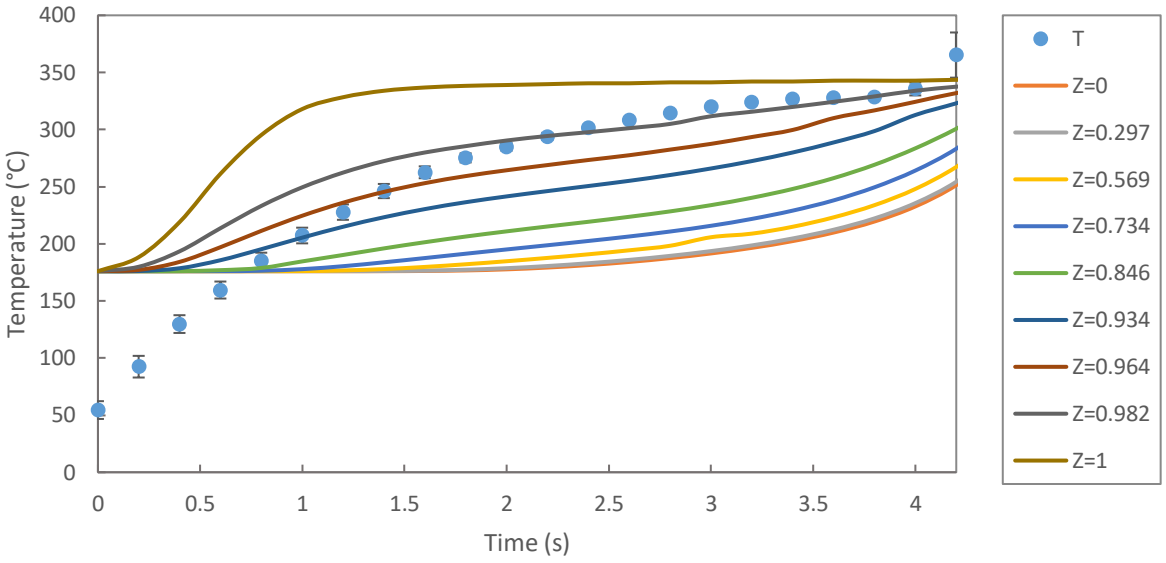

Figure 7-50: Droplet temperature and boiling temperature at different radial positions for biodiesel with 5% pentanol during droplet evaporation at 700°C, where Z=r/R
Note: Experimental points give the mean and standard deviation of 7 individual measurements

Figure 7-51 shows the droplet temperature and the boiling temperature at different radial positions for droplet evaporation of PROP20 at a furnace temperature of 700°C. The boiling temperature for most of the droplet, for Z=0 to 0.982, was lower than the droplet temperature from roughly 1 seconds to the end of the droplet's lifetime. The boiling temperature for the droplet surface remained above the droplet temperature for most of the droplet's lifetime up to 4 seconds, in which the boiling temperature drops below the droplet temperature.

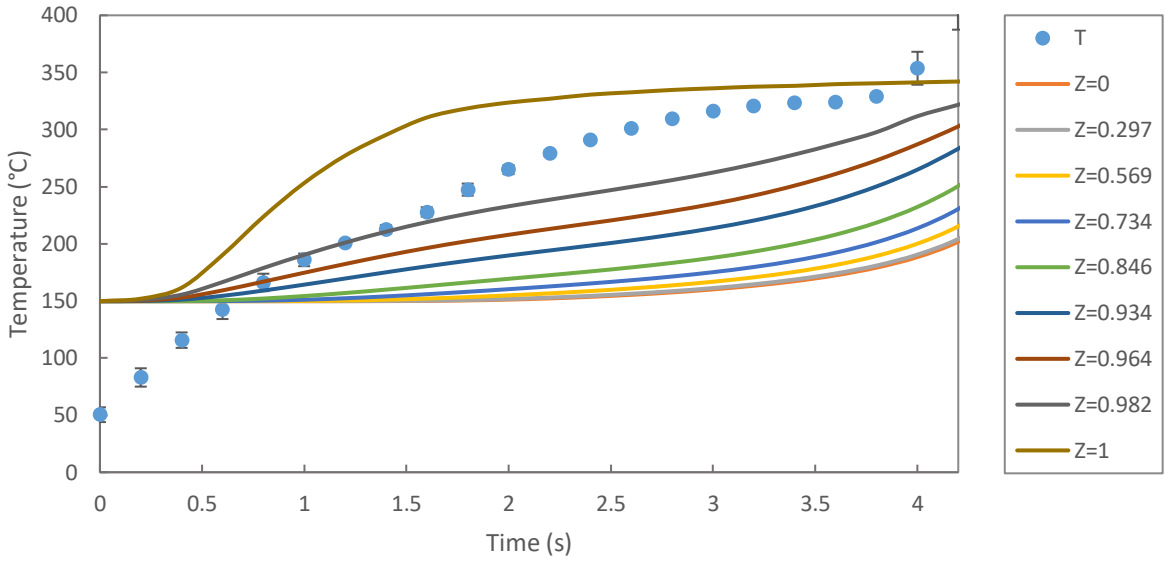

Figure 7-51: Droplet temperature and boiling temperature at different radial positions for biodiesel with 20% pentanol during droplet evaporation at 700°C, where Z=r/R
Note: Experimental points give the mean and standard deviation of 7 individual measurements

This section has confirmed that pentanol-biodiesel droplets show a similar behaviour to propanol-biodiesel droplets, in which the composition inside the droplet allows for boiling or bubble formation to occur. This was confirmed by checking if the boiling temperature of different portions of the droplet drops below the droplet temperature during the droplet's lifetime. However, the difference between pentanol-biodiesel droplets and propanol-biodiesel droplets is that the boiling temperatures for pentanol-biodiesel is below the droplet temperature for a smaller portion of the droplet volume and lifetime.

7.3.4 Summary of Results for Pentanol-Biodiesel

Droplet evaporation experiments of pentanol-biodiesel droplets have confirmed that, as with the propanol-biodiesel droplets, the liquid phase of alcohol-biodiesel droplets depends on liquid diffusion processes. Comparing droplet evaporation of pentanol-biodiesel droplets with propanol-biodiesel droplets have shown that difference between the well-mixed model and the diffusion-limited model is smaller for pentanol-biodiesel droplets, so that this difference become close to negligible for lower alcohol concentrations and lower furnace temperatures. Nonetheless, the diffusion-limited model was best able to represent droplet temperature data for pentanol-biodiesel droplets for all alcohol concentrations and furnace temperatures. The model was best able to represent the droplet diameters for the first half of the droplet's lifetime. For the second

half, the formation of large bubbles causes the experimental droplet diameters to be larger than the models. Neither model considers the formation of bubbles in the liquid phase, which is favoured by the cement bead that the droplet hangs, which acts as a nucleation site. The concentration of pentanol at the center of the droplet decreases the boiling temperature of the central liquid to below the droplet temperature. The experimental droplet diameters and temperatures with the well-mixed models and the diffusion-limited models for biodiesel with 10% (v/v) and 15% (v/v) pentanol can be found in Appendix E: Additional Results for Biodiesel Pentanol Mixtures.

7.4 Summary of Droplet Evaporation Results

Comparison of model results and experimental data for propanol-biodiesel and pentanol-biodiesel droplets have shown that non-uniform liquid concentrations and the radial movement of the liquid components by diffusion significantly affect droplet behaviour. Even though pentanol-biodiesel droplets show less of a difference between the two different models when compared to propanol-biodiesel droplets, the diffusion-limited model should be used to represent droplet evaporation of alcohol-biodiesel blends. The only discrepancy between the model and experimental results occurs in the last half of the droplet's lifetime in which the experimental droplet diameter is larger than the diffusion-limited model's droplet diameter due to the formation of a large bubble within the droplet. Bubble formation only occurs if there is a nucleation site present in the liquid and the liquid phase's boiling temperature is below the droplet's temperature. The liquid phase's boiling temperature does drop below the droplet's temperature due to a high concentration of alcohol component in the center of the droplet, and the experimental setup has the cement bead that the droplet hangs on act as a nucleation site. However, real-life applications of droplet evaporation have the liquid droplet's sprayed into air and the droplet evaporates in the atmosphere unsupported, so that in spray combustion there will not be anything to act as a nucleation site for bubble formation. Bubble formation is therefore not expected to occur in real-life applications of droplet evaporation unless the droplet temperature exceeds the limit of superheat of the liquid. Therefore, the diffusion-limited model does produce results that represent the droplet evaporation process in real-life applications.

8 Conclusion

The purpose of this work was to complete droplet evaporation experiments of alcohol-biodiesel blends and to determine the best numerical model to be used to represent the droplet evaporation process of these blends. A biodiesel sample was received from Innoltek and a distillation test was performed on this sample to determine its approximate composition. The experimental VLE data of some common FAMEs with ethanol and biodiesel with ethanol were compared with VLE calculations using Raoult's Law or a modified Raoult's Law with activity coefficients calculated using the UNIFAC method to determine the best method to be used to calculate the vapour pressure in droplet evaporation models. Droplet evaporation experiments of 2μL droplets of either propanol-biodiesel or pentanol-biodiesel blends were performed at 450°C and 700°C. The droplet evaporation process was numerical modeled using either the well-mixed continuous thermodynamics model or the diffusion-limited continuous thermodynamics model.

The comparison of experimental VLE data with VLE calculation has shown that mixtures of alcohol-FAMEs and alcohol-biodiesel exhibit non-ideal behaviour and require the use a modified Raoult's Law with activity coefficients found using the UNIFAC method to determine the vapour pressures of these mixtures. The droplet evaporation experiments of the alcohol-biodiesel blends have shown that the large difference in boiling points between the alcohol component and the biodiesel components creates a non-uniform radial composition of components within the droplet, and that it is necessary to use a model that includes liquid diffusion, in this case the diffusion-limited continuous thermodynamics model. This non-uniform radial composition also causes internal boiling and bubbling to occur, aided by bubble nucleation on the thermocouple bead that supports the droplet during the experiment. The diffusion-limited model agrees well with the experimental results, except when large bubble formation occurs within the droplet, in which case the experimental droplet diameter increases during the later half of the droplet evaporation process and then drops quickly if the bubble bursts. The inclusion of natural convection in both the well-mixed model and the diffusion-limited model has contributed to the good agreement of the model with experimental data.

Future work should look into expanding the diffusion-limited model to use more than two fuel fractions. In addition, the diffusion-limited model should be compared with experimental droplet

combustion/ignition of alcohol-biodiesel blends. Future work could also investigate droplets of alcohol-biodiesel blends that contain alcohol components with a high molecular weight, such as octanol, and whether the well-mixed model could be used to represents these blends. Additionally, droplet evaporation of alcohol-biodiesel blends with more volatile alcohols, such as methanol, should be investigated and determine whether a numerical model can represent a blend of a volatile alcohol with biodiesel. The possible occurrences of pyrolysis in biodiesel droplets should also be investigated.

References

[1] L. P. Koh and J. Ghazoul, "Biofuels, biodiversity, and people: Understanding the conflicts and finding opportunities," *Biological Conservation,* vol. 141, no. 10, pp. 2450-2460, 2008.

[2] BP p.l.c., "Statistical Review of World Energy, 70th edition," BP p.l.c., London, 2021.

[3] "Energy Information Administration (EIA)," [Online]. Available: https://www.eia.gov/totalenergy/data/annual/index.php. [Accessed 02 09 2021].

[4] S. Kumar, J. H. Cho, J. Park and I. Moon, "Advances in diesel-alcohol blends and their effects on the performance and emissions of diesel engines," *Renewable and Sustainable Energy Reviews,* vol. 22, pp. 46-72, 2013.

[5] "O. Reg. 663/20: Cleaner Transportation Fuels: Renewable Content Requirements For Gasoline And Diesel Fuels under Environmental Protection Act, R.S.O. 1990, c. E.19," 25 November 2020. [Online]. Available: https://www.ontario.ca/laws/regulation/r20663. [Accessed 12 September 2021].

[6] G. Knothe, J. Krahl and J. Gerpen, The Biodiesel Handbook, 2nd ed., Urbana, Illinois: Academic Press and AOCS Press, 2010.

[7] G. Knothe and L. F. Razon, "Biodiesel fuels," *Progress in Energy and Combustion Science,* vol. 58, pp. 36-59, 2017.

[8] W. L. H. Hallett and N. V. Leqault, "Modelling biodiesel droplet evaporation using continuous thermodynamics," *Fuel,* vol. 90, pp. 1221-1228, 2011.

[9] H. Joshi, B. R. Moser, J. Toler and T. Walker, "Preparation and fuel properties of mixtures of soybean oil methyl and ethyl esters," *Biomass and Bioenergy,* vol. 34, no. 1, pp. 14-20, 2010.

[10] L. Canoira, M. Rodriquez-Gamero, E. Querol, R. Alcantara, M. Lapuerta and F. Oliva, "Biodiesel from Low-Grade Animal Fat: Production Process Assessment and Biodiesel Properties Characterization," *Industrial & Engineering Chemistry Research,* vol. 47, no. 21, pp. 7997-8004, 2008.

[11] E. Torres-Jimenez, M. Svoljsak-Jerman, A. Gregorc, I. Lisec, M. P. Dorado and B. Kegl, "Physical and Chemical Properties of Ethanol-Biodiesel Blends for Diesel Engines," *Energy & Fuels,* vol. 24, no. 3, pp. 2002-2009, 2010.

[12] H. Aydin and C. Ilkilic, "Effect of ethanol blending with biodiesel on engine performance and exhaust emissions in a CI engine," *Applied Thermal Engineering,* vol. 30, no. 10, pp. 1199-1204, 2010.

[13] S. Rathinam, K. N. Balan, G. Subbiah, J. B. Sajin and Y. Devarajan, "Emission study of a diesel engine fueled with higher alcohol-biodiesel blended fuels," *International Journal of Green Energy,* vol. 16, no. 9, pp. 667-673, 2019.

[14] N. Yilmaz, F. M. Vigil, S. M. Davis and A. Calva, "Effect of biodiesel-butanol fuel blends on emissions and performance characteristics of a diesel engine," *Fuel,* vol. 135, pp. 46-50, 2014.

[15] N. Yilmaz and T. M. Sanchez, "Analysis of operating a diesel engine on biodiesel-ethanol and biodiesel-methanol blends," *Energy,* vol. 46, no. 1, pp. 126-129, 2012.

[16] N. Yilmaz, "Performance and emission characteristics of a diesel engine fuelled with biodiesel-ethanol and biodiesel-methanol blends at elevated air temperatures," *Fuel,* vol. 94, pp. 440-443, 2012.

[17] M. L. Botero, Y. Huang, D. L. Zhu, A. Molina and C. K. Law, "Synergistic combustion of droplets of ethanol, diesel and biodiesel mixtures," *Fuel,* vol. 94, pp. 342-347, 2012.

[18] K. L. Pan and M. C. Chiu, "Droplet combustion of blended fuels with alcohol and biodiesel/diesel in microgravity condition," *Fuel,* vol. 113, pp. 757-765, 2013.

[19] B. Coughlin and A. Hoxie, "Combustion characteristics of ternary fuel Blends: Pentanol, butanol and vegetable oil," *Fuel,* vol. 196, pp. 488-496, 2017.

[20] A. Hoxie, R. Schoo and J. Braden, "Microexplosive combustion behavior of blended soybean oil and butanol droplets," *Fuel,* vol. 120, pp. 22-29, 2014.

[21] C. K. Law, Combustion Physics, New Jersey: Cambridge University Press, 2006.

[22] A. Saha, R. Kumar and S. Basu, "Infrared thermography and numerical study of vaporization characteristics of pure and blended bio-fuel droplets," *International Journal of Heat and Mass Transfer,* vol. 53, no. 19-20, pp. 3862-3873, 2010.

[23] M. B. Oliveira, S. I. Miguel, A. J. Queimada and J. A. P. Coutinho, "Phase Equilibria of Ester + Alcohol Systems and Their Description with the Cubic-Plus-Association Equation of State," *Industrial & Engineering Chemistry Research,* vol. 49, no. 7, pp. 3452-3458, 2010.

[24] Y. Guo, J. Zhong, Y. Xing, D. Li and R. Lin, "Volatility of Blended Fuel of Biodiesel and Ethanol," *Energy Fuels,* vol. 21, no. 2, pp. 1188-1192, 2007.

[25] D. I. S. da Silva, M. R. Mafra, F. R. da Silva, P. M. Ndiaye, L. P. Ramos, L. C. Filho and M. L. Corazza, "Liquid-liquid and vapour-liquid equilibrium data for biodiesel reaction-separation systems," *Fuel,* vol. 108, pp. 269-276, 2013.

[26] P. M. S. Kalvelage, A. A. Albuquerque, A. A. C. Barros and S. L. Bertoli, "(Vapour + Liquid) Equilibrium for Mixtures Ethanol + Biodiesel from Soybean Oil and Frying Oil," *International Journal of Thermodynamics,* vol. 20, no. 3, pp. 159-164, 2017.

[27] J. Tamim and W. L. H. Hallett, "A Continuous Thermodynamics Model For Multicomponent Droplet Vaporization," *Chemical Engineering Science,* vol. 50, no. 18, pp. 2933-2942, 1995.

[28] W. L. H. Hallett, "A Simple Model for the Vaporization of Droplet with Large Numbers of Components," *Combustion and Flame,* vol. 121, pp. 334-344, 2000.

[29] F. R. Newbold and N. R. Amundson, "A model for evaporation of a multicomponent droplet," *AlChE Journal,* vol. 19, no. 1, pp. 22-30, 1973.

[30] C. K. Law, "Multicomponent droplet combustion with rapid internal mixing," *Combustion and Flame,* vol. 26, pp. 219-233, 1976.

[31] W. A. Sirignano and C. K. Law, "Transient Heating and Liquid-Phase Mass Diffusion in Fuel Droplet Evaporation," in *Evaporation-Combustion of Fuels,* Washington, American Chemical Society, 1978, pp. 3-26.

[32] C. A. Bergeron and W. L. H. Hallett, "Autoignition of Single Droplet of Two-Component Liquid Fuels," *Combustion Science and Technology,* vol. 65, no. 4-6, pp. 181-194, 1989.

[33] M. Mawid and S. K. Aggarwal, "Analysis of transient combustion of multicomponent liquid fuel droplet," *Combustion and Flame,* vol. 84, no. 1-2, pp. 1997-209, 1991.

[34] A. Y. Tong and W. A. Sirignano, "Multicomponent droplet vaporization in high temperature gas," *Combustion and Flame,* vol. 66, no. 3, pp. 221-235, 1986.

[35] S. K. Aggarwal, "Modeling of a dilute vaporizing multicomponent fuel spray," *International Journal of Heat and Mass Transfer,* vol. 30, no. 9, pp. 1949-1961, 1987.

[36] D. G. Talley and S. C. Yao, "A semi-empirical approach to thermal and composition transients inside vaporizing fuel droplets," *21st Symposium (International) on Combustion,* vol. 21, no. 1, pp. 609-616, 1988.

[37] A. J. Marchese and F. L. Dryer, "The effect of liquid mass transport on the combustion and extinction of bicomponent droplets of methanol and water," *Combustion and Flame,* vol. 105, no. 1-2, pp. 104-122, 1996.

[38] Z. Abdel-Qader and W. L. H. Hallett, "The role of liquid mixing in evaporation of complex multicomponent mixtures: modelling using continuous thermodynamics," *Chemical Engineering Science,* vol. 60, pp. 1629-1640, 2005.

[39] W. L. Hallett and S. Beauchamp-Kiss, "Evaporation of single droplets of ethanol-fuel oil mixtures," *Fuel,* vol. 89, pp. 2496-2504, 2010.

[40] N. S. Mousavi, A. Romero-Martinez and L. F. Ramirez-Verduzco, "Predicting the surface tension of mixtures of fatty acid ethyl esters and biodiesel fuels using UNIFAC activity coefficients," *Fluid Phase Equilibria,* vol. 507, p. 112430, 2020.

[41] F. R. do Carmo, N. S. Evangelista, R. S. de Santiago-Aguiar, F. A. N. Fernandes and H. B. de Sant'Ana, "Evaluation of optimal activity coefficient models for modeling and simulation of liquid-liquid equilibrium of biodiesel + glycerol + alcohol systems," *Fuel,* vol. 125, pp. 57-65, 2014.

[42] J. D. Jin and G. L. Borman, "A Model for Multicomponent Droplet Vaporization at High Ambient Pressures," *SAE Transactions,* vol. 94, no. 2, pp. 483-493, 1985.

[43] B. Abramzon and W. A. Sirignano, "Droplet vaporization model for spray combustion calculations," *International Journal of Heat and Mass Transfer,* vol. 32, no. 9, pp. 1605-1618, 1989.

[44] R. B. Bird, W. E. Steward and E. N. Lightfoot, Transport Phenomena, Wiley, 1960.

[45] W. L. H. Hallett and N. A. Clark, "A model for the evaporation of biomass pyrolysis oil droplets," *Fuel,* vol. 85, pp. 532-544, 2006.

[46] B. E. Poling, J. M. Prausnitz and J. P. O. Connell, The Properties of Gases and Liquids, Fifth ed., New York: McGraw-Hill, 2001.

[47] "Dortmund Data Bank, DDBST GmbH," [Online]. Available: www.ddbst.de. [Accessed January 2021].

[48] ASTM D86-20, "Standard Test Method for Distillation of Petroleum Products and Liquid Fuels at Atmospheric Pressure," ASTM International, 2020.

[49] H. B. Krop, M. J. M. v. Velzen, J. R. Parsons and H. A. J. Govers, "Determination of environmentally relevant physical-chemical properties of some fatty acid esters," *Journal of the American Oil Chemists' Society,* vol. 74, no. 3, pp. 309-315, 1997.

[50] W. Yuan, A. C. Hansen and Q. Zhang, "Vapor pressure and normal boiling point predictions for pure methyl esters and biodiesel fuels," *Fuel,* vol. 84, no. 7-8, pp. 943-950, 2005.

[51] S. K. Hoekman, A. Broch, C. Robbins, E. Ceniceros and M. Natarajan, "Review of biodiesel composition, properties, and specifications," *Renewable and Sustainable Energy Reviews,* vol. 16, pp. 143-169, 2012.

[52] U.S. Environmental Protection Agency, "CompTox Chemicals Dashboard, Glycerol 1-monostearate," [Online]. Available: https://comptox.epa.gov/dashboard/DTXSID7029160. [Accessed 06 10 2021].

[53] U.S. Environmental Protection Agency, "CompTox Chemicals Dashboard, 1,3-Distearoylglycerol," [Online]. Available: https://comptox.epa.gov/dashboard/DTXSID60892302. [Accessed 06 10 2021].

[54] E. Tolonen, "Evaporation Characteristics of a Liquid Bio-Fuel from Chicken Litter," Thesis (M.A.Sc.)--University of Ottawa, 2013.

[55] U.S. Environmental Protection Agency, "CompTox Chemicals Dashboard, 1-Pentanol," [Online]. Available: https://comptox.epa.gov/dashboard/DTXSID6021741. [Accessed 29 10 2021].

[56] U.S. Environmental Protection Agency, "CompTox Chemicals Dashboard, 1-Propanol," [Online]. Available: https://comptox.epa.gov/dashboard/DTXSID2021739. [Accessed 29 10 2021].

[57] C. K. Law and H. K. Law, "A d^2-Law for Multicomponent Droplet Vaporization and Combustion," *AIAA Journal,* vol. 20, no. 4, pp. 522-527, 1981.

Appendix A: Property Correlations Parameters Values

Table A-1: Parameter values used in property correlations

	Fatty Acid Methyl Esters (FAME)	Monoglycerides (MGC)	Alcohols
Boiling point (K)			
a_B	348.7	472.4	287.7
b_B	0.8478	0.5601	1.39221
s_{fg} (kJ/kmol·K)	108.1	143.4	107.2
Critical Temperature (K)			
a_{cr}	534.3	644.8	438.55
b_{cr}	0.7837	0.5188	1.6659
Critical Pressure (kPa)			
a_P	30.51	30.74	73.96
b_P	-0.06545	-0.0571	-0.37248
Diffusivity (m^2/s)			
a_D	2.404×10^{-9}	2.354×10^{-9}	4.2335×10^{-9}
b_D	-3.265×10^{-12}	-2.807×10^{-12}	-1.830×10^{-11}
b_Φ	205	235	140
Thermal Conductivity (W/m·K)			
a_{KC}	-2.092×10^{-2}	-1.869×10^{-2}	-2.476×10^{-2}
a_{KT}	1.019×10^{-4}	9.028×10^{-5}	1.299×10^{-4}
b_{KC}	8.782×10^{-6}	4.795×10^{-6}	1.807×10^{-5}
b_{KT}	-6.742×10^{-8}	-4.061×10^{-8}	-2.155×10^{-7}
Vapour Specific Heat (kJ/kmol·K)			
a_0	3.653	4.973	1.124
a_1	-3.225×10^{-2}	-4.938×10^{-2}	-1.013×10^{-2}
a_2	2.920×10^{-5}	3.640×10^{-5}	7.610×10^{-6}
a_3	-1.149×10^{-8}	-1.245×10^{-8}	-2.007×10^{-9}
b_0	-7.810×10^{-3}	-7.795×10^{-3}	-7.795×10^{-3}
b_1	8.162×10^{-4}	8.146×10^{-4}	8.146×10^{-4}
b_2	-4.674×10^{-7}	-4.665×10^{-7}	-4.665×10^{-7}
b_3	1.0224×10^{-10}	1.020×10^{-10}	1.020×10^{-10}
Enthalpy of vaporization (J/kmol)			
a_H	1.506×10^{7}	4.023×10^{7}	3.501×10^{7}
b_H	1.8136×10^{5}	1.678×10^{5}	1.007×10^{5}
$(T_{cr} - T_B)^{0.38}$	7.027	6.868	7.1151
Liquid Specific Heat (kJ/kmol·K)			
a_L	1.816	2.1848	6.9551
b_L	-1.462×10^{-3}	-1.255×10^{-3}	-3.474×10^{-2}
c_L	7.509×10^{-6}	8.670×10^{-6}	6.557×10^{-5}
Liquid Specific Volume (m^3/kmol)			
a_v	-3.50×10^{-3}	-5.290×10^{-2}	0.006667
b_v	1.16×10^{-3}	1.16×10^{-3}	1.163×10^{-3}
α_P	0.00085	1.10×10^{-3}	1.27×10^{-3}

Appendix B: Experimental Droplet Diameter Data from Droplet Evaporation Experiments

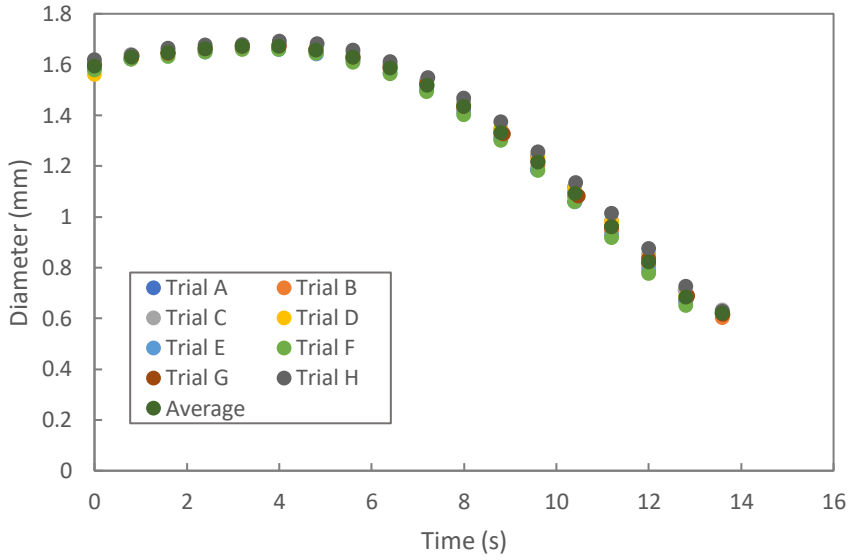

Figure B-1: Trial results of droplet diameter of biodiesel during droplet evaporation at 450°C

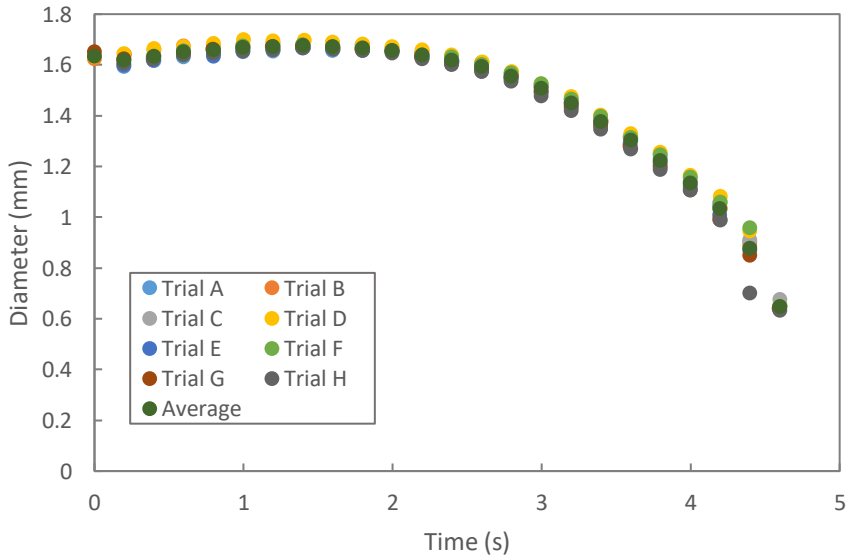

Figure B-2: Trial results of droplet diameter of biodiesel during droplet evaporation at 700°C

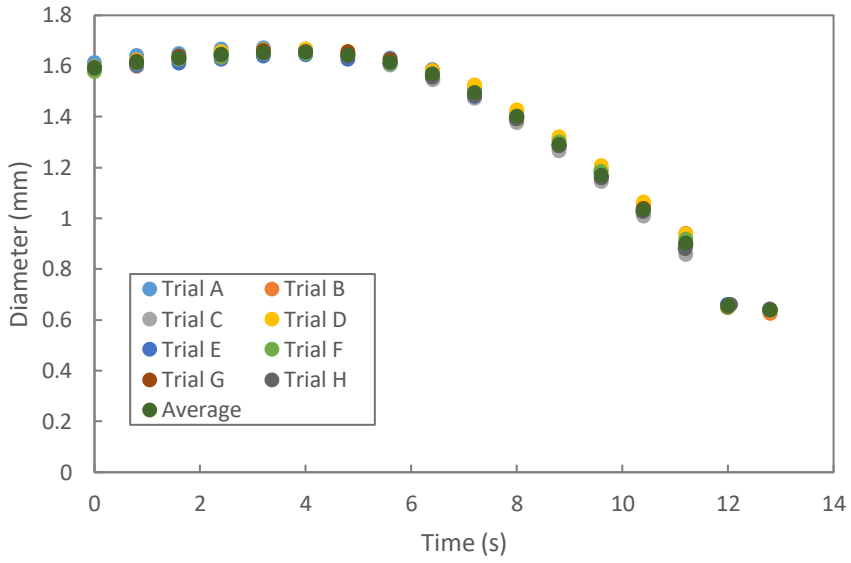

Figure B-3: Trial results droplet diameter of biodiesel with 5% propanol during droplet evaporation at 450°C

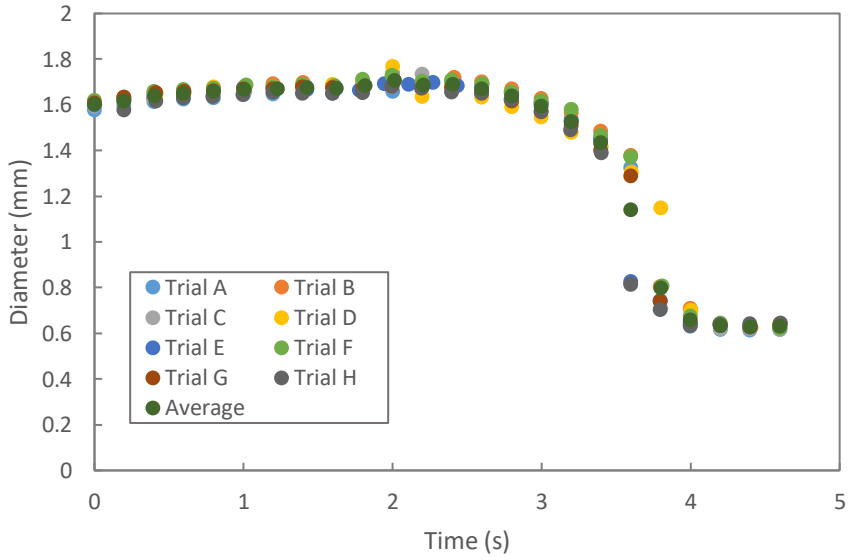

Figure B-4: Trial results droplet diameter of biodiesel with 5% propanol during droplet evaporation at 700°C

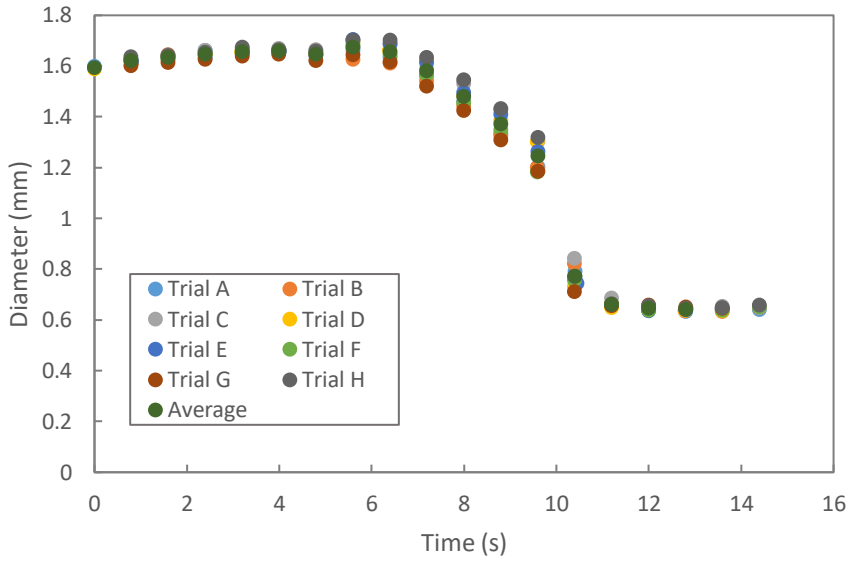

Figure B-5: Trial results droplet diameter of biodiesel with 10% propanol during droplet evaporation at 450°C

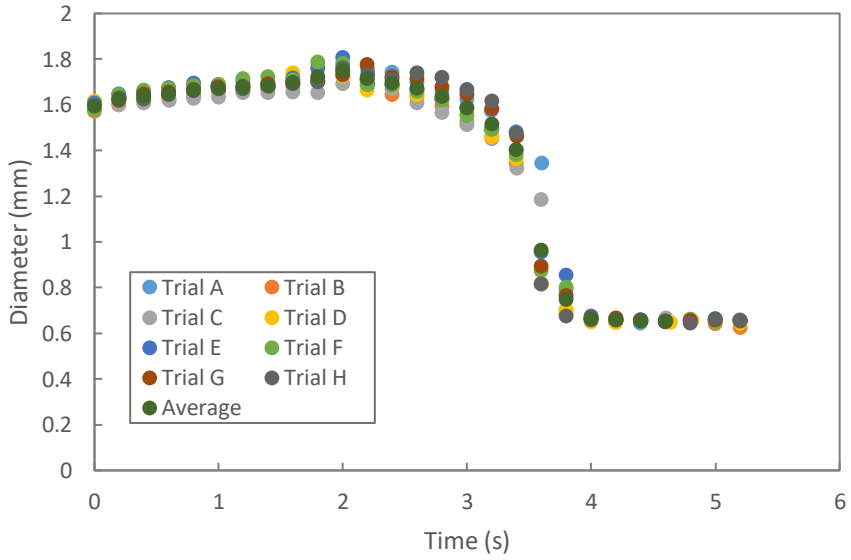

Figure B-6: Trial results droplet diameter of biodiesel with 10% propanol during droplet evaporation at 700°C

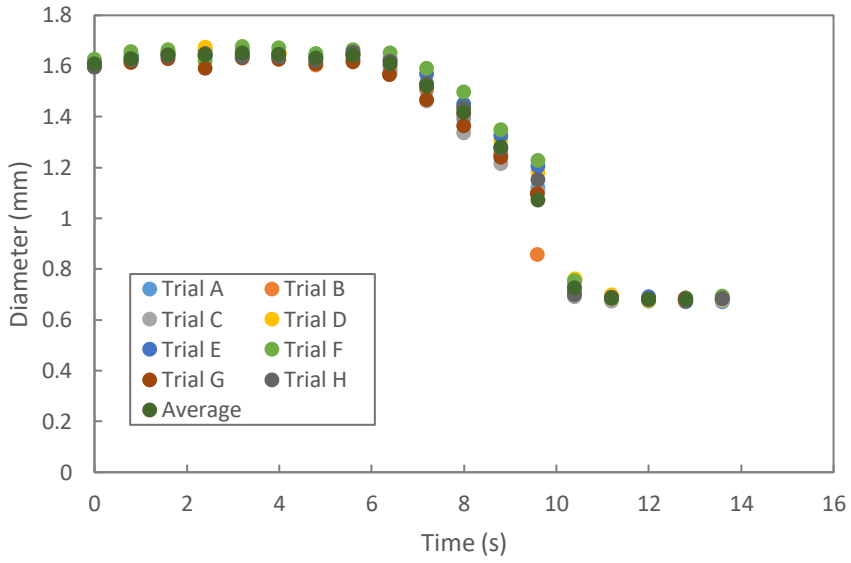

Figure B-7: Trial results droplet diameter of biodiesel with 15% propanol during droplet evaporation at 450°C

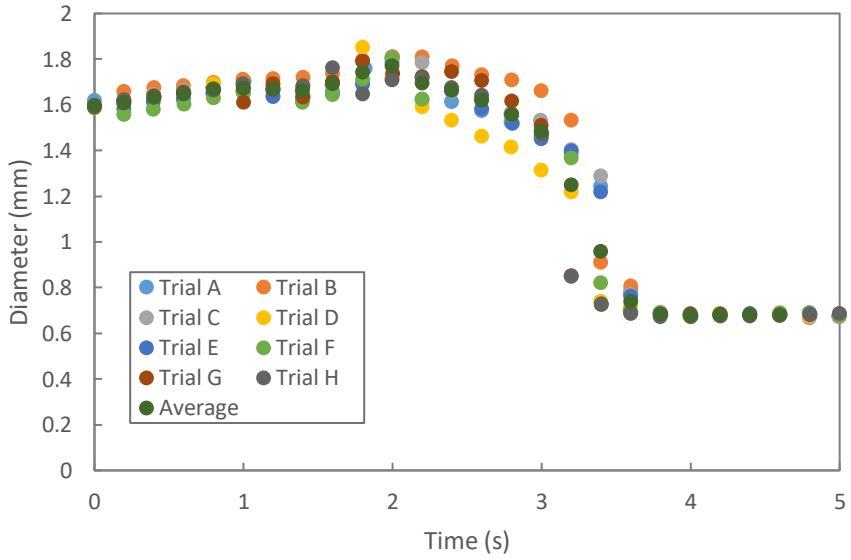

Figure B-8: Trial results droplet diameter of biodiesel with 15% propanol during droplet evaporation at 700°C

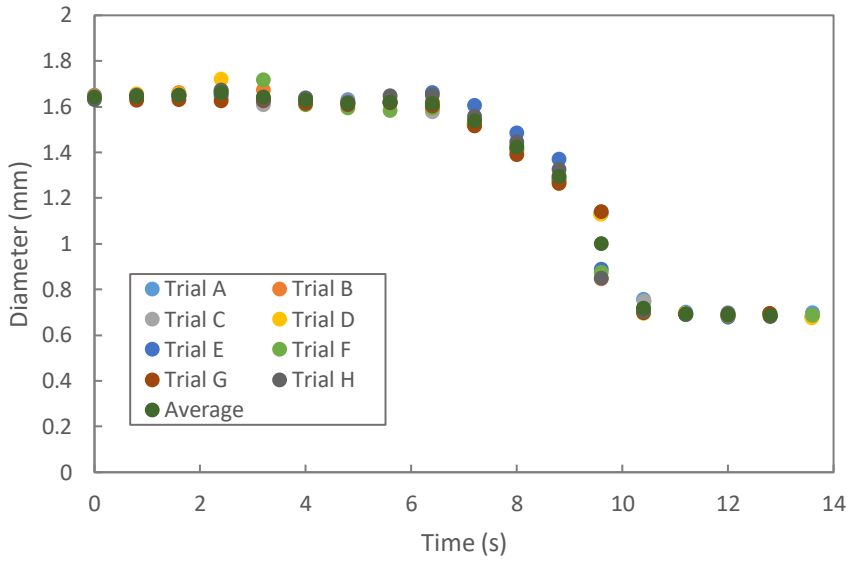

Figure B-9: Trial results droplet diameter of biodiesel with 20% propanol during droplet evaporation at 450°C

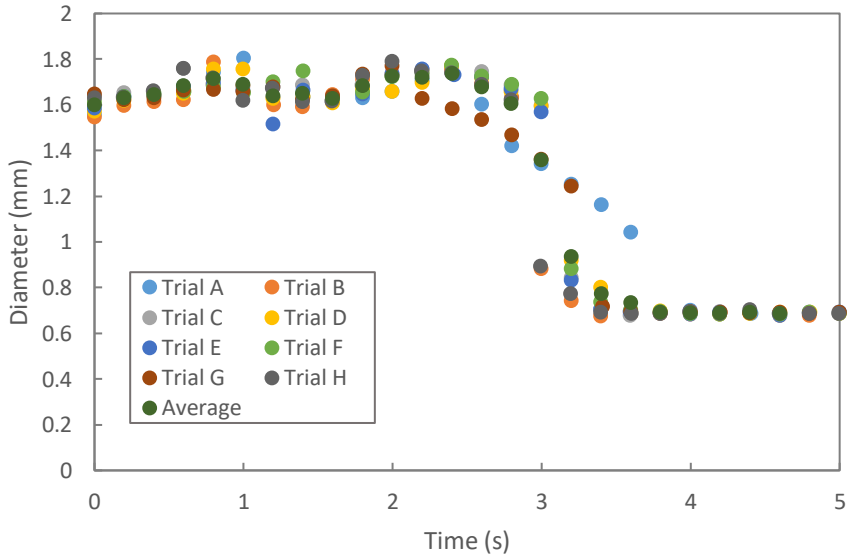

Figure B-10: Trial results droplet diameter of biodiesel with 20% propanol during droplet evaporation at 700°C

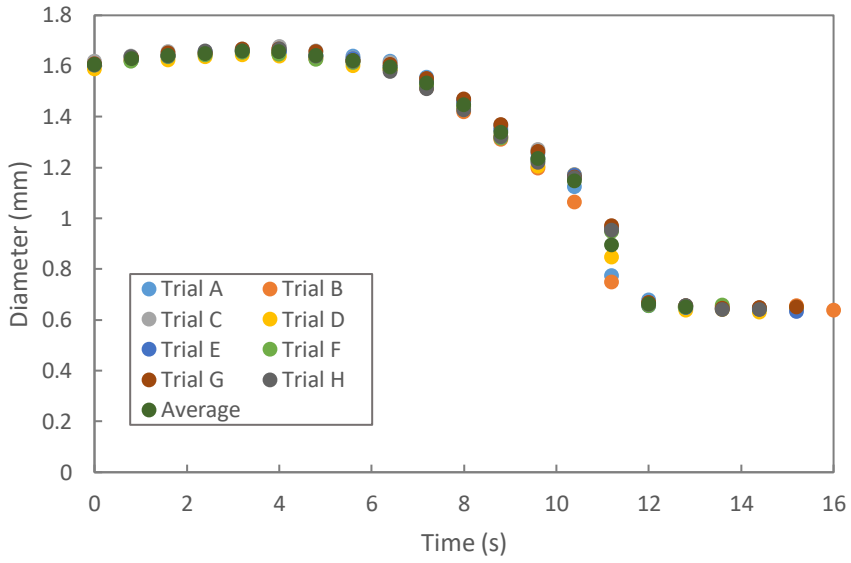

Figure B-11: Trial results droplet diameter of biodiesel with 5% pentanol during droplet evaporation at 450°C

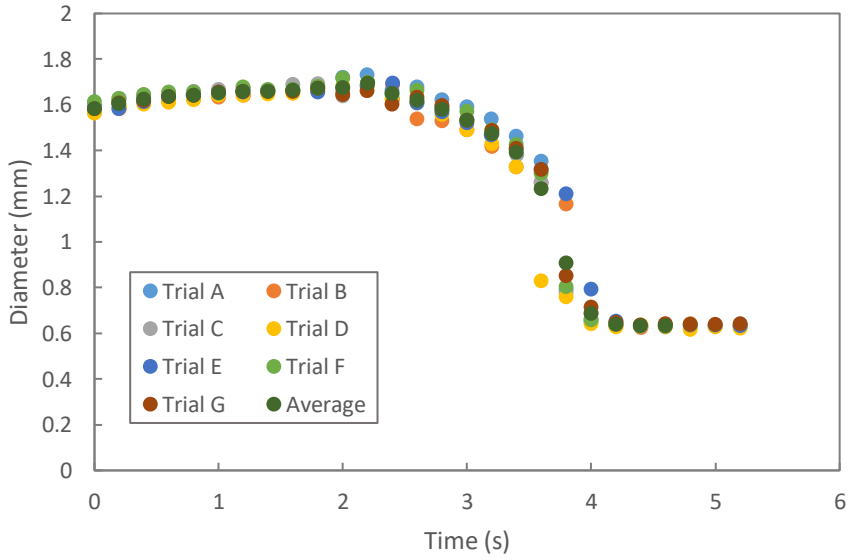

Figure B-12: Trial results droplet diameter of biodiesel with 5% pentanol during droplet evaporation at 700°C

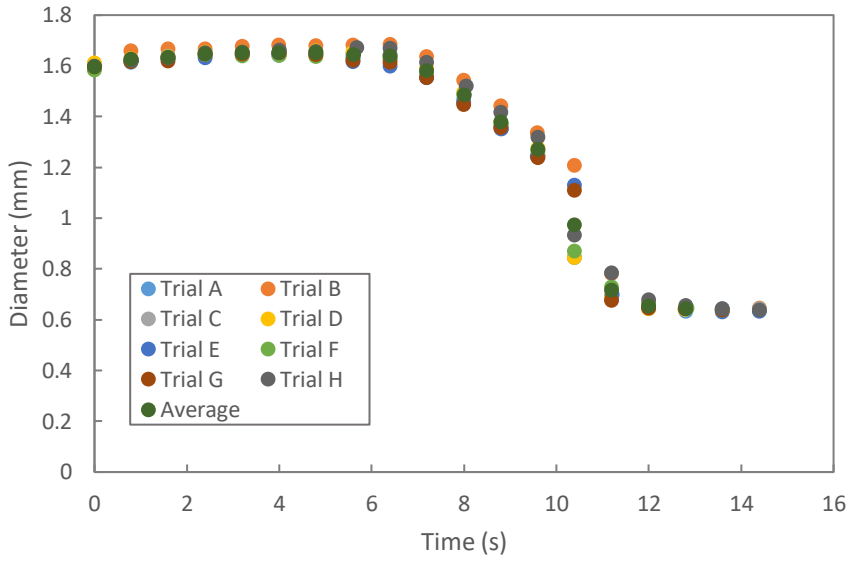

Figure B-13: Trial results droplet diameter of biodiesel with 10% pentanol during droplet evaporation at 450°C

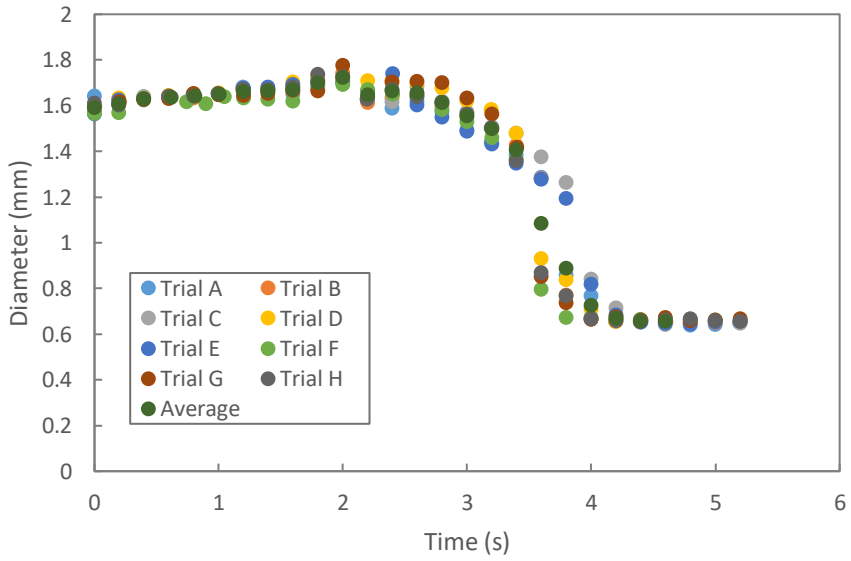

Figure B-14: Trial results droplet diameter of biodiesel with 10% pentanol during droplet evaporation at 700°C

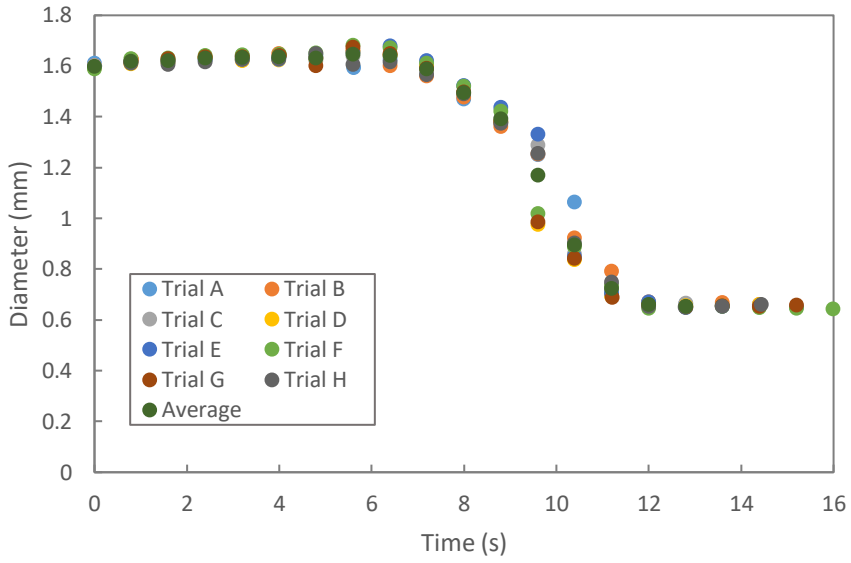

Figure B-15: Trial results droplet diameter of biodiesel with 15% pentanol during droplet evaporation at 450°C

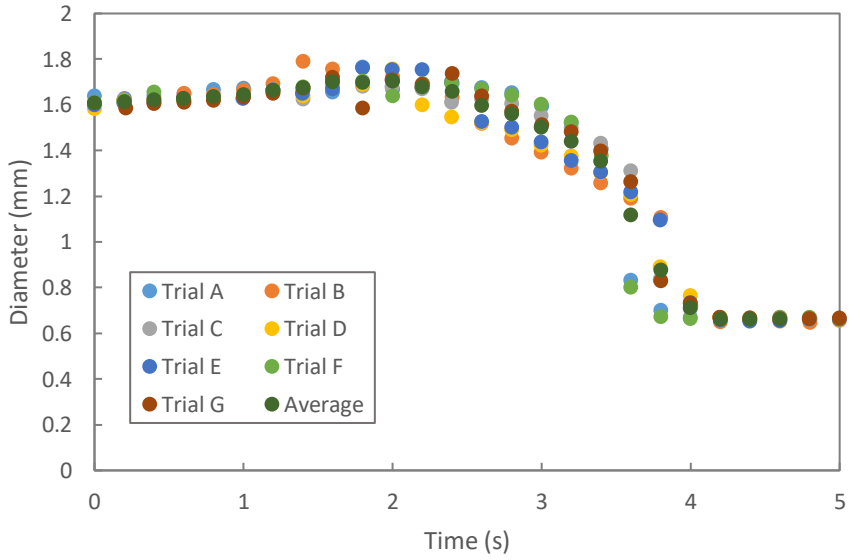

Figure B-16: Trial results droplet diameter of biodiesel with 15% pentanol during droplet evaporation at 700°C

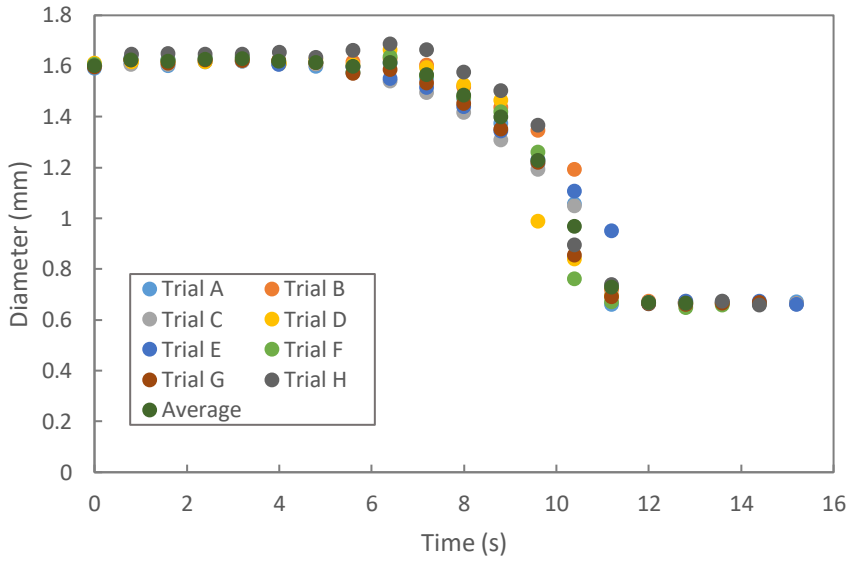

Figure B-17: Trial results droplet diameter of biodiesel with 20% pentanol during droplet evaporation at 450°C

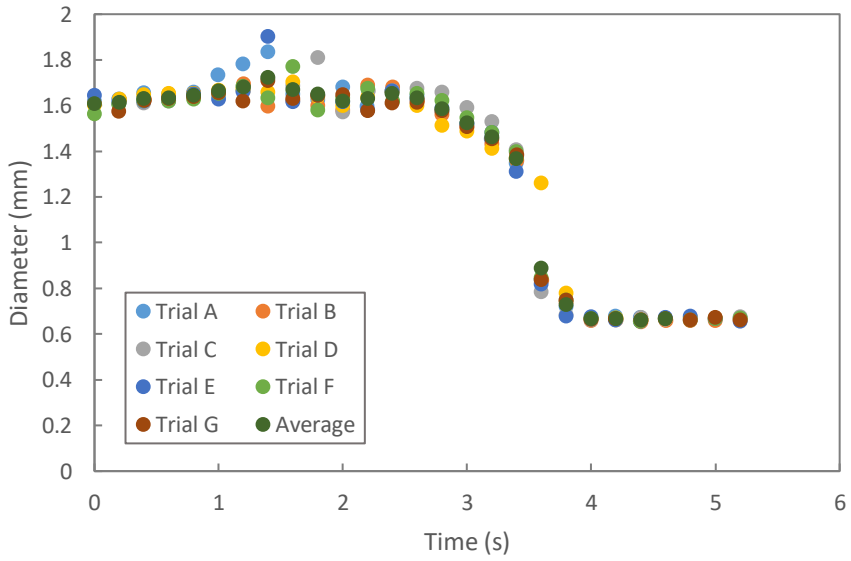

Figure B-18: Trial results droplet diameter of biodiesel with 20% pentanol during droplet evaporation at 700°C

Appendix C: Experimental Droplet Temperature Data from Droplet Evaporation Experiments

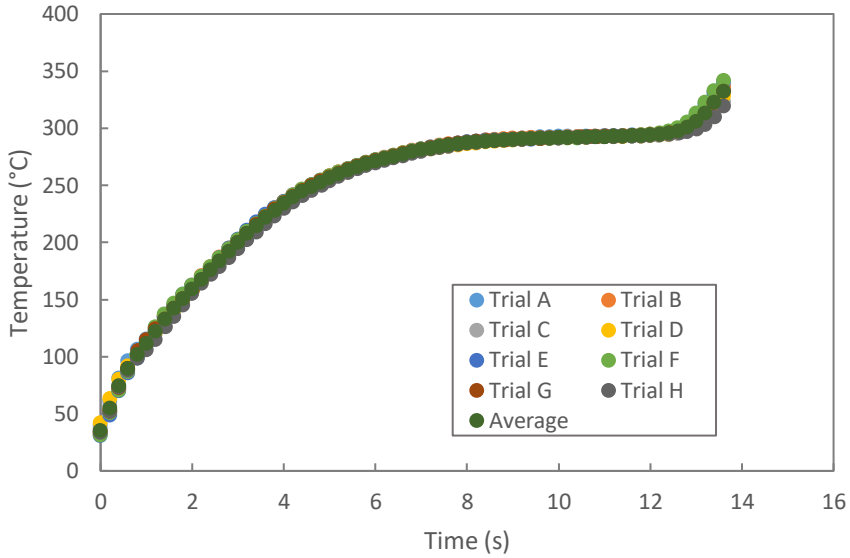

Figure C-1: Trial results of droplet temperature of biodiesel during droplet evaporation at 450°C

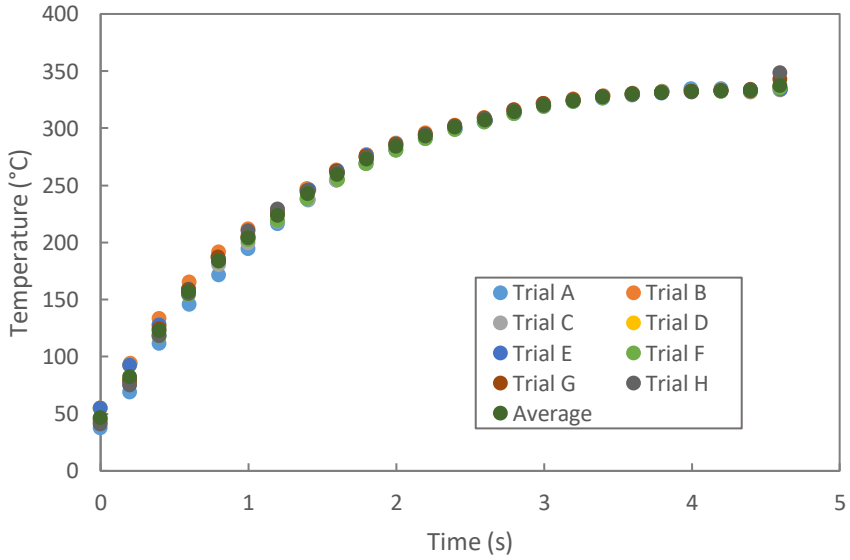

Figure C-2: Trial results of droplet temperature of biodiesel during droplet evaporation at 700°C

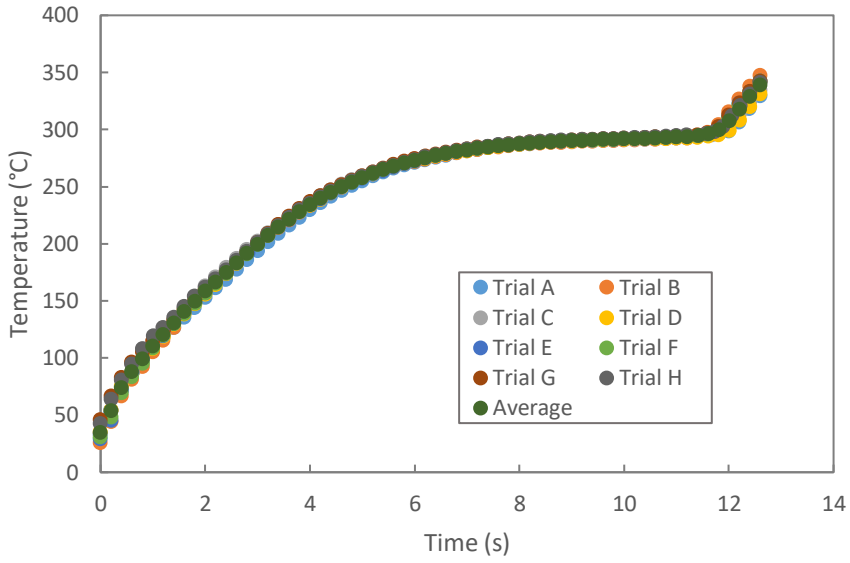

Figure C-3: Trial results droplet temperature of biodiesel with 5% propanol during droplet evaporation at 450°C

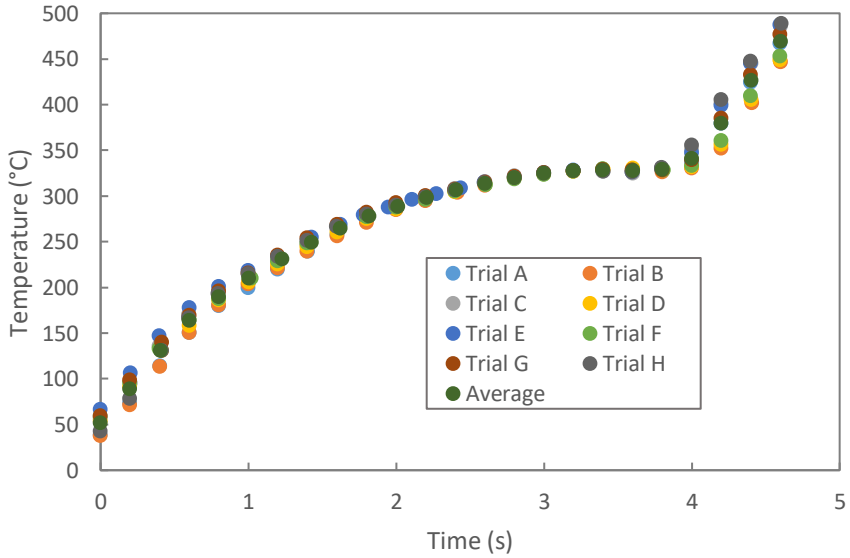

Figure C-4: Trial results droplet temperature of biodiesel with 5% propanol during droplet evaporation at 700°C

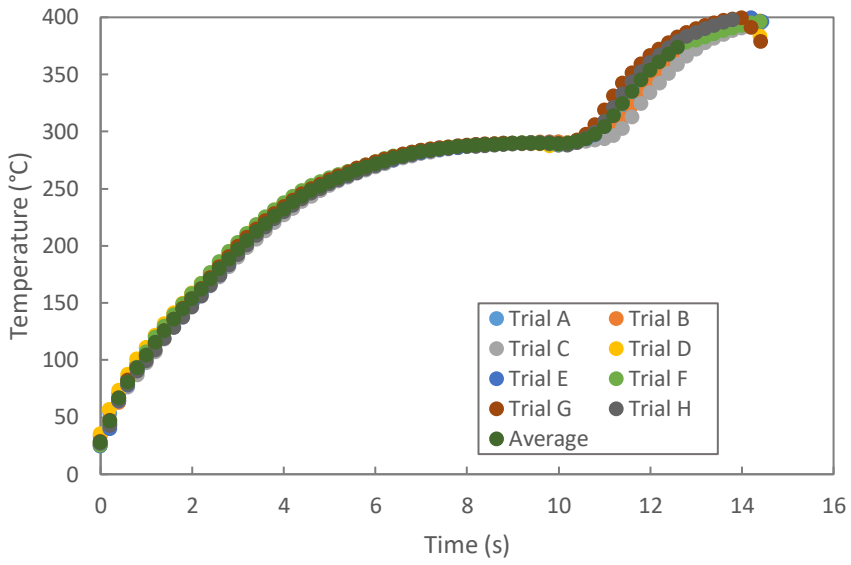

Figure C-5: Trial results droplet temperature of biodiesel with 10% propanol during droplet evaporation at 450°C

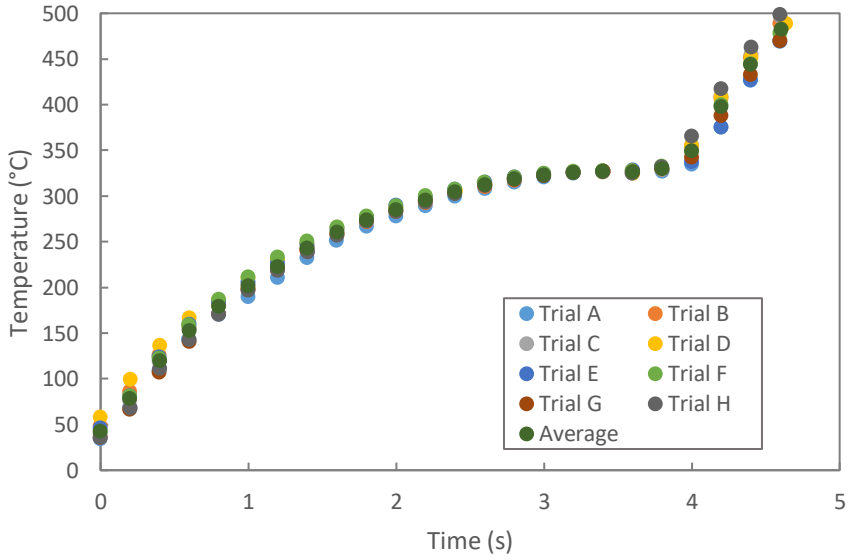

Figure C-6: Trial results droplet temperature of biodiesel with 10% propanol during droplet evaporation at 700°C

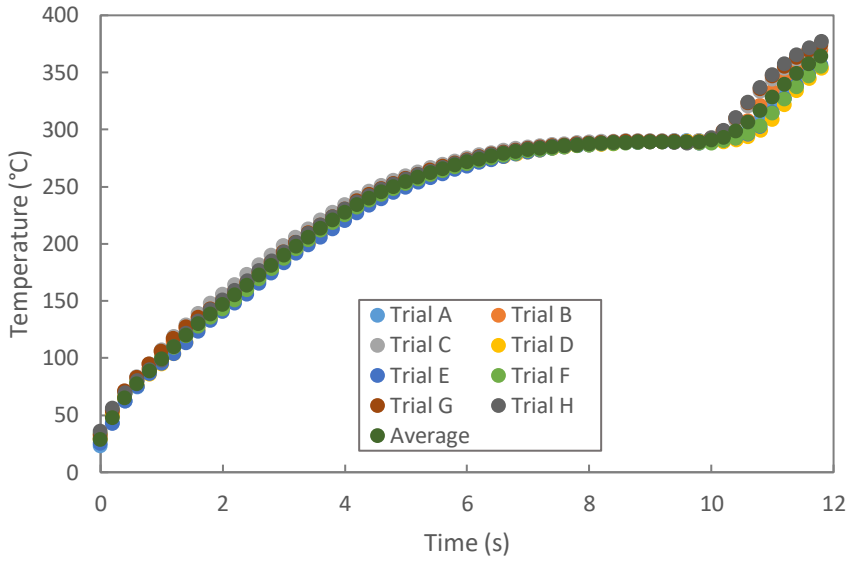

Figure C-7: Trial results droplet temperature of biodiesel with 15% propanol during droplet evaporation at 450°C

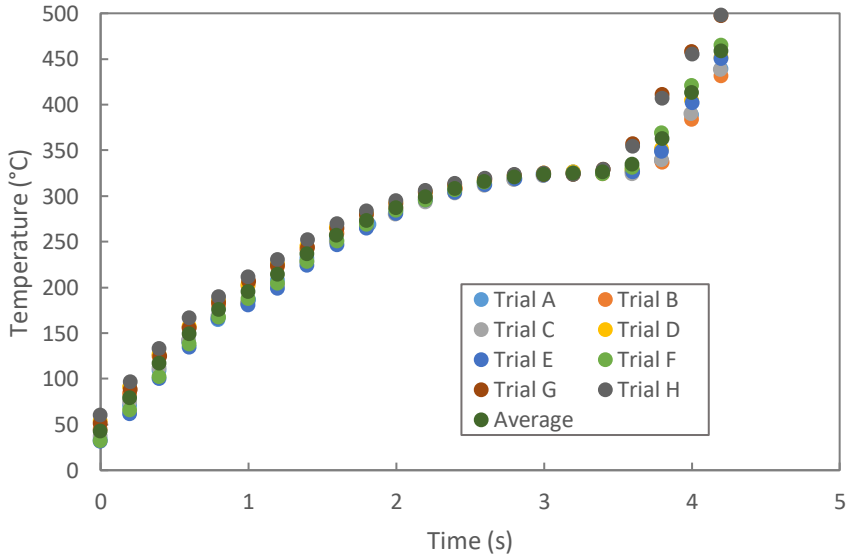

Figure C-8: Trial results droplet temperature of biodiesel with 15% propanol during droplet evaporation at 700°C

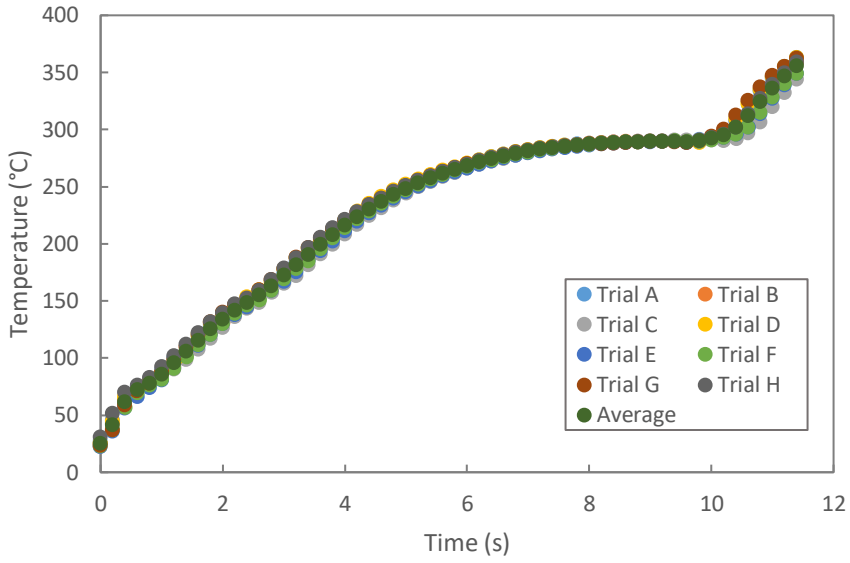

Figure C-9: Trial results droplet temperature of biodiesel with 20% propanol during droplet evaporation at 450°C

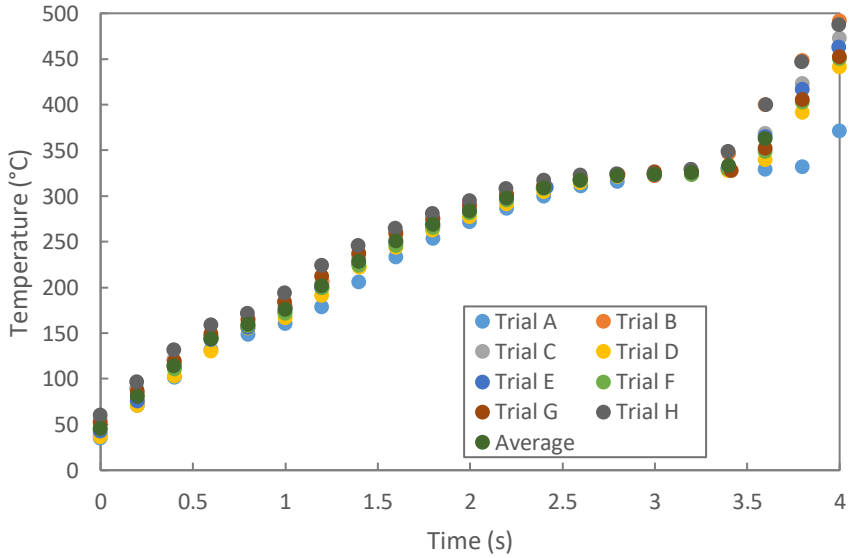

Figure C-10: Trial results droplet temperature of biodiesel with 20% propanol during droplet evaporation at 700°C

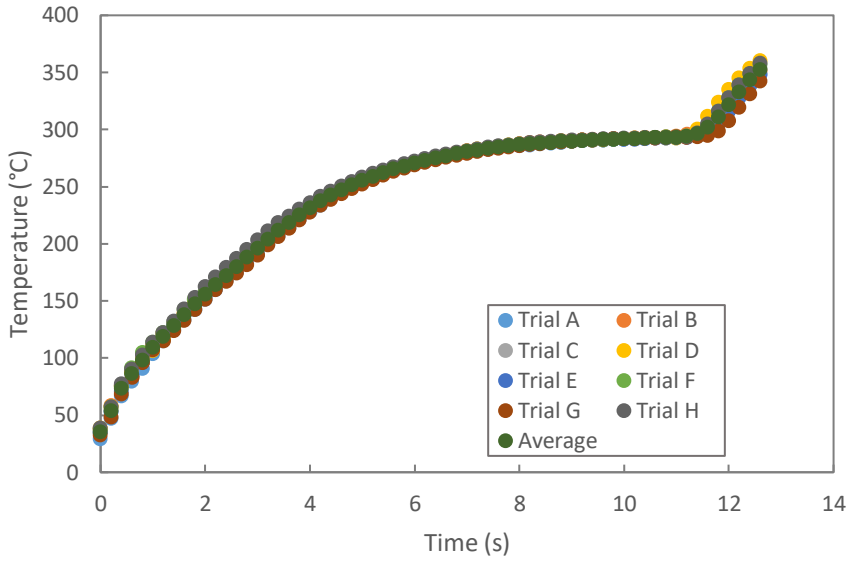

Figure C-11: Trial results droplet temperature of biodiesel with 5% pentanol during droplet evaporation at 450°C

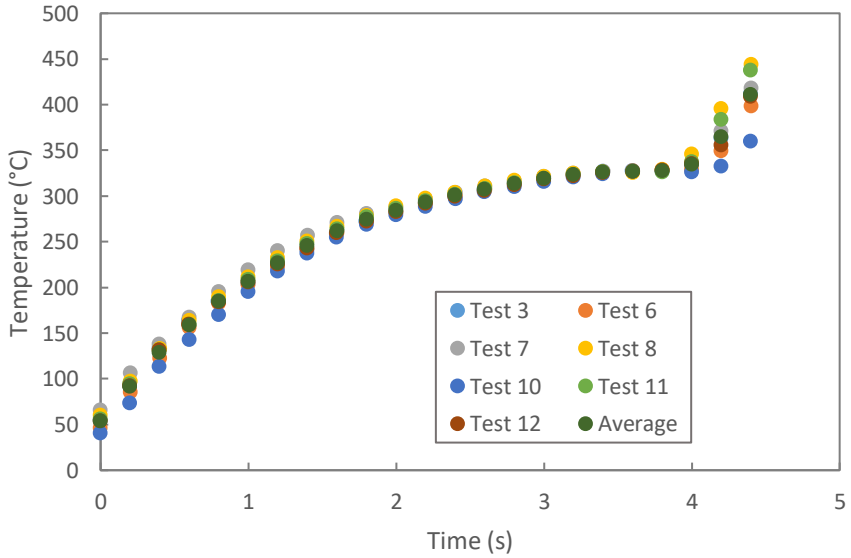

Figure C-12: Trial results droplet temperature of biodiesel with 5% pentanol during droplet evaporation at 700°C

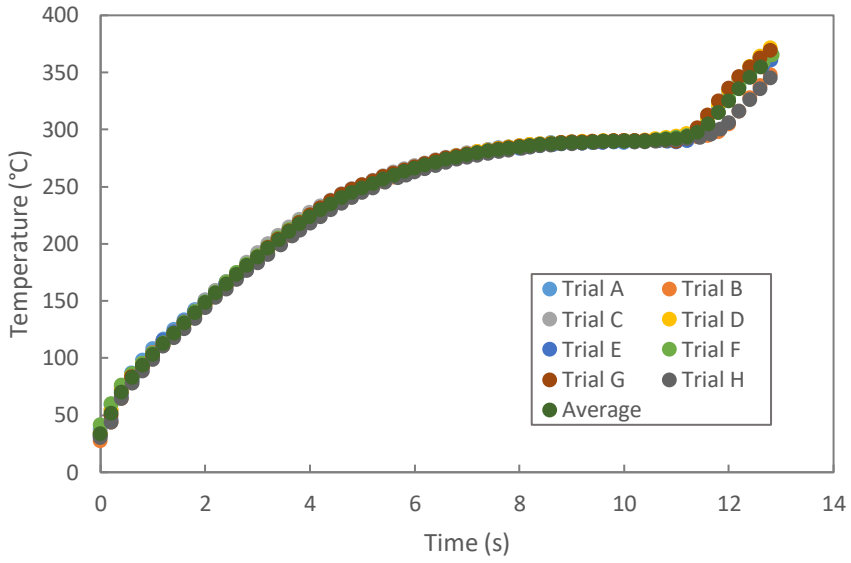

Figure C-13: Trial results droplet temperature of biodiesel with 10% pentanol during droplet evaporation at 450°C

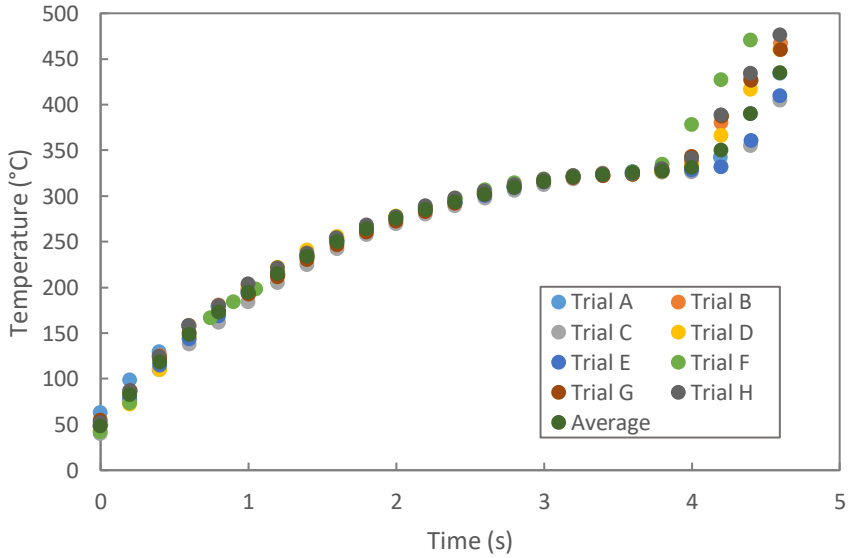

Figure C-14: Trial results droplet temperature of biodiesel with 10% pentanol during droplet evaporation at 700°C

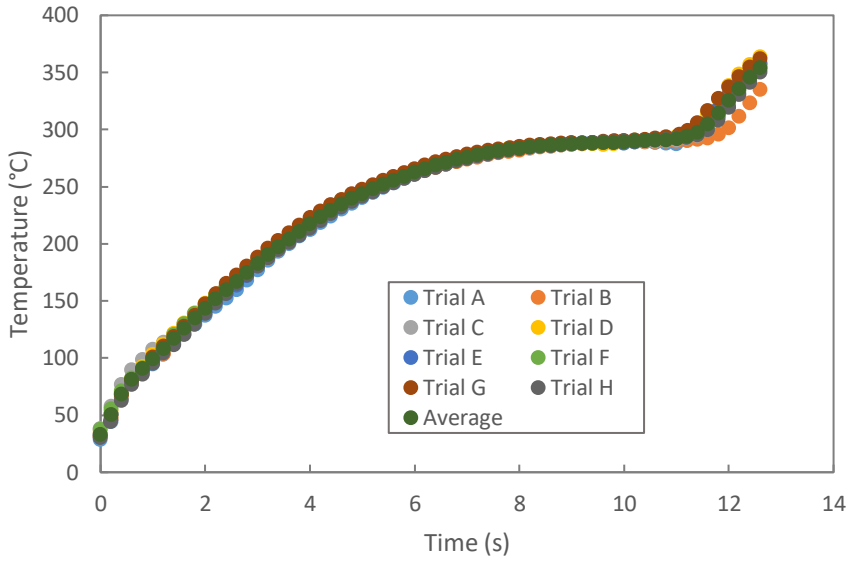

Figure C-15: Trial results droplet temperature of biodiesel with 15% pentanol during droplet evaporation at 450°C

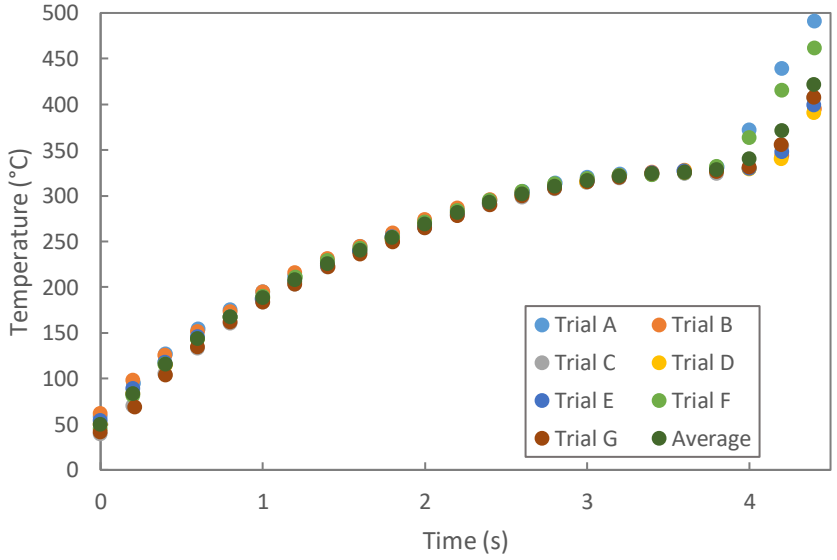

Figure C-16: Trial results droplet temperature of biodiesel with 15% pentanol during droplet evaporation at 700°C

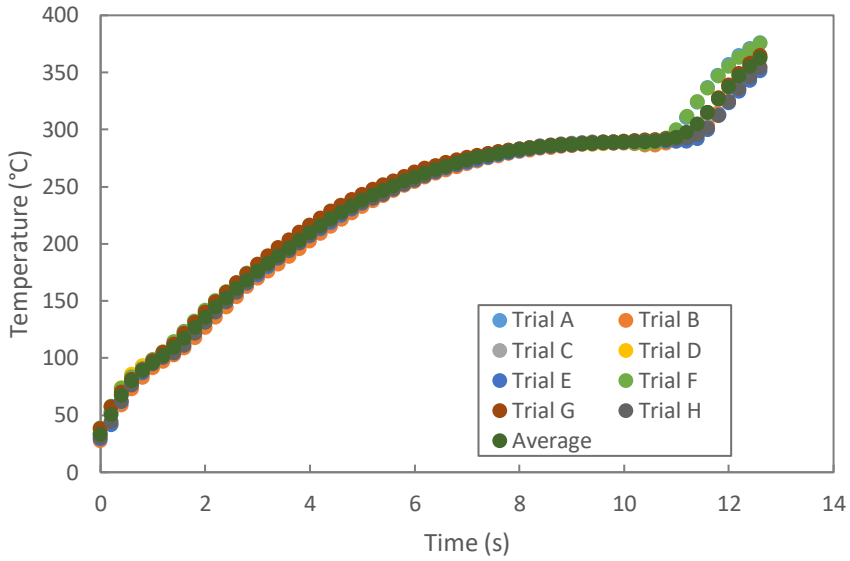

Figure C-17: Trial results droplet temperature of biodiesel with 20% pentanol during droplet evaporation at 450°C

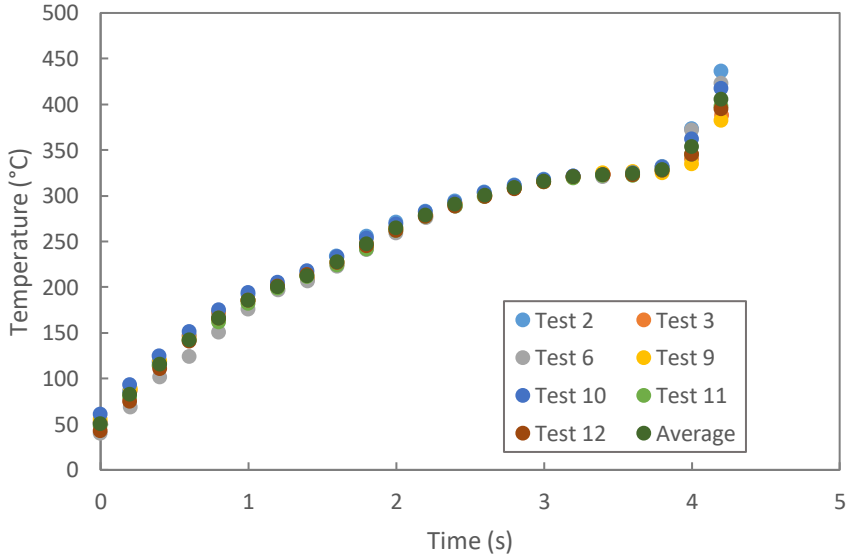

Figure C-18: Trial results droplet temperature of biodiesel with 20% pentanol during droplet evaporation at 700°C

Appendix D: Additional Results for Biodiesel Propanol Mixtures

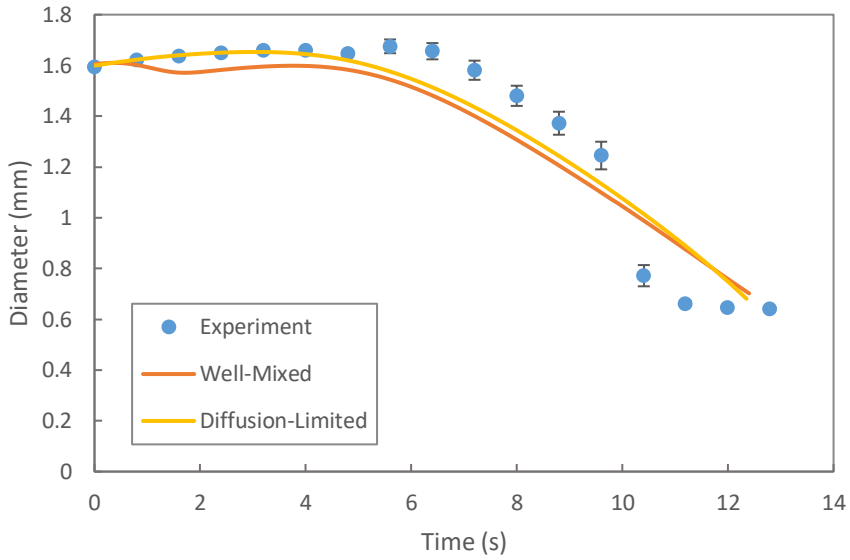

Figure D-1: Droplet diameter of biodiesel with 10% propanol during droplet evaporation at 450°C

Note: Experimental points give the mean and standard deviation of 8 individual measurements

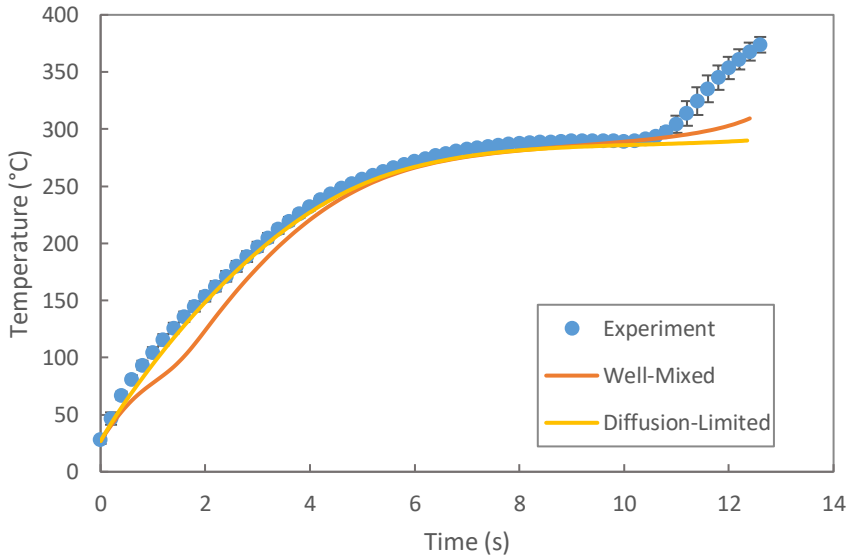

Figure D-2: Droplet temperature of biodiesel with 10% propanol during droplet evaporation at 450°C

Note: Experimental points give the mean and standard deviation of 8 individual measurements

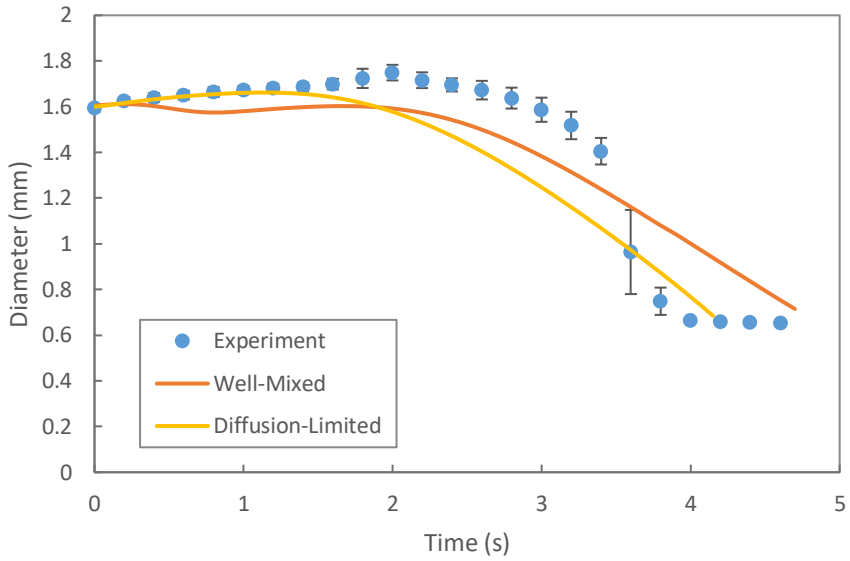

Figure D-3: Droplet diameter of biodiesel with 10% propanol during droplet evaporation at 700°C

Note: Experimental points give the mean and standard deviation of 8 individual measurements

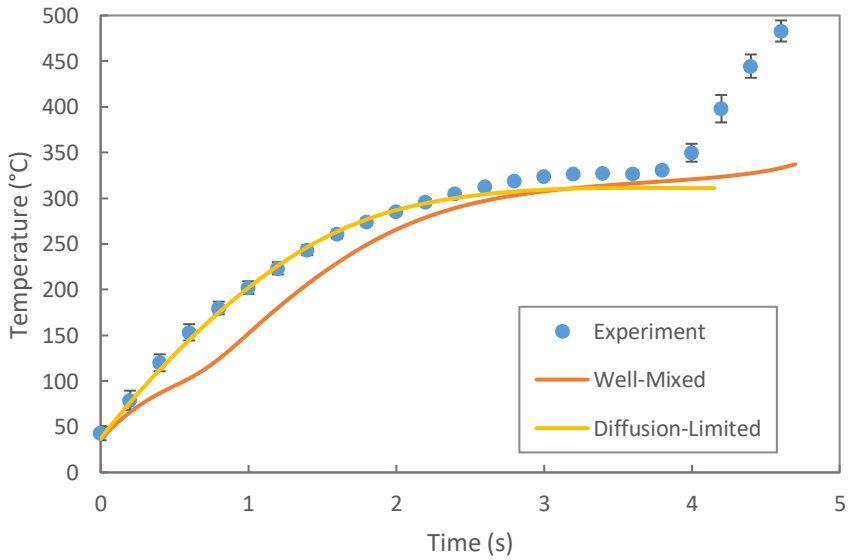

Figure D-4: Droplet temperature of biodiesel with 10% propanol during droplet evaporation at 700°C

Note: Experimental points give the mean and standard deviation of 8 individual measurements

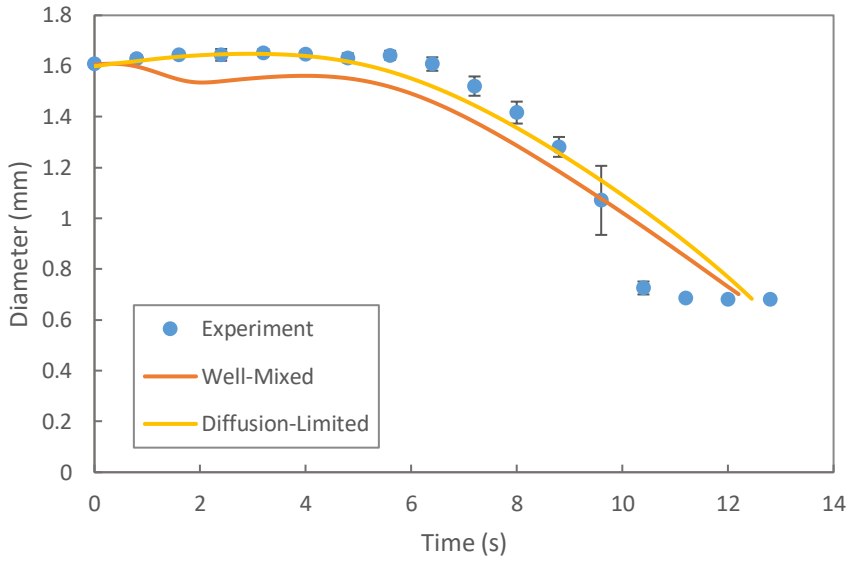

Figure D-5: Droplet diameter of biodiesel with 15% propanol during droplet evaporation at 450°C

Note: Experimental points give the mean and standard deviation of 8 individual measurements

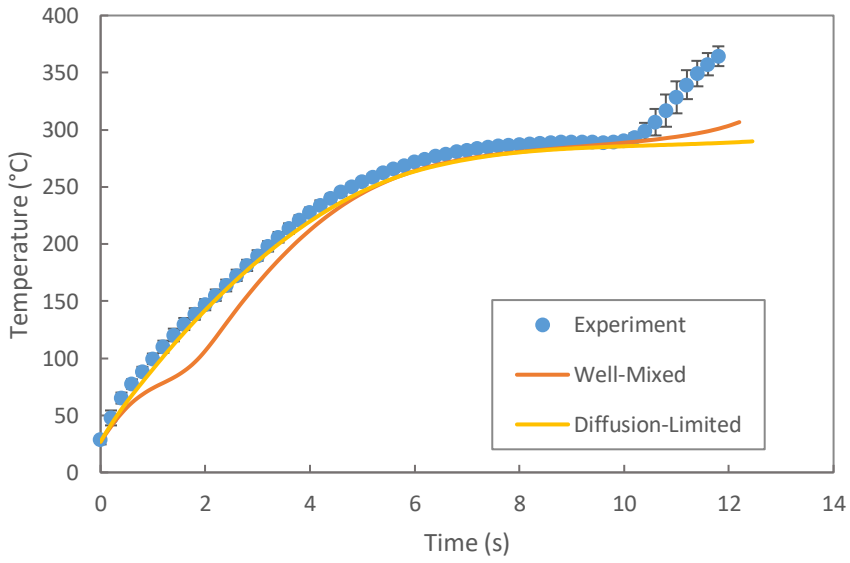

Figure D-6: Droplet temperature of biodiesel with 15% propanol during droplet evaporation at 450°C

Note: Experimental points give the mean and standard deviation of 8 individual measurements

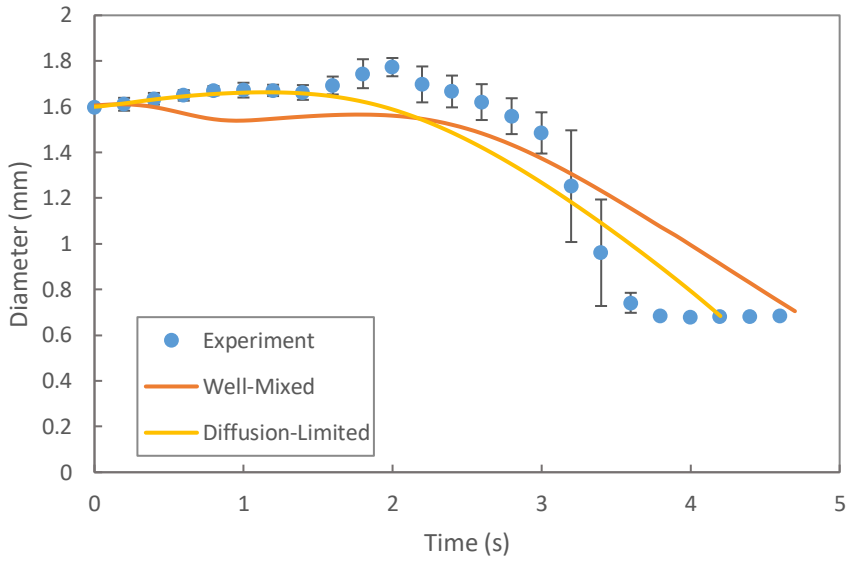

Figure D-7: Droplet diameter of biodiesel with 15% propanol during droplet evaporation at 700°C

Note: Experimental points give the mean and standard deviation of 8 individual measurements

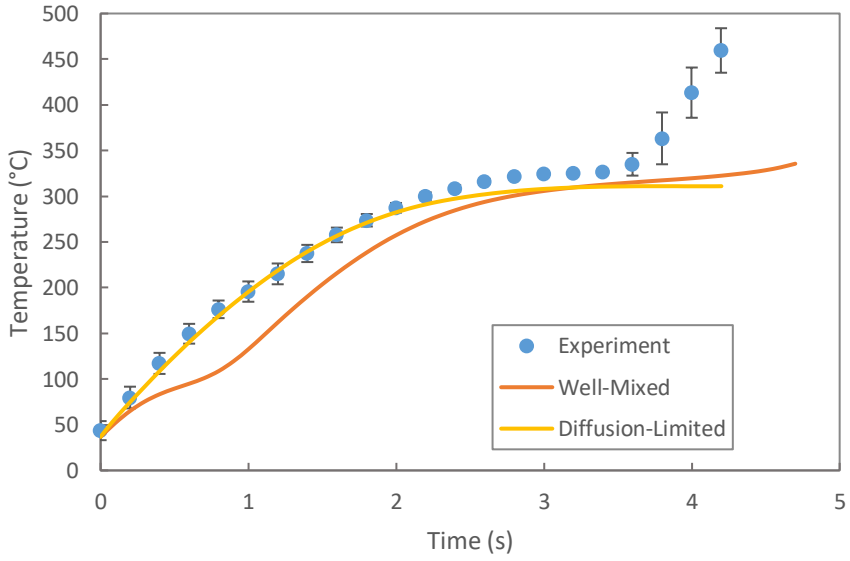

Figure D-8: Droplet temperature of biodiesel with 15% propanol during droplet evaporation at 700°C

Note: Experimental points give the mean and standard deviation of 8 individual measurements

Appendix E: Additional Results for Biodiesel Pentanol Mixtures

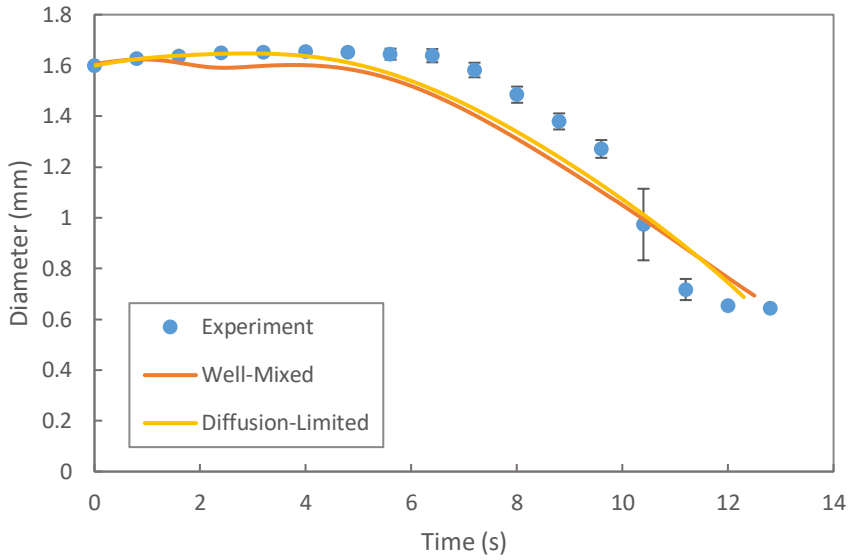

Figure E-1: Droplet diameter of biodiesel with 10% pentanol during droplet evaporation at 450°C

Note: Experimental points give the mean and standard deviation of 8 individual measurements

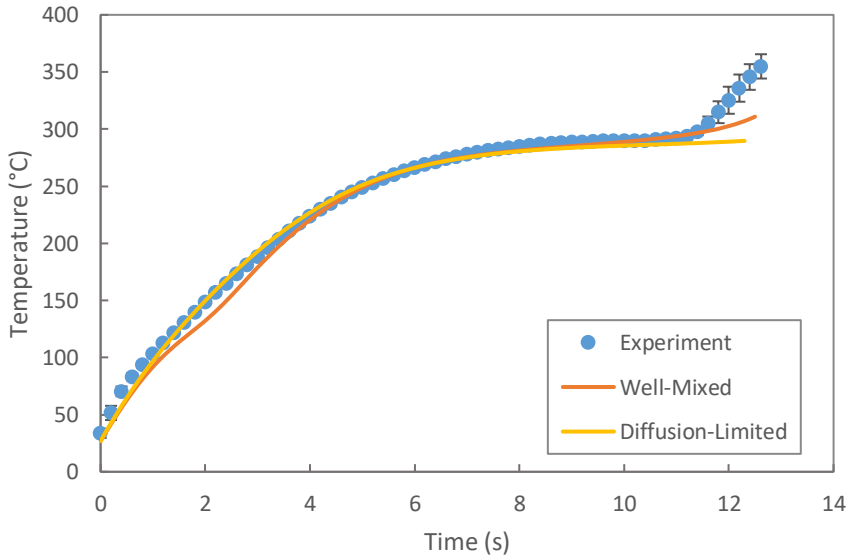

Figure E-2: Droplet temperature of biodiesel with 10% pentanol during droplet evaporation at 450°C

Note: Experimental points give the mean and standard deviation of 8 individual measurements

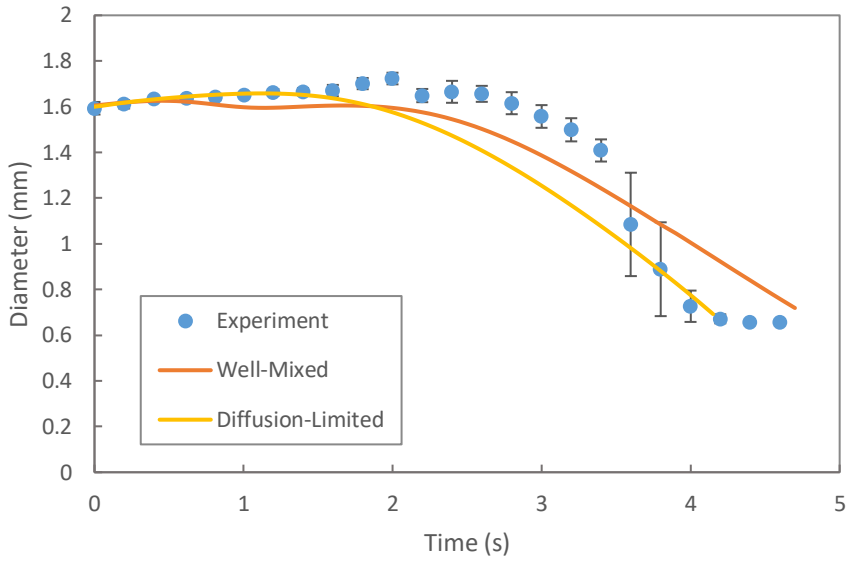

Figure E-3: Droplet diameter of biodiesel with 10% pentanol during droplet evaporation at 700°C

Note: Experimental points give the mean and standard deviation of 8 individual measurements

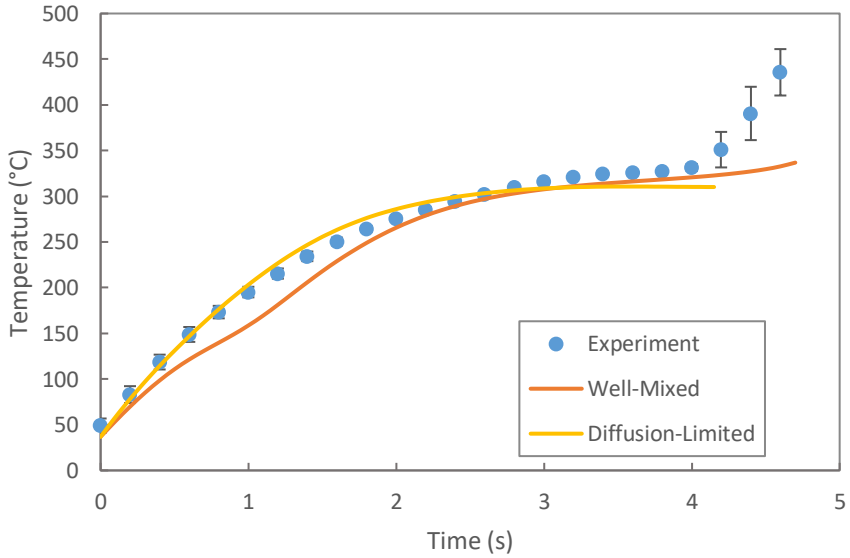

Figure E-4: Droplet temperature of biodiesel with 10% pentanol during droplet evaporation at 700°C

Note: Experimental points give the mean and standard deviation of 8 individual measurements

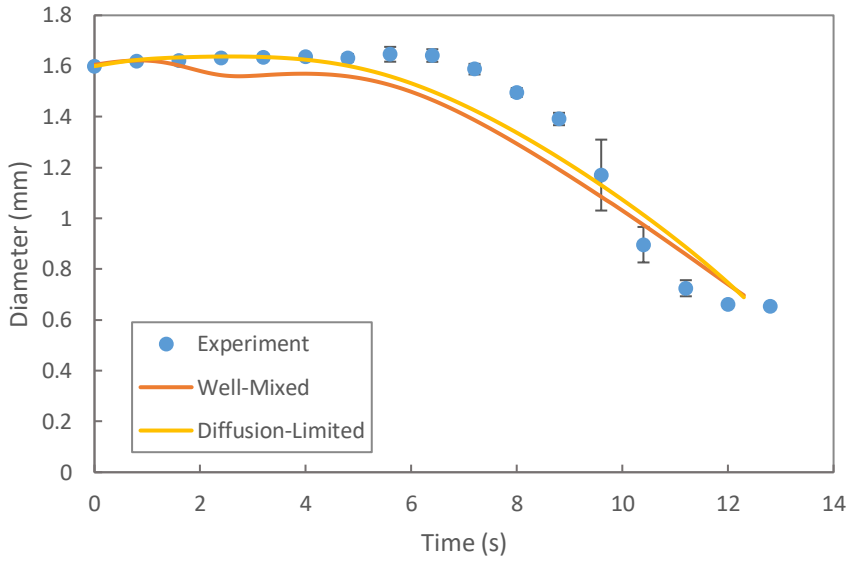

Figure E-5: Droplet diameter of biodiesel with 15% pentanol during droplet evaporation at 450°C

Note: Experimental points give the mean and standard deviation of 8 individual measurements

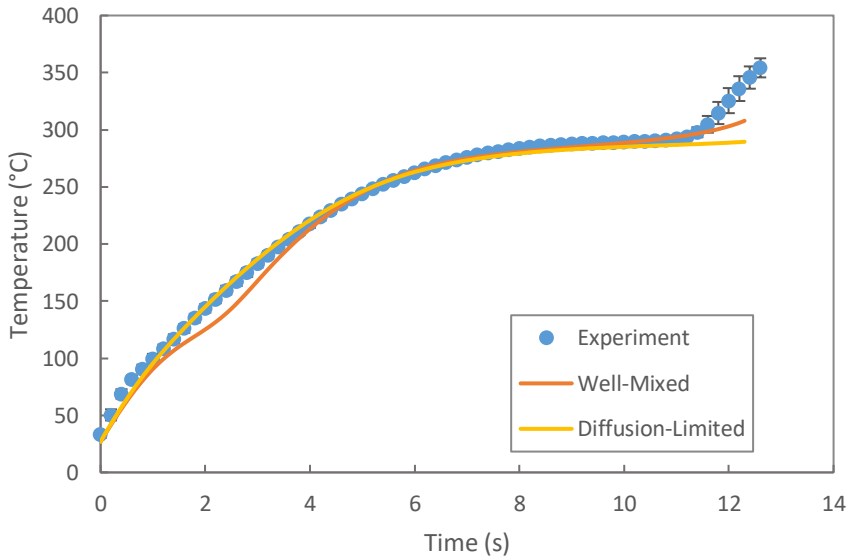

Figure E-6: Droplet temperature of biodiesel with 15% pentanol during droplet evaporation at 450°C

Note: Experimental points give the mean and standard deviation of 8 individual measurements

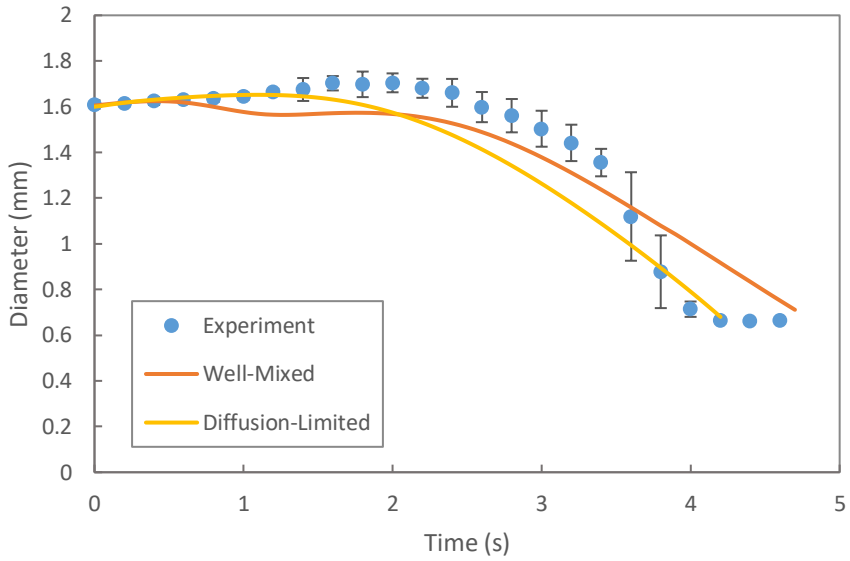

Figure E-7: Droplet diameter of biodiesel with 15% pentanol during droplet evaporation at 700°C

Note: Experimental points give the mean and standard deviation of 7 individual measurements

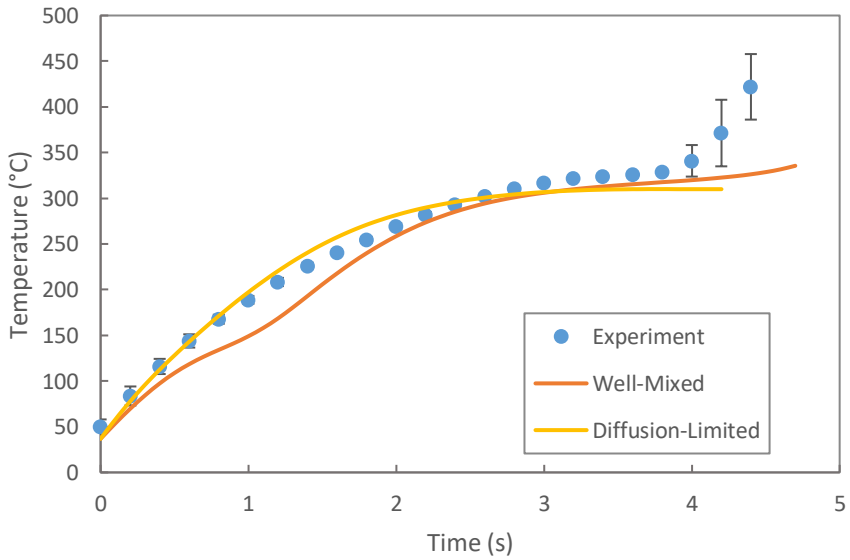

Figure E-8: Droplet temperature of biodiesel with 15% pentanol during droplet evaporation at 450°C

Note: Experimental points give the mean and standard deviation of 7 individual measurements